AD NUMBER

AD887076

NEW LIMITATION CHANGE

TO

Approved for public release, distribution unlimited

FROM

Distribution authorized to U.S. Gov't. agencies only; Test and Evaluation; MAY 1971. Other requests shall be referred to Air Force Armament Lab., Attn: DLRA, Eglin AFB, FL 32542.

AUTHORITY

Air Force Armament Lab ltr dtd 22 Mar 1978

AFATL-TR-71-57

VOLUTE STABILIZATION OF CYLINDRICAL SUBMUNITIONS

VALAERO, INC.

TECHNICAL REPORT AFATL-TR-71-57

MAY 1971

Distribution limited to U. S. Government agencies only; this report documents tests and evaluation of potential military hardware; distribution limitation applied May 1971. Other requests for this document must be referred to the Air Force Armament Laboratory (DLRA), Eglin Air Force Base, Florida 32542.

AIR FORCE ARMAMENT LABORATORY
AIR FORCE SYSTEMS COMMAND • UNITED STATES AIR FORCE
EGLIN AIR FORCE BASE, FLORIDA

UNCLASSIFIED
Security Classification

DOCUMENT CONTROL DATA - R & D

(Security classification of title, body of abstract and indexing annotation must be entered when the overall report is classified)

1 ORIGINATING ACTIVITY (Corporate author)	2a. REPORT SECURITY CLASSIFICATION
Valaero, Inc. Valparaiso, Florida 32580	UNCLASSIFIED 2b. GROUP

3 REPORT TITLE

VOLUTE STABILIZATION OF CYLINDRICAL SUBMUNITIONS

4 DESCRIPTIVE NOTES (Type of report and inclusive dates)

Final Report - March 1970 to March 1971

5 AUTHOR(S) (First name, middle initial, last name)

Robert W. Conlan
Dewey E. Calfee

6 REPORT DATE	7a. TOTAL NO. OF PAGES	7b. NO OF REFS
May 1971	135	4

8a CONTRACT OR GRANT NO.	9a. ORIGINATOR'S REPORT NUMBER(S)
F08635-70-C-0071 b. PROJECT NO. 2547 c. Task No. 01 d. Work Unit 011	9b. OTHER REPORT NO(S) (Any other numbers that may be assigned this report) AFATL-TR-71-57

10. DISTRIBUTION STATEMENT

Distribution limited to U. S. Government agencies only: this report documents tests and evaluation of potential military hardware; distribution limitation applied May 1971. Other requests for this document must be referred to the Air Force Armament Laboratory (DLRA), Eglin Air Force Base, Florida 32542

11 SUPPLEMENTARY NOTES	12. SPONSORING MILITARY ACTIVITY
Available in DDC	Air Force Armament Laboratory Air Force Systems Command Eglin Air Force Base, Florida 32542

13 ABSTRACT

~~This~~ report is the first of a two-year effort for determining the dynamic and static aerodynamic stability derivatives for volute stabilized cylindrical forebodies. The complete analytical treatment of both rigid and flexible models is dealt with and these results compared to data obtained from the Eglin low speed wind tunnel. The theory presents several methods that give the designer necessary techniques for estimating ~~$C_{m\alpha}$~~ and ~~$(C_{mq} + C_{m\dot{\alpha}})$~~ for a variety of different volute shapes and cylindrical forebodies. These techniques yield reasonable answers for both rigid and flexible models operating at $R_n = 2 \times 10^5$ and $M_\infty = 0.2$ with volute tails sufficiently long so that the potential flow theory used is valid. The complete data obtained at both the Eglin facility and at Arnold Engineering Development Center, Arnold Air Force Station, Tennessee, joined with the analysis presented, served to show that the volute provides an effective yet compact stabilizer for $R_n = 2 \times 10^5$ to 1×10^6 for $M_\infty = 0.2$ to 0.5 for cylindrical forebodies.

DD FORM 1 NOV 65 1473

UNCLASSIFIED
Security Classification

14 KEY WORDS	LINK A		LINK B		LINK C	
	ROLE	WT	ROLE	WT	ROLE	WT
Aerodynamic Stability Derivatives						
Volute Stabilizer						
Cylindrical Submunitions						
Rigid Volute Tails						
Flexible Volute Tails						
Wind Tunnel Tests						
Two Degree Angular Freedom Analysis						

Volute Stabilization

of

Cylindrical Submunitions

Robert W. Conlan

Dewey E. Calfee

FOREWORD

This report documents a study conducted during the period March 1970 to March 1971 by Valaero, Inc., Valparaiso, Florida, under Contract F08635-70-C-0071 with the Air Force Armament Laboratory, Air Force Systems Command, Eglin Air Force Base, Florida. Dr. Mark O. Glasgow (DLRA) was program monitor for the Armament Laboratory. This effort was conducted under Project 2547, Task 01, and Work Unit 011.

Principal investigators for contractor were Messrs. Robert W. Conlan and Dewey E. Calfee.

This report has been reviewed and is approved.

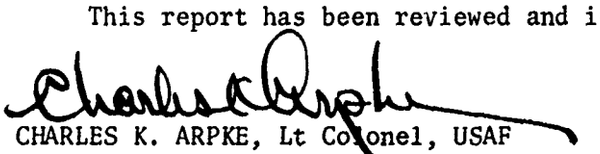

CHARLES K. ARPKE, Lt Colonel, USAF
Chief, Technology Division

ABSTRACT

This report is the first of a two-year effort for determining the dynamic and static aerodynamic stability derivatives for volute stabilized cylindrical forebodies. The complete analytical treatment of both rigid and flexible models is dealt with and these results compared to data obtained from the Eglin low speed wind tunnel. The theory presents several methods that give the designer necessary techniques for estimating $C_{m\alpha}$ and $(C_{mq} + C_{m\dot{\alpha}})$ for a variety of different volute shapes and cylindrical forebodies. These techniques yield reasonable answers for both rigid and flexible models operating at $R_n = 2 \times 10^5$ and $M_\infty = 0.2$ with volute tails sufficiently long so that the potential flow theory used is valid. The complete data obtained at both the Eglin facility and at Arnold Engineering Development Center, Arnold Air Force Station, Tennessee, joined with the analysis presented, served to show that the volute provides an effective yet compact stabilizer for $R_n = 2 \times 10^5$ to 1×10^6 for $M_\infty = 0.2$ to 0.5 for cylindrical forebodies.

(The reverse of this page is blank)

TABLE OF CONTENTS

LIST OF FIGURES

LIST OF FIGURES (Concluded)

LIST OF TABLES

LIST OF ABBREVIATIONS AND SYMBOLS

h_b' - Moment arm measured forward from the model cg to the center of pressure of cylindrical portion forward of the model cg.

h_b - Moment arm measured aft of the model cg to the center of pressure of the cylindrical portion of the model aft of the cg.

h_t' - Moment arm measured from the model cg to the center of pressure of the volute stabilizer.

h_t - Moment arm measured aft of the model cg to the center of pressure of aft portion of the model.

h_v - Moment arm measured from the volute hinge line to the volute center of pressure.

$\hat{x}_t$ - Accounts for the rotary velocity field aft of the cg.

$\hat{x}_b'$ - Accounts for the rotary velocity field forward of the model cg.

$\hat{x}_b$ - Accounts for the rotary velocity field for the aft portion of the cylinder relative to the model cg.

$\hat{x}_{v_t}$ - Accounts for the rotary velocity about the volute measured from the model cg.

x_v - Accounts for the rotary velocity field about the volute measured from the volute hinge line.

S_b' - The planform area of the cylindrical portion of the model measured forward of the model cg.

S_b - The planform area of the cylindrical portion of the model measured aft of the model cg.

S_v - Planform area of the volute.

S_t - $S_t = S_b' + S_v$

S - Total planform area of the model.

l_b - Forebody length

l_v - Volute length

LIST OF ABBREVIATIONS AND SYMBOLS (Continued)

l_o	- Length of the cylinder aft of the model cg.
x_{cg}	- Model center of gravity measured relative to model nose.
x	- Variable running along the model longitudinal axis.
d_c	- Diameter of the cylinder.
d_v	- Diameter of the volute.
d_v'	- Diameter of the truncated portion of the volute.
q	- Dynamic pressure.
C_{nt_o}	- Normal force coefficient of the area aft of the model cg at 90 degrees.
C_{nb_o}	- Normal force coefficient of the cylindrical portion of the model.
C_{nv_o}	- Normal force coefficient of the volute.
C_m	- Total pitching coefficient.
C_{m_s}	- Static portion of C_m.
C_{m_α}	- Pitching moment slope coefficient.
$(C_{m_q} + C_{m_{\dot\alpha}})$	- Damping coefficient.
C_{m_δ}	- Represents the static pitching contribution of the volute.
$C_{m_{\dot\delta}}$	- Represents the amount of intrinsic damping power of the volute.
$C_{m_{\alpha f}}$	- Flexible pitching slope coefficient.
$(C_{m_q} + C_{m_{\dot\alpha}})_f$	- Flexible damping coefficient.
J	- A number which proportions the effects of flexible volutes as related to rigid ones.
Φ	- Proportionality constant for flexible analysis.
$\hat\theta$	- Proportionality constant for rigid analysis.

ΔB - Forebody contribution to the C_{m_α} equations.

$\Delta B'$ - Forebody contribution to the $(C_{m_q} + C_{m_{\dot{\alpha}}})$ equation.

V - Represents the moment developed by the volute.

k_V - Lateral spring constant of the volute.

a_{ij} - Coefficients of the two-degree angular freedom equations.

I_b - Mass moment of inertia of the cylinder about the model pitch axis.

I - Total body moment of inertia

K_V - Mass moment of inertia term resulting from two-degree angular freedom moment summation.

I_V - Mass moment of inertia of the volute measured about the hinge line.

M_V - Mass of the volute.

R_V - Distance from the pitch axis to the hinge axis.

$\bar{r}_V$ - Distance from the volute hinge line to the volute mass center.

w_V - Volute weight.

V_∞ - Relative velocity.

C_{ij} - Coefficients on the characteristic equation for the flexible models.

θ - Angle subtended by the free stream velocity vector and the model longitudinal axis.

ρ - Air density.

s - Characteristic equation variable.

d_i - Coefficients of the quadratic factors of the 4th degree characteristic equations.

p_{ij} - Elements in the Routh-Hurwitz stability scheme.

LIST OF ABBREVIATIONS AND SYMBOLS (Concluded)

R - Cylinder cavity radius.

t_1 - Volute spring material thickness.

t_2 - Volute spring material width.

n - Number of volute helical coils.

δ_o - Volute half-angle.

δ - Deflection of volute relative to cylinder longitudinal axis.

SECTION I

INTRODUCTION

This report documents the results of investigations of the mechanical behavior of volute stabilized cylindrical forebodies. The cylinder model flight characteristics were determined through experimental and analytical programs which yielded values for the stability derivatives and several predictive schemes for evaluating C_{m_α}, $(C_{m_q} + C_{m_{\dot{\alpha}}})$.

The volute stabilizer is essentially a tapered helical spring which can be packaged conveniently in a small area at the base of a forebody (Figure 1). Spring steel, which provides strength and flexibility, is an ideal material for volute stabilizer construction.

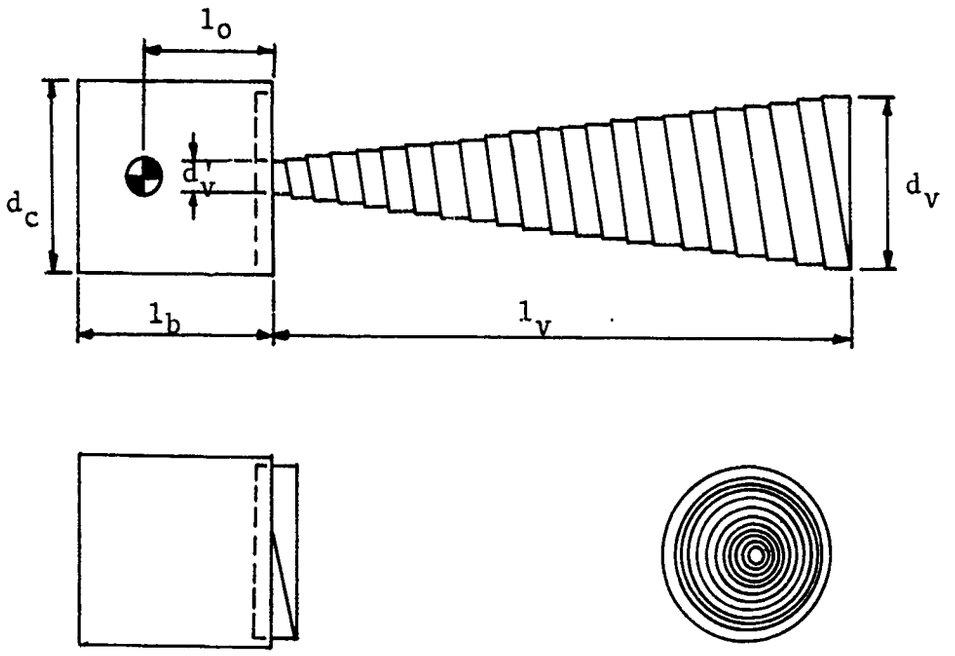

Figure 1. Volute Stabilizer

The basic dimensionless ratios are: l_V/d_V, d_V/d_C, l_V/l_b. The volute is considered to be fully characterized once l_V, d_V, d_V, k_V (spring constant) w_V, and I_V have been specified.

For a given volute planform area and forebody, the volute stabilizer is considered effective if C_{m_α} and $(C_{m_q} + C_{m_{\dot{\alpha}}})$ are negative. The determination of these derivatives as functions of forebody-volute dimensions represents the core of the following sections. Once they are determined, the frequency equation can be solved for the characteristic roots of the model. The determination of C_{m_α} and $(C_{m_q} + C_{m_{\dot{\alpha}}})$ is complicated by the fact that volutes are flexible and are forced to operate in the slipstream of the forebody.

Because of the success of linear aerodynamics in predicting stability and motion for small coordinate perturbations of many shapes, the first approach to the problem was to force the nonlinear rigid body equation of motion Equation (5) into a linear form. The basic moment summation required:

$$\text{Constrained cg, pitch only, } I\ddot{\theta} = q_\infty dSC_m \tag{1}$$

$$\text{Where, } \quad C_m = C_{trim} + C_{m_\alpha}\,\theta + (C_{m_q} + C_{m_{\dot{\alpha}}})\dot{\theta}\frac{d}{2V_\infty} \tag{2}$$

C_m was derived in terms of dimensions of the forebody-volute combination and the normal force coefficient C_n. Nonlinear effects were later entered into the basic form by allowing for forebody interference and $\sin^2\theta$ variation of the normal force. The results of the rigid body analysis are divided into three parts corresponding to three approaches used to solve for C_m. The first is a linear theory, the second includes forebody interference, the third involves interference and $\sin^2\theta$ variation of C_m.

Because the volute tail is flexible, serious questions arise as to whether a volute equipped cylinder will be dynamically stable. Insuring dynamic stability is a much more profound problem than the simpler problem of guaranteeing static stability, criteria for which are set up in the rigid body analysis. Dynamic stability may be inferred from the following set of equations which describe an elastic model having only two degrees of angular freedom:

$$\text{cg moment, } a_{11}\ddot{\theta}+a_{12}\ddot{\delta}+a_{13}\dot{\theta}+a_{14}\theta+a_{15}\dot{\delta}+a_{16}\delta = 0 \tag{3}$$

$$\text{Hinge moment, } a_{21}\ddot{\theta}+a_{22}\ddot{\delta}+a_{23}\theta+a_{24}\dot{\theta}+a_{25}\dot{\delta}+a_{26}\delta = 0 \tag{4}$$

The entire flexible section deals with these equations. It is shown in the analysis that, depending upon the mass and inertia of the elastic tail, characteristic equations (frequency equations) may be second or fourth order polynominals. Stability is investigated by invoking the Routh-Hurwitz criteria.

Basic supporting data was obtained from both static and dynamic test stands. Dynamic tests utilize two special stands developed under the contract: The first utilized a piezoelectric-equipped model to drive an oscillograph which gave acceleration versus time data and the second forced the test model into resonance (forced oscillation testing). Free-flight data was also gathered and reduced.

SECTION II

RIGID BODY ANALYSIS

The rigid model equation of motion is obtained from a simple moment summation about the forebody-volute mass center. As shown in Appendix I, the relative velocity is the vector sum of the free stream velocity and a rotary velocity field which coexists with any rotational motion. The entire stabilizing aerodynamic moment is equated to the normal pressure force multiplied by an effective moment arm. The resulting equation is nonlinear:

$$\begin{aligned} -I\ddot{\theta} = {} & \tfrac{1}{2}\rho C_{n_{t_o}} h_t \left(V_\infty\theta + \hat{x}_t\dot{\theta}\right)\left|V_\infty\theta + \hat{x}_t\dot{\theta}\right| S_t \\ & - \tfrac{1}{2}\rho C_{n_{b_o}} h_b \left(V_\infty\theta - \hat{x}_b\dot{\theta}\right)\left|V_\infty\theta - \hat{x}_b\dot{\theta}\right| S_b \end{aligned} \tag{5}$$

It is shown that Equation (5) reduces to a linear form if a number of assumptions are made. When this is done:

$$\begin{aligned} -I\ddot{\theta} = qd_cS\Bigg(& \left[\frac{2C_{n_{b_o}}\hat{x}_t h_t S_t}{d_c{}^2 S}\right]\left[1 + \frac{C_{n_{b_o}}\hat{x}_b h_b S_b}{C_{n_{t_o}}\hat{x}_t h_t S_t}\right]\hat{\theta}\frac{d_c}{2V_\infty}\dot{\theta} \\ & + \left[\frac{C_{n_{t_o}} h_t S_t}{d_c S}\right]\left[1 - \frac{C_{n_{b_o}} x_b S_b}{C_{n_{t_o}} x_t S_t}\right]\hat{\theta}\theta\Bigg) \end{aligned} \tag{6}$$

Linear aerodynamics require:

$$I\ddot{\theta} = qd_cS\left[\left(C_{m_q} + C_{m_{\dot{\alpha}}}\right)\frac{d_c}{2V_\infty}\dot{\theta} + C_{m_\alpha}\theta\right] \tag{7}$$

where,

$$C_{m_{trim}} = 0$$

By identification of the common terms in Equations (6) and (7):

$$C_{m_\alpha} = -\left[\frac{C_{n_{t_o}} h_t S_t}{d_c S}\right]\left[1 - \frac{C_{n_{b_o}} h_b S_b}{C_{n_{t_o}} h_t S_t}\right]\hat{\theta} \tag{8}$$

$$(C_{m_q} + C_{m_{\dot{\alpha}}}) = -\left[\frac{2C_{n_{t_o}} \hat{x}_t h_t S_t}{d_c^2 S}\right]\left[1 + \frac{C_{n_{b_o}} \hat{x}_b h_b S_b}{C_{n_{t_o}} \hat{x}_t h_t S_t}\right]\hat{\theta} \tag{9}$$

The stability derivatives are in terms of $\hat{\theta}$, $C_{n_{v_o}}$, $C_{n_{b_o}}$, $C_{n_{t_o}} = f(C_{n_{v_o}}, C_{n_{b_o}})$ and the geometrical properties of the cylinder and volute. $\hat{\theta}$ is a proportionality constant which is evaluated from 0 to 40 degrees. It is defined to be:

$$\hat{\theta} = 1.432 \int_0^{40°} \sin\theta d\theta = 0.335 \tag{10}$$

$C_{n_{v_o}}$ and $C_{n_{b_o}}$ are the normal force coefficients of the volute and cylinder evaluated at 90°. $C_{n_{v_o}}$ decreases with an increase of the ratio l_v/d_v (Appendix II). The final results have justified approximating $C_{n_{v_o}}$ and $C_{n_{b_o}}$ with average values for volutes having l_v/d_v ranging from 0.78 to 4.79 and cylinders with l_c/d_c ranging from 1.48 to 2.36. $C_{n_{v_o}}$ and $C_{n_{b_o}}$ will be replaced by:

$$C_{n_{v_o}} = 1.100 \tag{11}$$

$$C_{n_{b_o}} = 0.833 \tag{12}$$

The remaining variables are:

S_b - Planform area of the cylinder forward of the cg.

S_b' - Planform area of the cylinder aft of the cg.

S_v - Planform area of the volute.

S_t - Equal to $S_b' + S_v$.

S - Equal to the total model planform area.

C_{nb_o} - Equal to 0.833.

C_{nt_o} - The effective normal force coefficient of the tail area aft of the cg.

$$C_{nt_o} = 0.267 \frac{S_v}{S_t} + 0.833.$$

h_b - Moment arm used to account for the adverse moment set up by that portion of the cylinder forward of the cg. $h_b = \frac{1}{2}x_{cg}$

h_t - Moment arm used to account for the stabilizing moment set up by that portion of the cylinder aft of the cg plus the entire volute. h_t is:

$$\frac{h_t}{l_o} = \frac{1}{C_{nt_o}}\left[\left(1 - \frac{S_v}{S_t}\right)0.416 + 1.1\frac{S_v}{S_t}\left[1 + 1.33\left(\frac{S_v/S_t}{1-S_v/S_t}\right)\right]\right] \quad (13)$$

$\hat{x}_b$ - Linear dimension used to proportion the magnitude of the rotary velocity field. It accounts for the field forward of the cylinder cg giving an approximate value to $(x)\theta$. $\hat{x}_b = \frac{1}{2}x_{cg}$.

$\hat{x}_t$ Serves the same purpose as $\hat{x}_b$. $\hat{x}_t$ is complicated because it deals with two different planforms, i.e., rectangular and triangular. For all analytical work to follow it is defined to be $\hat{x}_t = \frac{1}{2}l_v + \frac{2}{3}l_v$.

The evaluation of h_t and $\hat{x}_t$ is actually more involved than is indicated by their simple definitions. The assigned values followed a detailed analysis into the behavior of each with variations of l_v/l_o, θ, and $\dot{\theta}$. $\hat{x}_t$ was found by evaluating the following integral equated to an average expression:

$$\iint_S (V_\infty\theta + x\dot{\theta})^2 dS = (V_\infty\theta + \hat{x}_t\dot{\theta})^2 S \quad (14)$$

The integration gives a complex equation revealing the dependence of $\hat{x}_t$ on θ and $\dot{\theta}$. The primary interest, however, is in the range over which $\hat{x}_t$ can vary. This was found by setting first $\theta = 0$ and then $\dot{\theta} = 0$ in the results of Equation (14). When this was done $\hat{x}_t$ was found to obey:

$$\hat{x}_t = \frac{l_o^2 + l_v l_o + \frac{2}{3}l_v^2}{2l_o + l_v}, \quad \dot{\theta} = 0 \quad (15)$$

$$\hat{x}_t^2 = \frac{\frac{2}{3}l_o^3 + \frac{4}{3}l_o l_v^2 + l_v l_o^2 + \frac{1}{2}l_v^3}{2l_o + l_v}, \quad \theta = 0 \tag{16}$$

These equations represent the upper and lower bounds over which $\hat{x}_t$ may vary. The value for $\hat{x}_t$, defined earlier and used in deriving other expressions, differs from Equation (15) or Equation (16) (i.e., $\frac{1}{2}l_o + \frac{2}{3}l_v$). $\hat{x}_t$, as defined, represents a compromise between the two extremes at $\theta = 0$ and $\dot{\theta} = 0$. However, it may be necessary for some design problems to have a better value for $\hat{x}_t$, and for this purpose Equation (15) and Equation (16) are graphed (Figures 2 and 3). For a given l_o, $\hat{x}_t$ may be found as the volute changes length (l_v varies) for $\theta = 0$ and $\dot{\theta} = 0$. The same argument shows that h_t likewise varies with θ and $\dot{\theta}$. The integral to be evaluated does not follow directly because of the way in which h_t was originally derived. h_t was found after a moment summation about the model cg which took into account only the normal force acting aft of the cg. The equation is:

$$C_{n_{t_o}} h_t S_t = C_{n_{b_o}} h_b' S_b' + C_{n_{v_o}} h_t' S_v \tag{17}$$

Evidently h_t is a function of two other moment arms h_b' and h_t'. h_b offers no problem since to good accuracy it can be approximated by $\frac{1}{2}l_o$.

$$h_b' = \tfrac{1}{2}l_o \tag{18}$$

However, h_t' does vary with θ and $\dot{\theta}$. h_t varies with h_t' and h_t is found by integrating over the volute. The result is:

$$h_t' = \frac{1}{\hat{x}_t^2 V_t}\left(\frac{3}{5}l_o l_v^2 + \frac{1}{2}l_o^2 l_v + l_o^3 + \frac{2}{5}l_v^3\right), \theta = 0 \tag{19}$$

$$h_t' = l_o + \tfrac{2}{3}l_v, \dot{\theta} = 0 \tag{20}$$

h_t' is graphed (Figure 4) for values of l_o and l_v. Equation (17) with the corrected h_t' should be used in lieu of Equation (13), if the extra accuracy is deemed necessary. Some guidelines on this point will be provided in the discussion on stability.

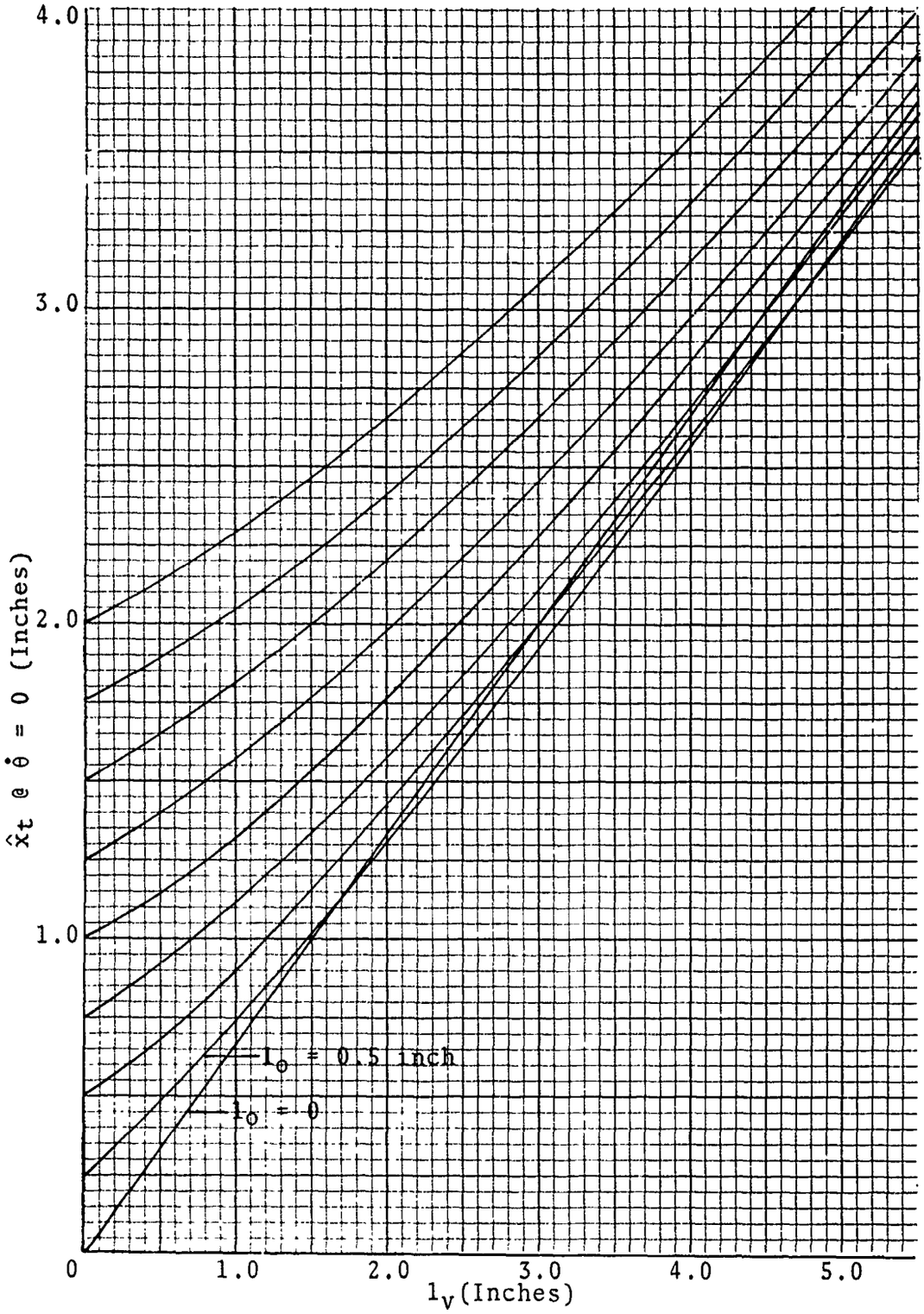

Figure 2. l_V Versus $\hat{x}_t$ @ $\dot{\theta} = 0$

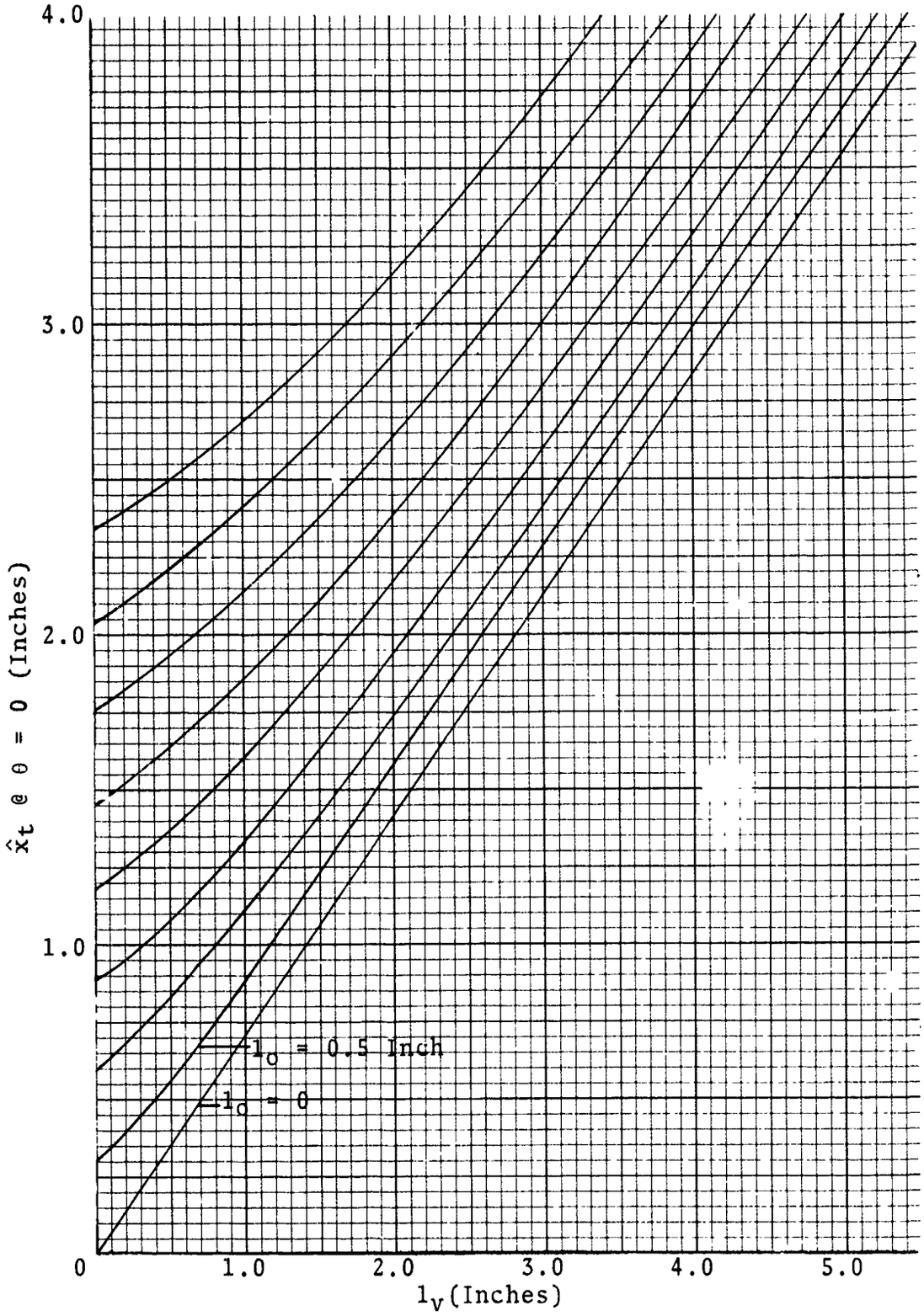

Figure 3. l_V Versus $\hat{x}_t$ @ θ = 0

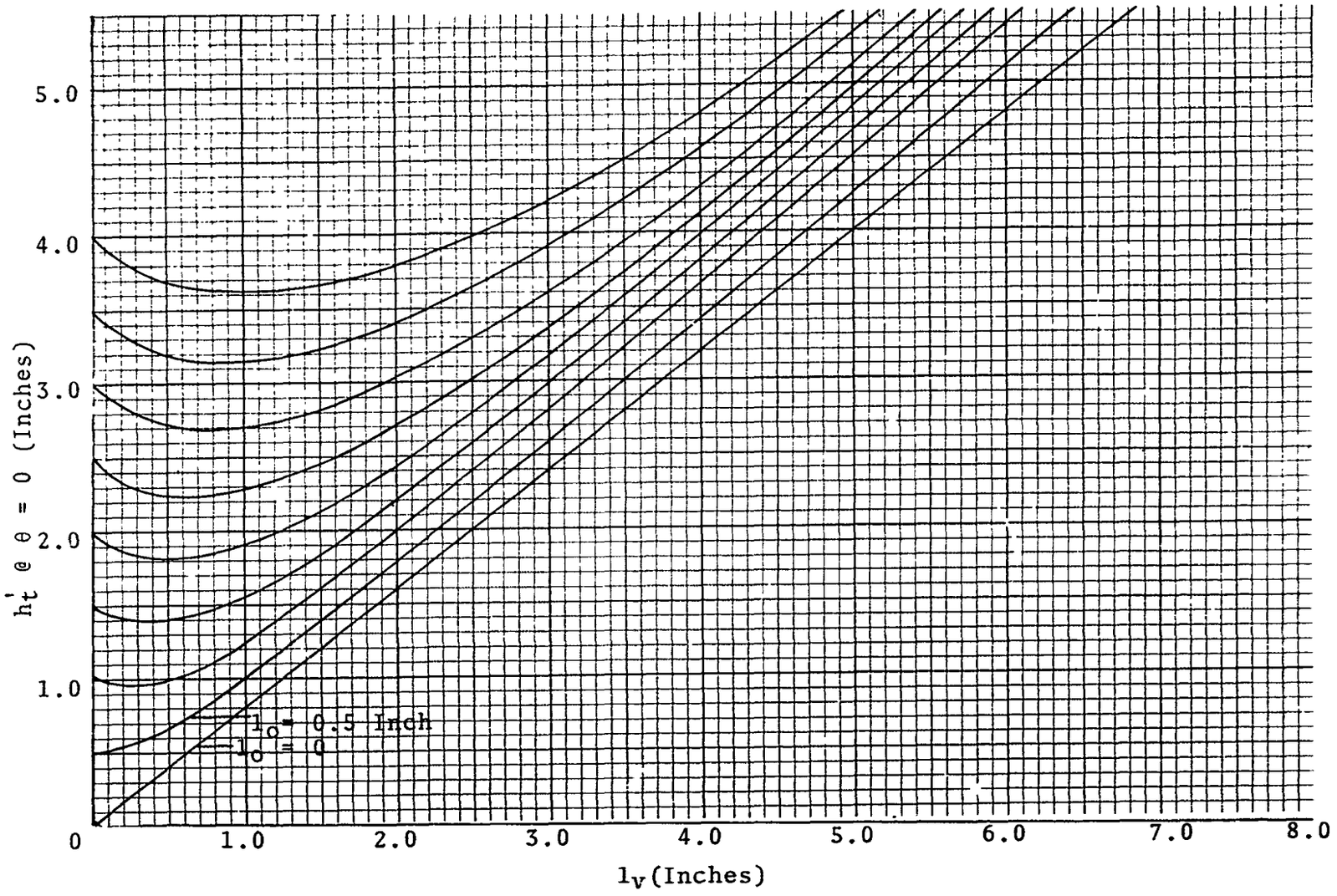

Figure 4. l_v Versus h_t' @ θ = 0

Although it is not used in the linear expressions presented thus far, $\hat{x}_{v_t}$ serves a similar purpose in future work as $\hat{x}_t$. It deals with the rotary velocity field over the volute only (whereas $\hat{x}_t$ dealt with the whole tail portion aft of the cg). Values for $\hat{x}_{v_t}$ are (Figure 5):

$$\hat{x}^2_{v_t} = l_o^2 + \tfrac{4}{3} l_o l_v + l_v^2/2 \,, \dot{\theta} = 0 \qquad (21)$$

$$\hat{x}_{v_t} = l_o + \tfrac{2}{3} l_v \,, \dot{\theta} = 0 \qquad (22)$$

Detailed work concerning derivation of all the above forms for $\hat{x}_t$, h_t, and $\hat{x}_{v_t}$ are included in Appendix I.

The first thing that is apparent from Equation (8) is a convenient stability criteria. For static stability it is required that $C_{m_\alpha} < 0$ or that:

$$1 - \frac{C_{n_{b_o}} h_b S_b}{C_{n_{t_o}} h_t S_t} > 0 \qquad (23)$$

which is,

$$h_t S_t > \frac{.833}{C_{n_{t_o}}} h_b S_b$$

The largest that $0.833/C_{n_{t_o}}$ can be is 1.00 so that Equation (22) may also be written as:

$$h_t S_t > h_b S_b \qquad (24)$$

It is required by Equation (24) that the tail planform area and h_t multiplied must be greater than the analogous parameters $h_b S_b$ measured forward of the cg. For many combinations of cylinders and volutes it is possible to have $S_t = S_b$ in which case stability depends upon:

$$h_t > h_b \qquad (25)$$

The importance of h_t is evident. Normally the cylinder-volute combination will be designed to insure that $S_t > S_b$, otherwise stability may be compromised by variations of h_t with θ or $\dot{\theta}$ Large S_t relieves the necessity of having precise values for h_t. For determining the angular frequency and damping exponent ($e^{-\beta t}$), use the best obtainable value for h_t. Equation (17) will serve this purpose.

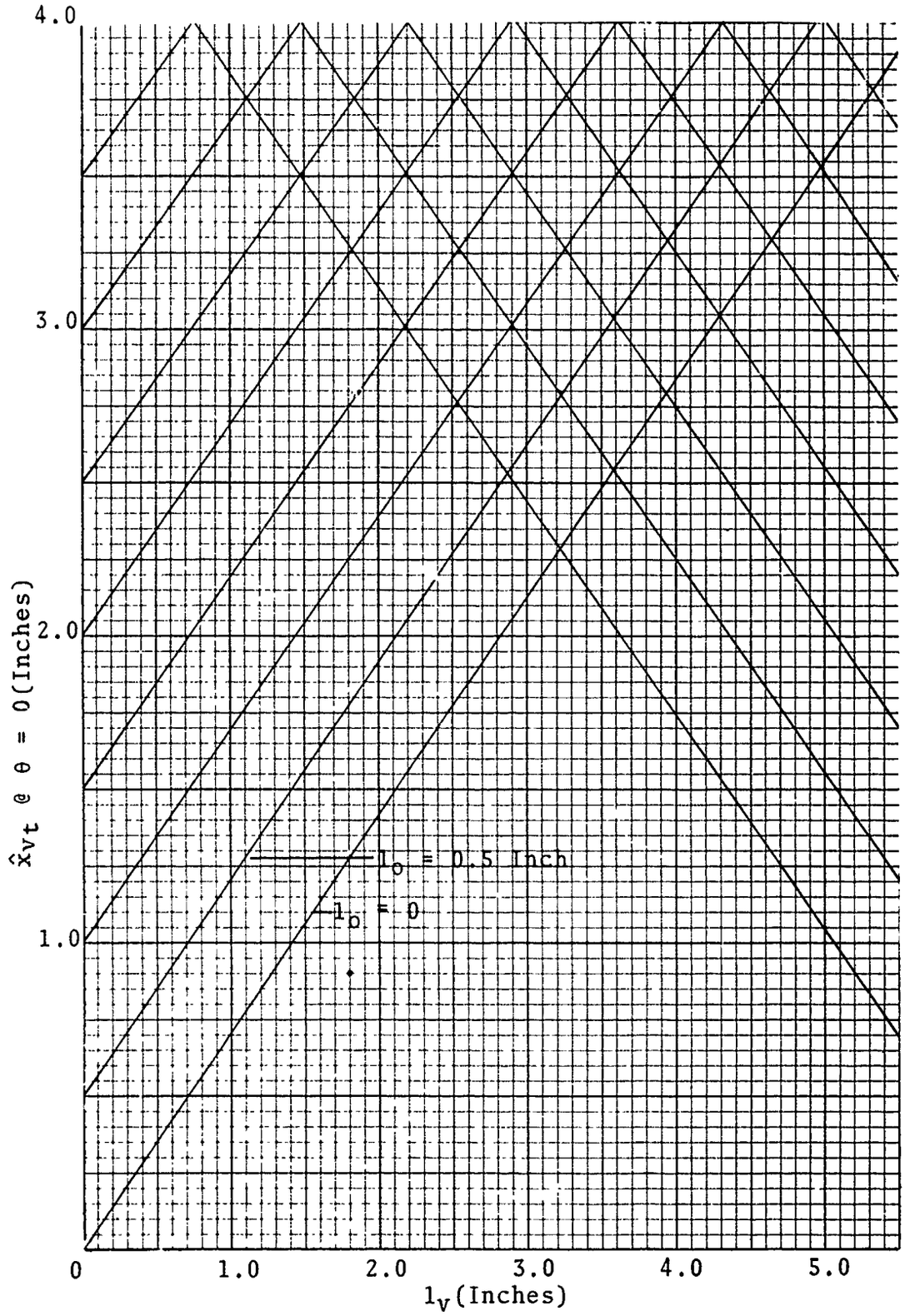

Figure 5. l_v Versus $\hat{x}_{vt}$ @ θ = 0

Because of the method in which Equation (5) was derived, it is impossible for the rigid model to be dynamically unstable. This is evident from Equation (9) which can never be greater than zero. The equation is nearly the same as Equation (8) but includes $\hat{x}_t$ and $\hat{x}_b$. Accurate determination of these variables will be manifest in β, the damping constant. Dynamic or static stability of the rigid model does not depend on $\hat{x}_t$. As will be shown, this is not the case for the flexible model.

Before discussing the numerical results of the preceding analysis, two additional methods for computing C_{m_α} and subsequently C_{m_S} will be presented. Although the linear analysis gives good answers, it fails to indicate the interference effects from the forebody and nonlinear variation of the normal force coefficient. Returning to Equation (5), it is evident that there exists a θ^2 term which approximates $\sin^2\theta$. Writing the exact expression for the static pitching moment:

$$C_{m_S} = \frac{C_{m_\alpha}}{\hat{\theta}} |\sin\theta| \sin\theta, -90 < \theta < 90 \qquad (26)$$

The pitching moment coefficient in linear form follows directly from Equation (26) and is again:

$$C_{m_S} = \left(\frac{C_{m_\alpha}}{\hat{\theta}}\right)\hat{\theta}\theta \qquad (27)$$

The pitching moment slope coefficient is:

$$\frac{\partial C_{m_S}}{\partial \theta} = C_{m_\alpha} \quad \text{i.e., [Equation (8)]} \qquad (28)$$

To account for forebody blanking of the volute, the area S_V must be altered to reflect a reduction in the tail surface which can act to stabilize the forebody. The detailed derivation is in Appendix I. The results are:

$$\frac{S_V'}{\bar{d}^2} = \frac{l_V}{2\bar{d}} - \frac{\bar{d}}{8l}\left[\frac{1}{\left[\tan\theta + \frac{\bar{d}}{2l_V}\right]^2}\right] \qquad (29)$$

$$\bar{d} = d_V - d_V'$$

Figure 6 and Equation (29) represent the variation of $S_V = S_V'$ with θ, if the area planform is a triangle ($d_V' = 0$). Most volutes end at the forebody blunted and, therefore, the planform is trapezoidal. This can be accounted for by adding to Equation (29):

$$S_V'' = d_V'(l_V - x') \tag{30}$$

where

$$x' = \frac{1}{2}\tan\theta + \frac{(d_c - d_V')}{\dfrac{d_V - d_V'}{2l_V}} \tag{31}$$

the total area acting in the wind stream for a given angle of attack is:

$$S_V = S_V' + S_V'' \tag{32}$$

S_V' will be good enough to approximate the area if d_V' is not large or not more than about 1/10 d_V. S_V' is plotted for different values of $l_V/\bar{d}$. To use the new area in the C_{m_α} expression, an alternate form of Equation (8) has to be used and is:

$$C_{m_\alpha} = -\frac{C_{n_{V_o}} h_t' S_V}{d_c S}\left[1 + \frac{C_{n_{b_o}} h_b' S_b'}{C_{n_{V_o}} h_t' S_V} - \frac{C_{n_{b_o}} h_b S_b}{C_{n_{V_o}} h_t' S_V}\right]\hat{\theta} \tag{33}$$

This expression for C_{m_α} is not new since Equation (8) was derived directly from it. The new variables are:

- $\hat{x}_b'$ - Serves the same purpose as did $\hat{x}_b$ but is equal to $\frac{1}{2}l_o$.
- h_b' - Moment arm for the normal force which acts on that portion of the cylinder aft of the cg. $h_b = \frac{1}{2}l_o$
- S_b' - Planform area of the cylinder aft of the model cg.

The new stability criteria is:

$$(C_{n_{V_o}} h_t' S_V + C_{n_{b_o}} h_b' S_b') > C_{n_{b_o}} h_b S_b \tag{34}$$

at $\theta \cong 0$ the criteria reduces to:

$$C_{n_{b_o}} h_b' S_b' > C_{n_{b_o}} h_b S_b \tag{35}$$

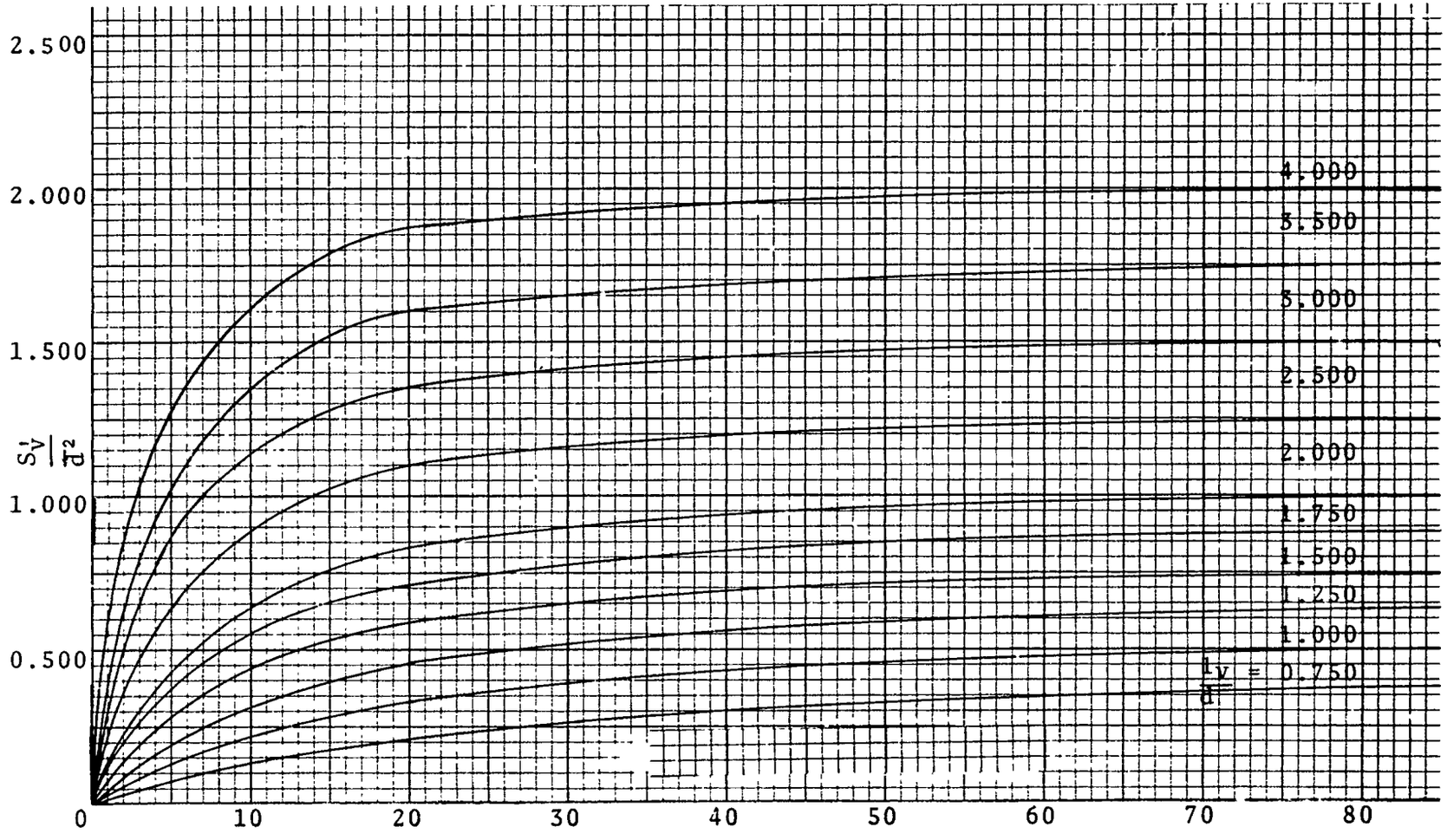

Figure 6. θ Versus $S_V'/\bar{d}^2$

If Equation (35) is not satisfied, the inference is that the model will tend towards static instability. This is partially correct. As soon as the model tends to overturn, Equation (34) becomes valid. Since S_V rises rapidly with θ, increase in θ immediately tends to restore stable motion. The length of the volute is the critical parameter since short volutes do not have the sharp rise in S_V' exhibited by long volutes (Figure 6). With the new values for S_V, C_{m_S} becomes a function of θ. With this new form for C_{m_S}, two nonlinear theories are evident. Equation (26) is the most nonlinear form investigated. Replacing $\sin^2\theta$ with $\theta\sin\theta$ yields a third form which is a compromise between the linear theory and the $\sin^2\theta$ theory. The three theories are listed below for reference and hereafter referred to as Methods 1, 2, and 3.

$$C_{m_S} = \frac{C_{m_\alpha}}{\hat{\theta}}\,\hat{\theta}\theta \qquad \text{Method 1} \tag{36}$$

$$C_{m_S} = \left(\frac{C_{m_\alpha}}{\hat{\theta}}\right)_b \hat{\theta}\sin\theta \qquad \text{Method 2} \tag{37}$$

$$C_{m_S} = \left(\frac{C_{m_\alpha}}{\hat{\theta}}\right)_b \sin^2\theta \qquad \text{Method 3} \tag{38}$$

Equation (37) represents the pitching moment coefficient for large angles (40°) and is an extension of the linear form with tail blanking. Equation (38) is included because it accounts for the $\sin^2\theta$ variation of the normal force coefficient C_n which has been substantiated for cylindrical shapes for large angles. The pitching moment slope coefficient follows directly by differentiating Equations (36),(37) and (38) giving:

$$\partial C_{m_S}/\partial\theta = C_{m_\alpha} \tag{39}$$

$$\partial C_{m_S}/\partial\theta = \frac{\partial}{\partial\theta}(C_{m_\alpha})_b\sin\theta + (C_{m_\alpha})_b\cos\theta \tag{40}$$

$$\partial C_{m_S}/\partial\theta = \frac{\partial}{\partial\theta}\left(\frac{C_{m_\alpha}}{\hat{\theta}}\right)_b \sin^2\theta + 2\left(\frac{C_{m_\alpha}}{\hat{\theta}}\right)_b \sin\theta\cos\theta \tag{41}$$

Equations (37), (38), and (41) contain the expression $(C_{m_\alpha}/\hat{\theta})_b$, which is the nonlinear variation of C_{m_α} with θ discussed earlier.

C_{m_s} was determined experimentally for five models. Referring to the experimental section of the report (Appendix II), the Models were 3+1, 3+2, 3+3, 3+5, and 3+6. The cylinder had $l_c/d_c = 2.36$ and the volute l_v/d_v ranged from 0.78 to 4.79. C_{m_s} for each model along with the theoretical values obtained from Equations (36),(37) and (38) were plotted for each model (Figures 7 through 11). 3+1 shows the widest variation from the predicted values of the three methods. This is so because the greatest portion of volute 1 ($l_v/d_v = 0.79$) is forced to act in the turbulent slipstream curling around the cylinder edge. For this reason, short volutes should be avoided. C_{m_α} varies from a positive to negative number throughout the first portion of the plot straightening out at around 30 to 40 degrees. The erratic behavior is undesirable and should be expected if l_v/d_v is less than about 1.5 for $d_v \simeq d_c$. The tendency toward a more stable and predictable C_{m_s} with increasing l_v/d_v is evident from the plots. The linear theory is surprisingly accurate and can be used to predict C_{m_s}. Method 2 is more accurate and tends to follow the contour of the data points for the larger volutes (Figure 11). Method 3 tends to follow the data points for θ larger than 30 degrees up to the maximum range plotted. For initial design it is recommended that the linear theory be used. If the volute l_v/d_v is less than one, only wind tunnel testing should be trusted.

Equations (40) and (41) are plotted (Figures 12 and 13). The C_{m_s} data was not smoothed and numerical differentiation was unproductive because the somewhat erratic behavior of most data points was greatly exaggerated. However, the C_{m_s} plots for the five models show that the general slope of the data points comes very close to the slopes of Methods 1 and 2. The closest agreement corresponds to the middle volute (3). The tabulated values for C_{m_α}/radian are as follows:

TABLE I. C_{m_α}/Rad

Model	Method 1	*Method 2	*Method 3	Data
3+1	-0.126	-0.087	-0.065	-0.053
3+2	-0.196	-0.155	-0.114	-0.181
3+3	-0.275	-0.225	-0.172	-0.212
3+5	-0.470	-0.399	-0.301	-0.447
3+6	-0.927	-0.816	-0.626	-0.762

$$*C_{m_\alpha} = \frac{1}{40^\circ}\int_0^{40^\circ} \frac{\partial C_{m_s}}{\partial \theta} d\theta$$

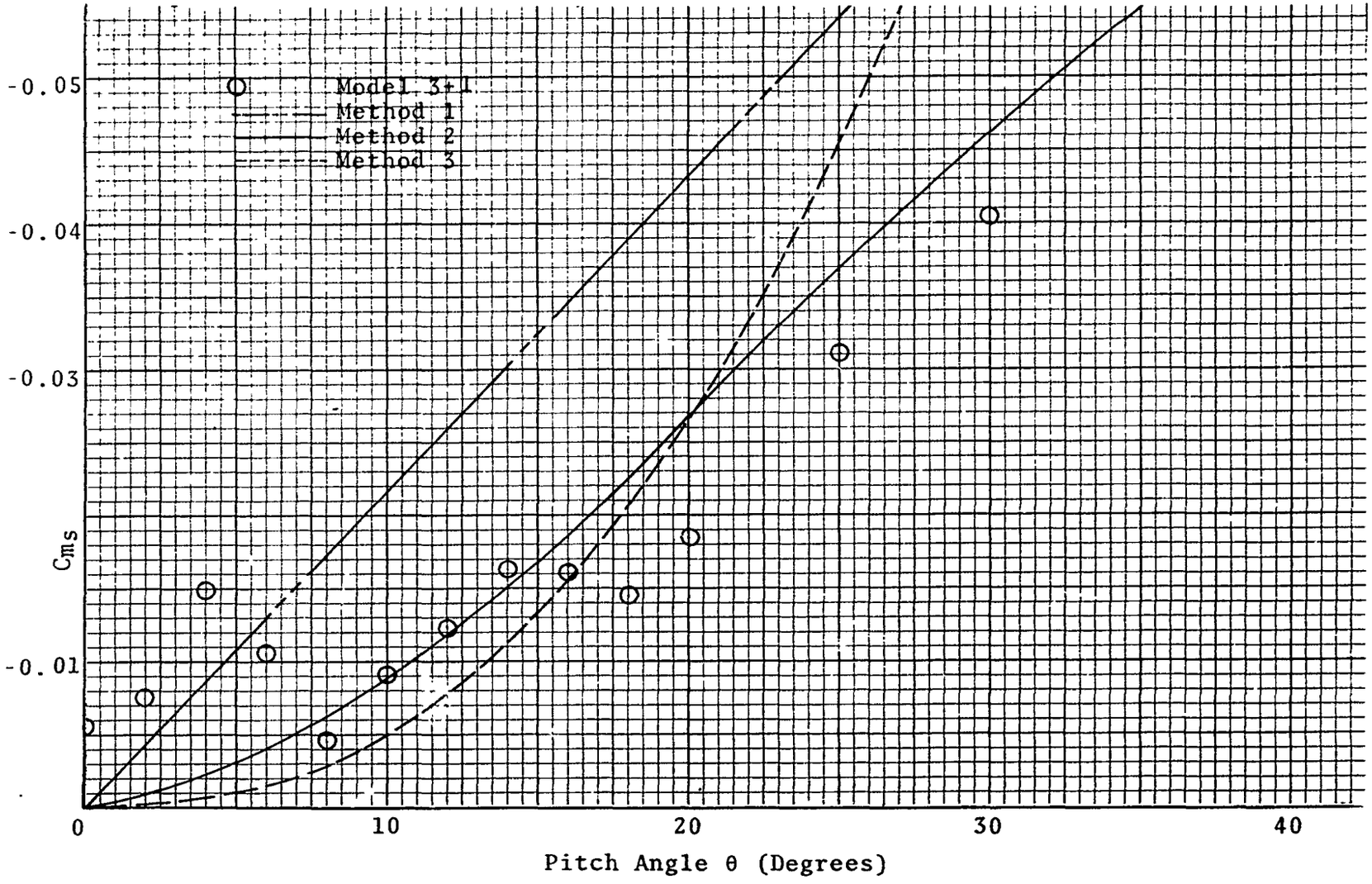

Figure 7. θ Versus C_{m_s} Model 3+1

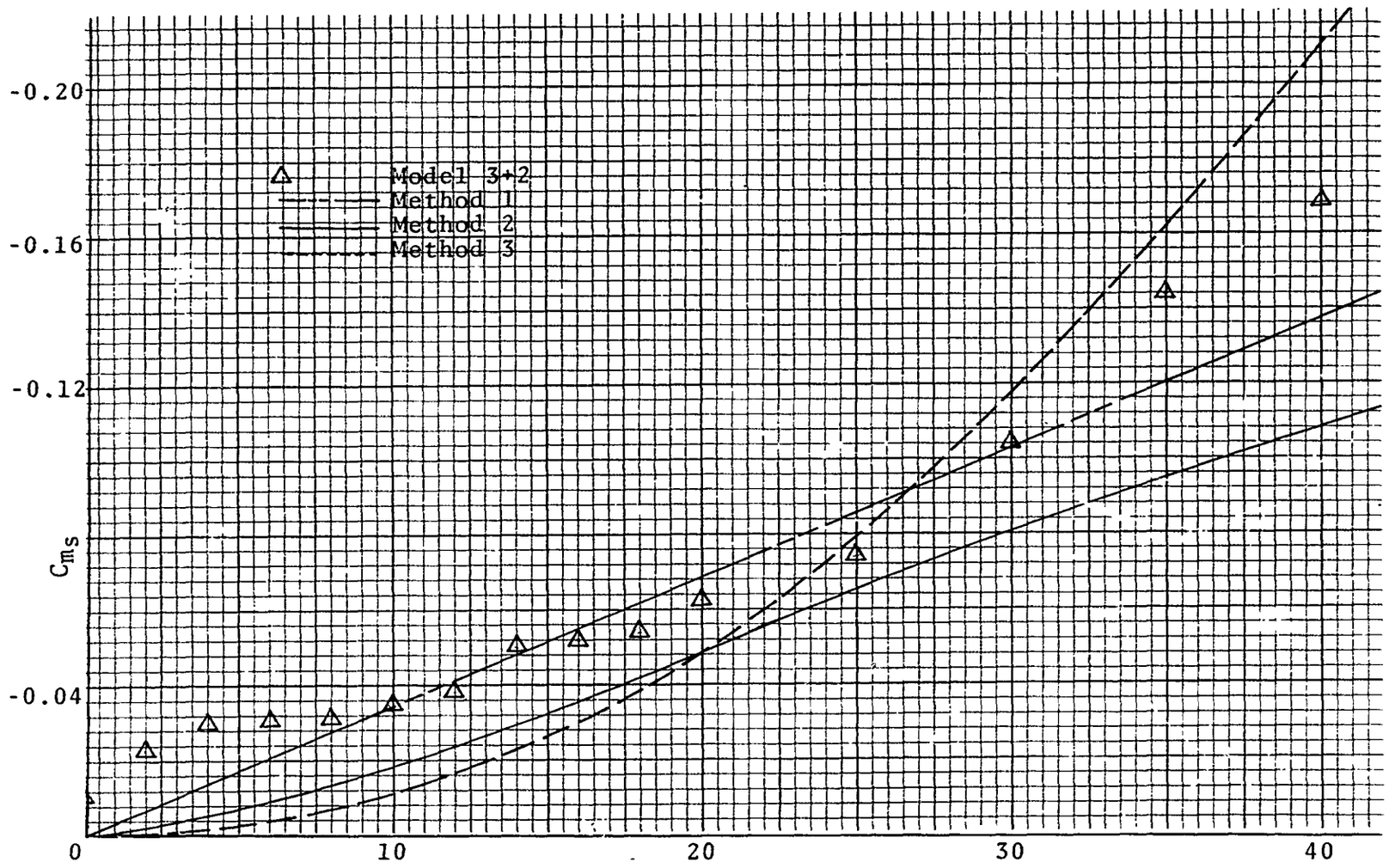

Figure 8. θ Versus C_{m_s} Model 3+2

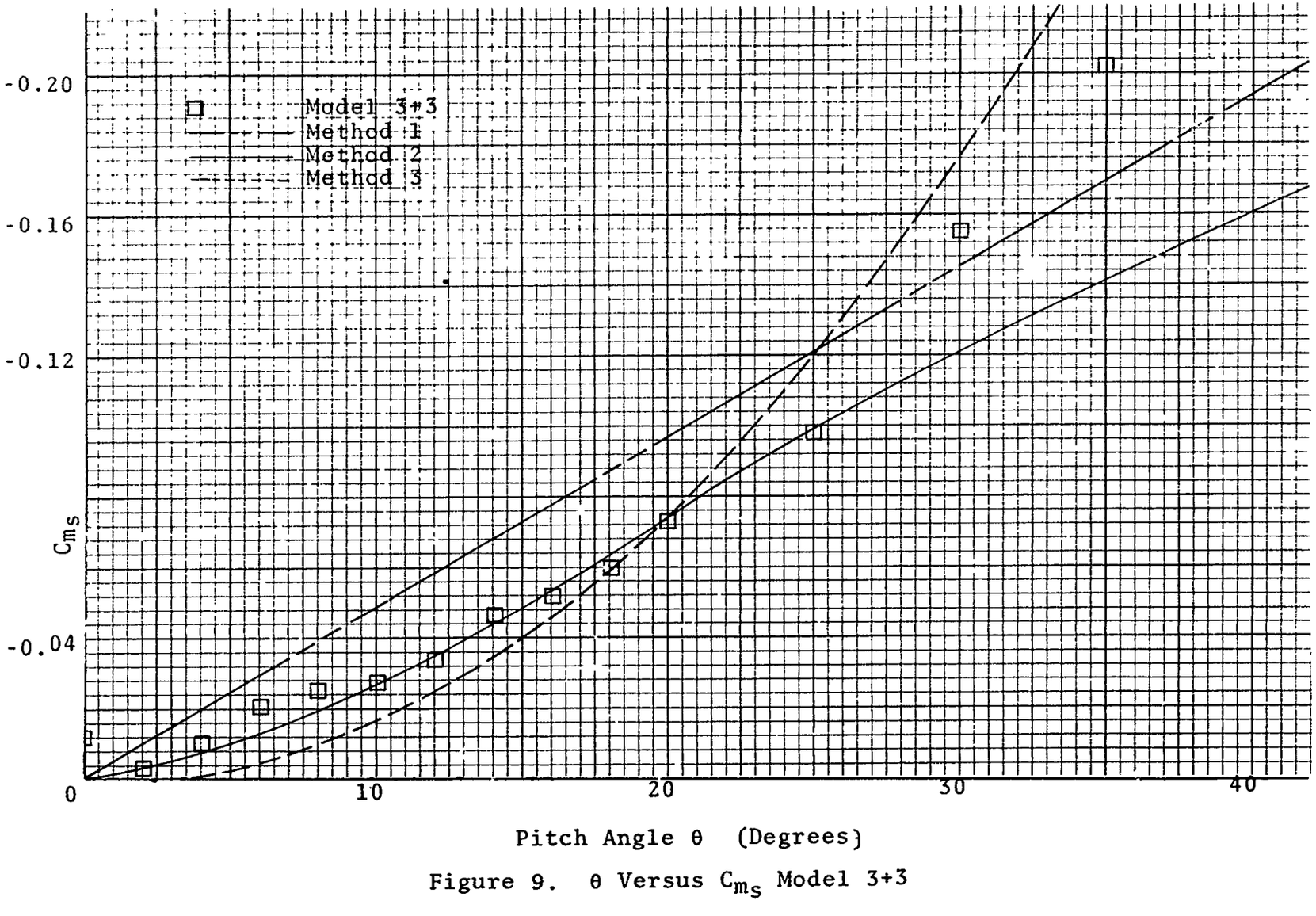

Figure 9. θ Versus C_{m_s} Model 3+3

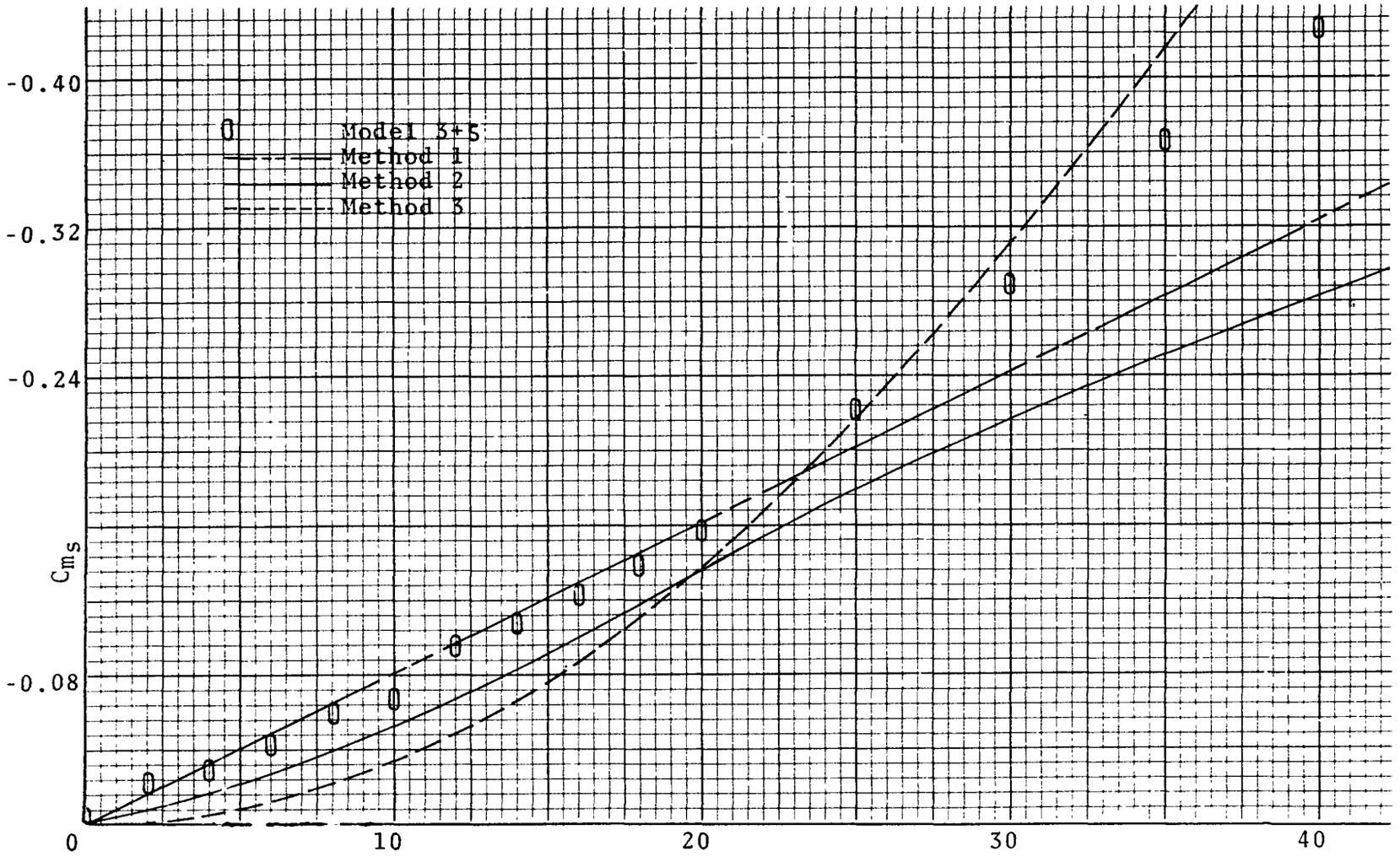

Figure 10. θ Versus C_{m_s} Model 3+5

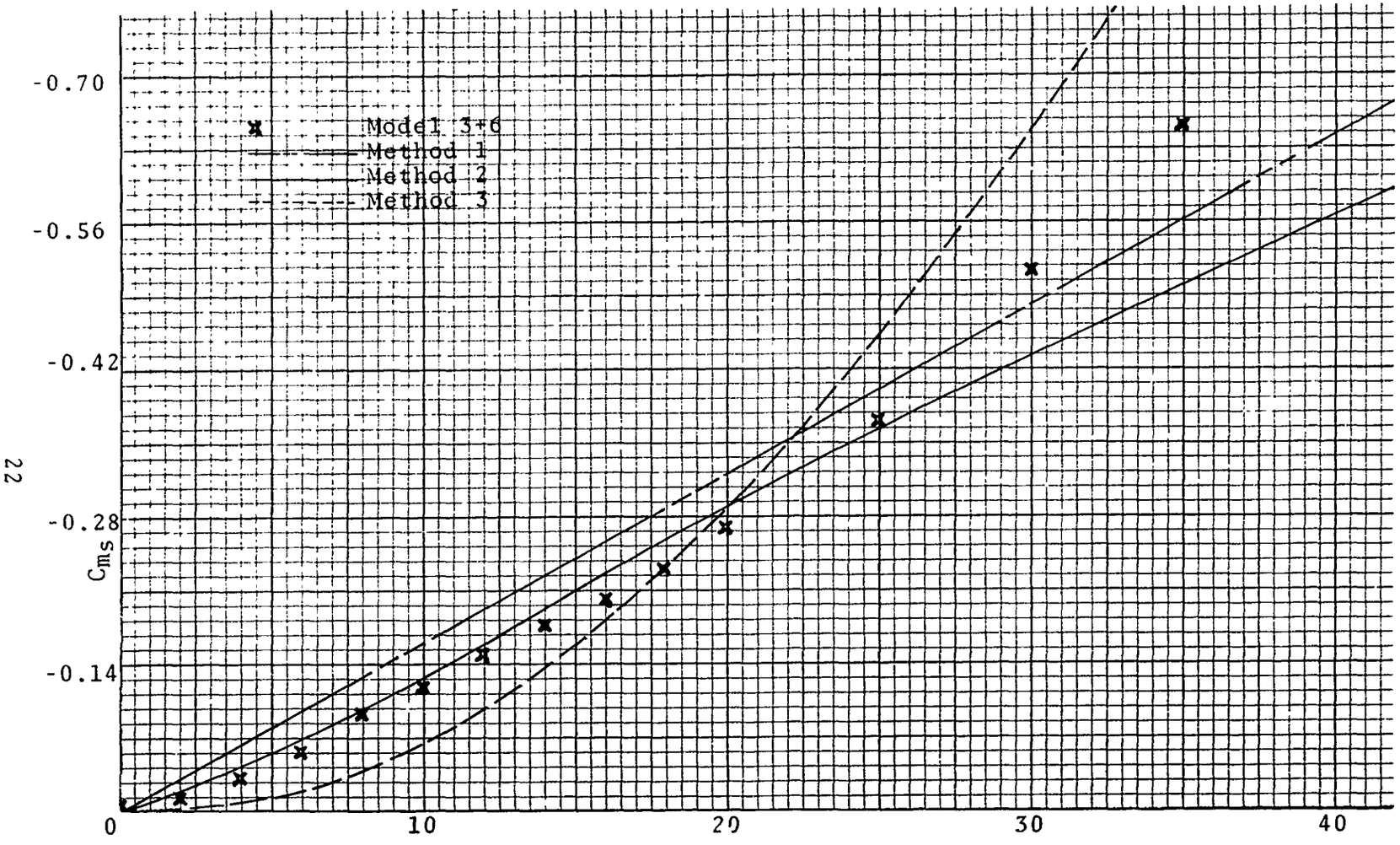

Figure 11. θ Versus C_{m_s} Model 3+6

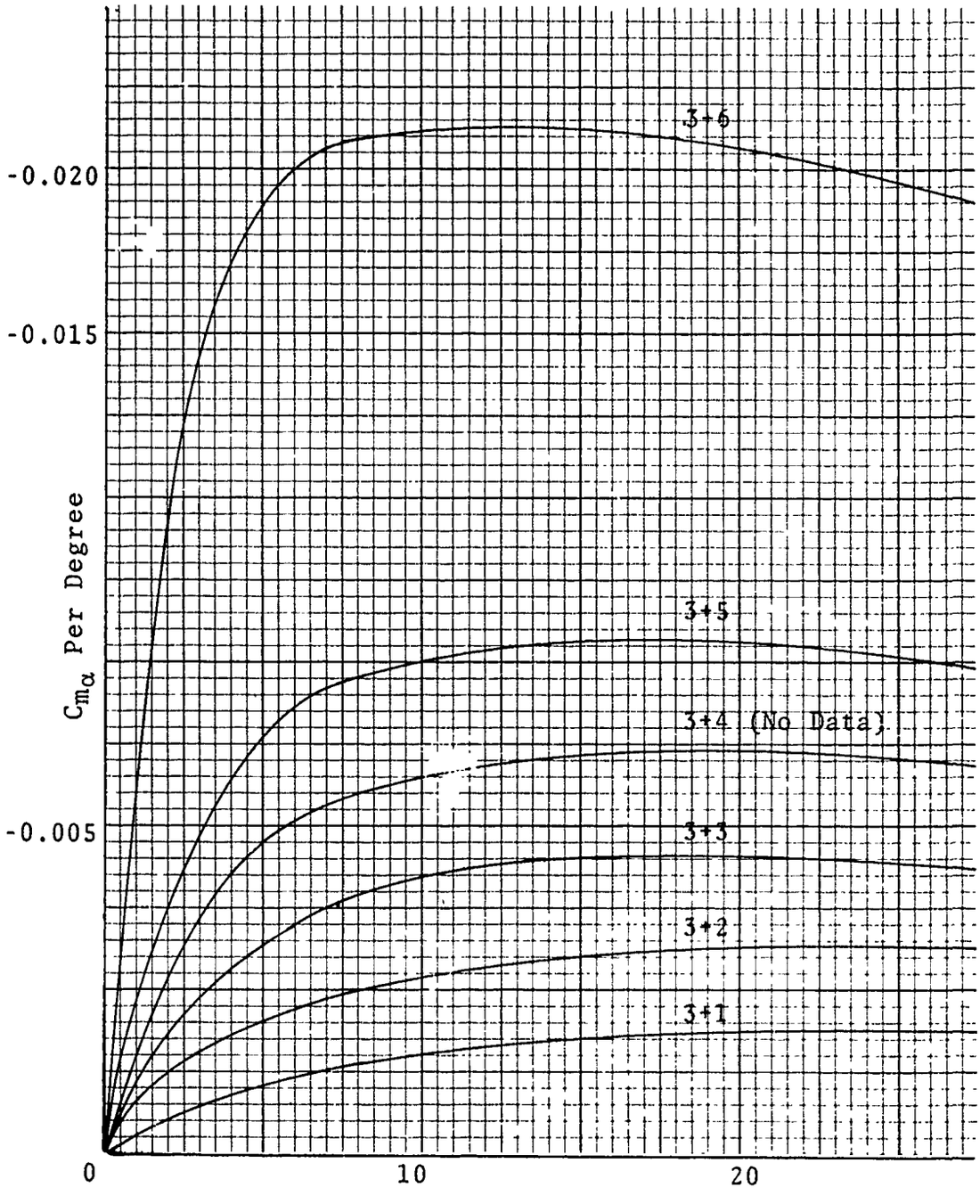

Figure 12. θ Versus C_{m_α} Method 2

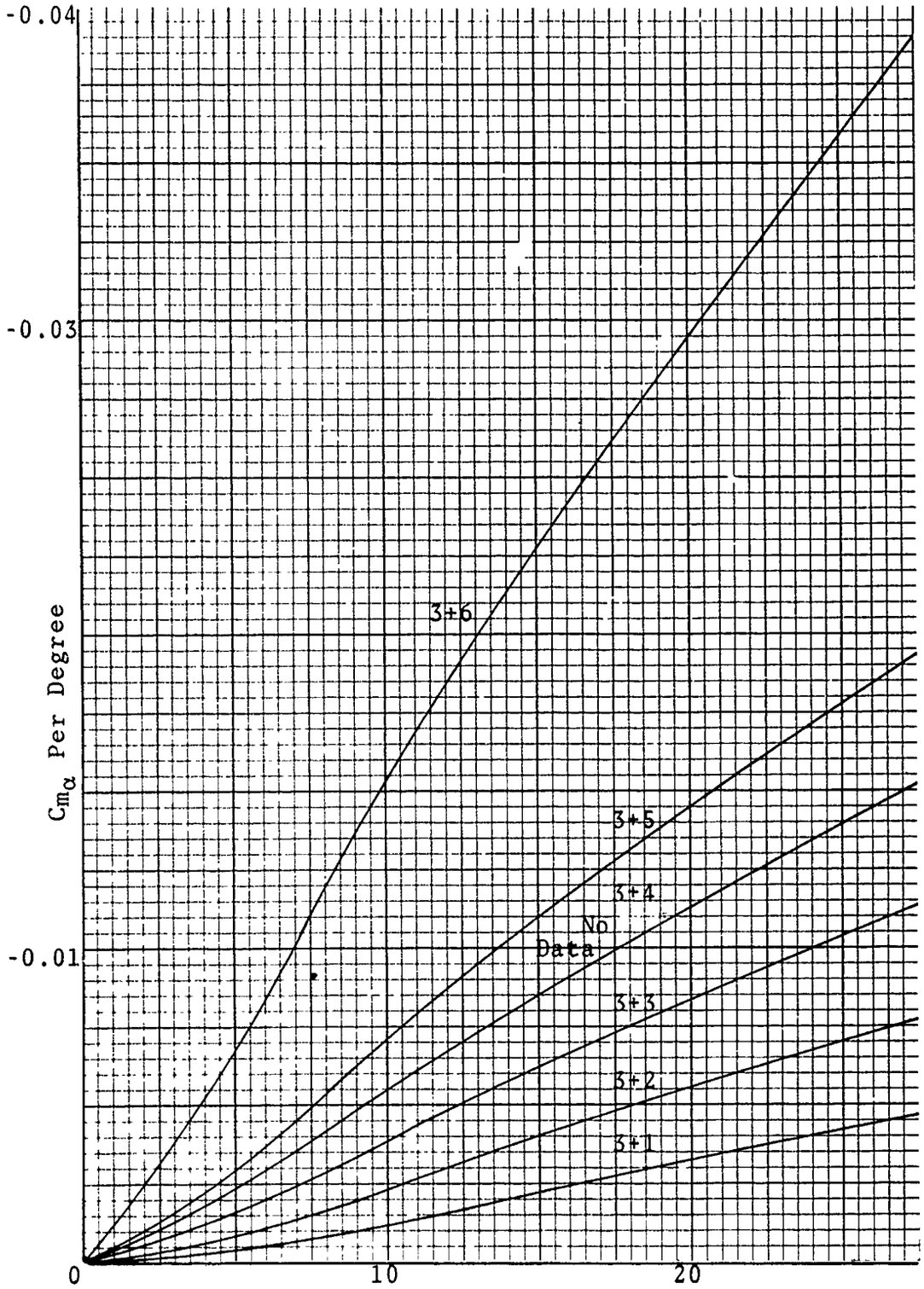

Figure 13. θ Versus C_{m_α} Method 3

Since the linear form is accurate enough for at least preliminary design work, it is possible to generate design curves for C_{m_α} that are simple to use. The design curves provided depend upon S_v/S_t, $C_{n_{t_o}}$, h_t, $h_b S_b C_{n_{b_o}}$ (designated B). Recalling the definition of $C_{n_{t_o}}$, it is possible to plot $C_{n_{t_o}}$ as a function of S_v/S_t. This is the first design curve. Once the forebody cylinder has been selected and volute stabilizer chosen, $C_{n_{t_o}}$ can be found. (h_t/l_o) is tabulated as a function of S_v/S_t and $C_{n_{t_o}}$ in Table II. Since S_v/S_t and $C_{n_{t_o}}$ are now known, (h_t/l_o) is fixed and found by interpolating between the two variables S_v/S_t and $C_{n_{t_o}}$. l_o is known since the cg location was fixed for the selected forebody-volute combination. The tail parameters, $C_{n_{t_o}} h_t S_t$ are all known and the forebody parameters, $B = C_{n_{b_o}} h_b S_b$, are fixed once the cg location is specified. Equation (8) can now be solved for C_{m_α}, remembering that $\bar{\theta} = 0.335$. Equation (8) can be used directly or the master design curve for C_{m_α} may be used.

(1) Example: Find C_{m_α} for Model 3+6, using Equation (8)

Selection of volute 6 and specifying the cylinder pitch axis fixes the following variables:

$S_b = 2.357 in^2$; $h_b = 0.81$ in; $C_{n_{b_o}} = 0.833$;

$l_o = 1.820$ in; $S_t = 9.027$ in^2; $S_v = 6.370$ in

For $S_v/S_t = 0.7056$, Figure 14 gives $C_{n_{t_o}} = 1.020$

The h_t/l_o matrix shows:

S_v/S_t \ $C_{n_{t_o}}$	1.008	1.033
0.700	3.264	3.185
0.800	5.619	5.483

Interpolating between the values gives $h_t/l_o = 3.226$

Thus, $h_t = (1.820)(3.226) = 5.871$ in

The parameter $B = h_b C_{n_{b_o}} S_b = (0.81)(0.833)(2.357) = 1.590$ in^3. The quantity dS in Equation (8) is $(1.47)(11.392) = 16.746$ in^3

Inserting the numbers into Equation (8):

$$C_{m_\alpha} = -\frac{0.335}{16.746}((1.02)(5.871)(9.027) - 1.59) = -1.049/rad$$

* TABLE II. h_t/l_o MATRIX

$S_v S_t$	$\cot_{t_o}$ 0.833	0.858	0.873	0.908	0.933	0.958	0.983	1.008	1.033	1.058	1.083	1.100
0.000	0.500	0.486	0.473	0.459	0.447	0.435	0.424	0.414	0.404	0.394	0.385	0.379
0.100	0.601	0.584	0.568	0.552	0.537	0.523	0.509	0.497	0.485	0.473	0.462	0.455
0.200	0.752	0.731	0.710	0.690	0.672	0.655	0.638	0.622	0.607	0.593	0.579	0.569
0.300	0.972	0.945	0.918	0.892	0.868	0.846	0.824	0.804	0.784	0.766	0.748	0.736
0.400	0.296	1.259	1.224	1.189	1.158	1.128	1.098	1.071	1.045	1.021	0.997	0.982
0.500	1.791	1.741	1.692	1.644	1.601	1.559	1.518	1.481	1.445	1.411	1.378	1.357
0.600	2.576	2.503	2.433	2.364	2.302	2.242	2.184	2.129	2.078	2.029	1.982	1.952
0.700	3.948	3.836	3.728	3.622	3.527	3.435	3.346	3.264	3.185	3.109	3.037	2.991
0.800	6.796	6.604	6.417	6.236	6.072	5.913	5.760	5.619	5.483	5.353	5.228	5.149
0.900	15.494	15.055	14.629	14.216	13.842	13.480	13.132	12.809	12.499	12.202	11.918	11.737

* Valid only for triangular volute planform

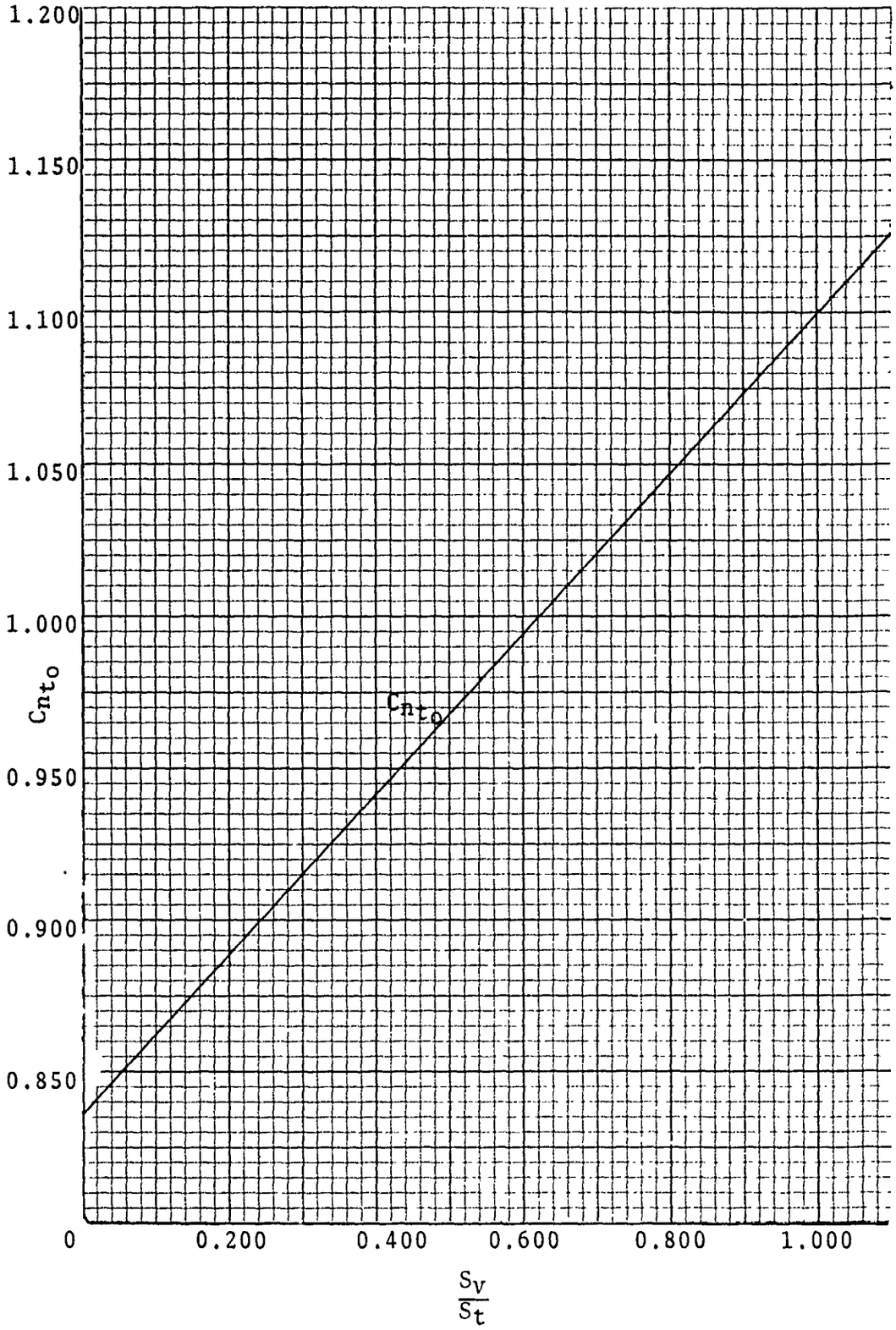

Figure 14. S_v/S_t Versus C_{nt_o}

Comparing this answer with Method 1 in Table I shows a difference of about 8 percent. This follows from the earlier comments regarding approximating the volute planform area as a triangle, which was done in the above calculation. Table II requires the planform to be triangular since this approximation was used to get h_t/l_o in the nondimensional form. Method 1 answers in Table I were obtained from Equation (33), using the more correct trapezoidal planform area. Note for volute 6, $d_V/d_V' = 4.56$.

(2) Example: Find C_{m_α} for Model 3+3, using the design chart (Figure 15).

The following variables are fixed once again:

$S_b = 2.357$ in^2; $h_b = 0.810$ in; $C_{nb_o} = 0.833$;
$l_o = 1.820$ in; $S_t = 4.946$ in^2 ; $S_V = 2.289$ in^2,
$S_V/S_t = 0.463$
For $S_V/S_t = 0.460$, Figure 14 gives $C_{nt_o} = 0.955$
Find h_t using Table II: $h_t = 2.523$ in.
The quantity B is the same as example 1, $B = 1.590$ in^3
The quantity dS is: $1.46(7.679) = 11.21$ in^3
Find the vertical axis labeled S_t and enter there with the value for $S_t = 4.946$. Project a line and find the line labeled $h_t = 2.520$. Project a line perpendicular to the first through the point defined by the first projection and the line $h_t = 2.520$. In a similar manner, locate the line labeled 0.958 and project a third line perpendicular to the second, and through the point defined by $C_{nt_o} = 0.958$ and the second projection. Proceed around the graph, choosing next the proper line for B = 1.59 and, finally, the value for dS = 11.21. Read the answer on the left side of the vertical axis labeled $C_{m_\alpha}/\hat{\theta}$

$$C_{m_\alpha}/\hat{\theta} = 0.900$$

$$C_{m_\alpha} \cong 0.302/\text{rad}$$

Comparison with the answer in Table I indicates that the preceding method is high. This is due to the volute planform area used in developing the graph being triangular. One advantage to using Figure 15 instead of Equation (8) or Equation (33) is that it enables the designer to pick different values for the many variables and see directly what the effect upon C_{m_α} will be. For accurate determination of C_{m_α}, use Equation (33).

(3) Example: Use Equation (33) to find C_{m_α} for model illustrated below and investigate its stability.

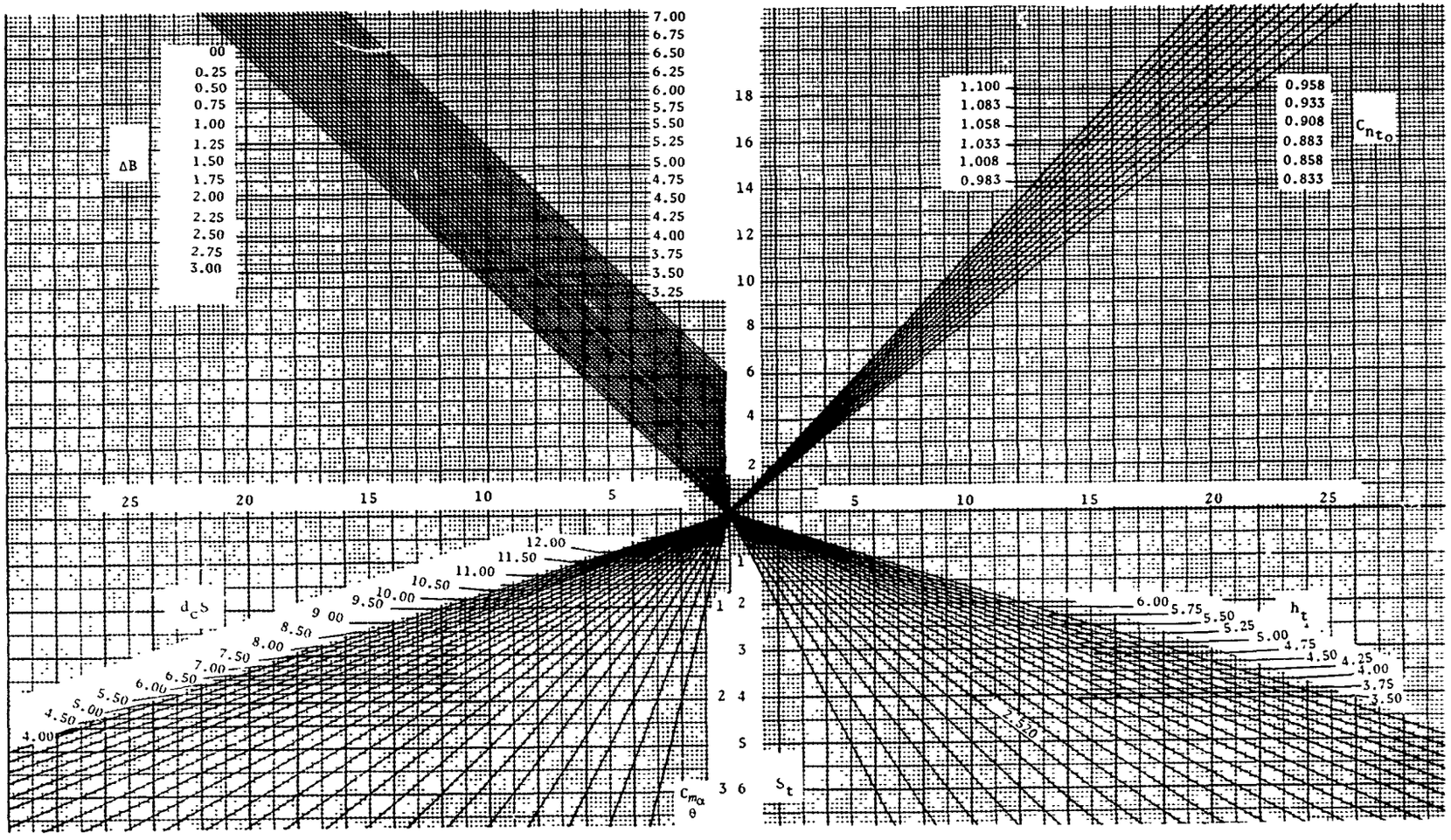

Figure 15. Master Design Curve

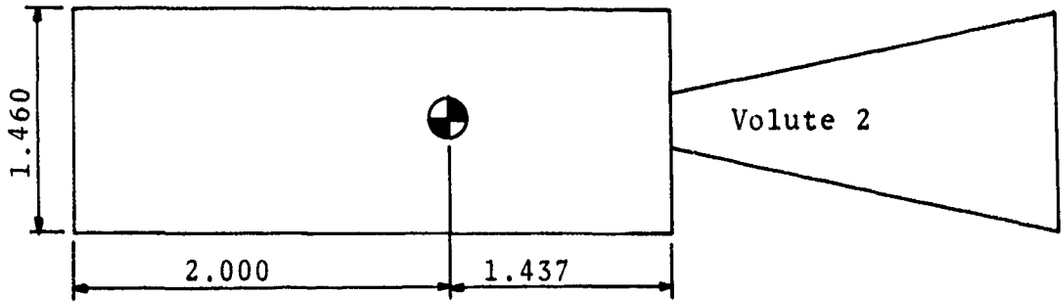

S_b= 2.920 in^2; S_b' = 2.0981 in^2; S_V = 1.568 in^2;
h_b= 1.000 in; h_b' = 0.719 in; h_t' = 2.652 in
which gives:

$$C_{m_\alpha} = -\frac{(3.3811)(0.335)}{9.62} = -0.118/\text{rad}$$

The low value indicates possible static stability problems. Invoking the stability criteria of Equation (23):

$$h_t S_t > 0.883/C_{n_{t_o}}[h_b S_b]$$

$$6.64 > 2.560$$

According to Equation (23) the forebody-volute combination is stable; however, the volute is masked by the forebody for the early portion of the oscillatory motion. If the volute l_V/d_V is less than 1.5, the nonlinear stability criteria stated by Equation (34) should be used. In the above case, l_V/d_V = 1.313. Equation (35) for the above model gives:

$$C_{n_{b_o}} h_b' S_b' > C_{n_{b_o}} h_b S_b, \quad @\ \theta \simeq 0$$

and $\quad C_{n_{b_o}} h_b' S_b' = 1.508 < 2.920 = C_{n_{b_o}} h_b S_b$

This is equivalent to stating that the model will have a trim angle different from zero. The model will tend to pitch over until the volute balances the adverse moment set up by the large area in front of the cg. That the model will stabilize out at all was verified by satisfying Equation (23). The trim angle can be found by using the following procedure:

$$C_{n_{V_o}} h_t' S_V = C_{n_{b_o}} h_b S_b - C_{n_{b_o}} h_b' S_b', \text{ i.e., } C_m = 0$$

therefore, $$S_V \cong S_V' = 0.4046$$

$$S_V' \cong 1.268 - 0.1839 \frac{1}{(\tan\theta + 0.3808)^2}$$

$$\tan\theta = 0.0806$$

$$\theta = 4°36$$

To find the trim coefficient note,

$$C_m = C_{m_{trim}} + C_{m_\alpha}\theta = 0$$

$$C_{m_{trim}} = -C_{m_\alpha}\theta = 0.118(0.0785) = 0.0093/\text{rad}$$

The model was placed in the wind tunnel operating at a dynamic pressure of about 60 lbs/ft^2. It immediately diverged and oscillated weakly about the 10 degree radial with an amplitude ranging over approximately 8 to 15 degrees. A trim angle will always be present if Equation (35) is not satisfied. If this is the case, the magnitude of the angle will depend upon the length of the volute, small angles corresponding to long volutes, and large angles corresponding to short volutes. Since it may be necessary that the forebody being stabilized not exceeds a certain trim angle after transients have damped out, it is important to check any design for steady state trim angle. In this respect, the above model was analyzed for different trim angles by varying the volute length. The results are shown in Figure 16.

Another point which demands consideration deals with the ratio d_V/d_C assumed to be close to one. Actual fabrication of the forebody does not allow this since the volute must fit inside the cylinder rim (Figure 1) and thus $d_V < d_C$. This is undesirable for stability since the volute must now be rotated a small angle before being impinged upon by the free stream. This is distinct from the previous cases which assume that the volute starts producing a stabilizing moment for the slightest pitch of the forebody. The diameter of the cylinder and volute must be kept as close as possible, consistent with structural requirements. Test work on a special rigid model shows that

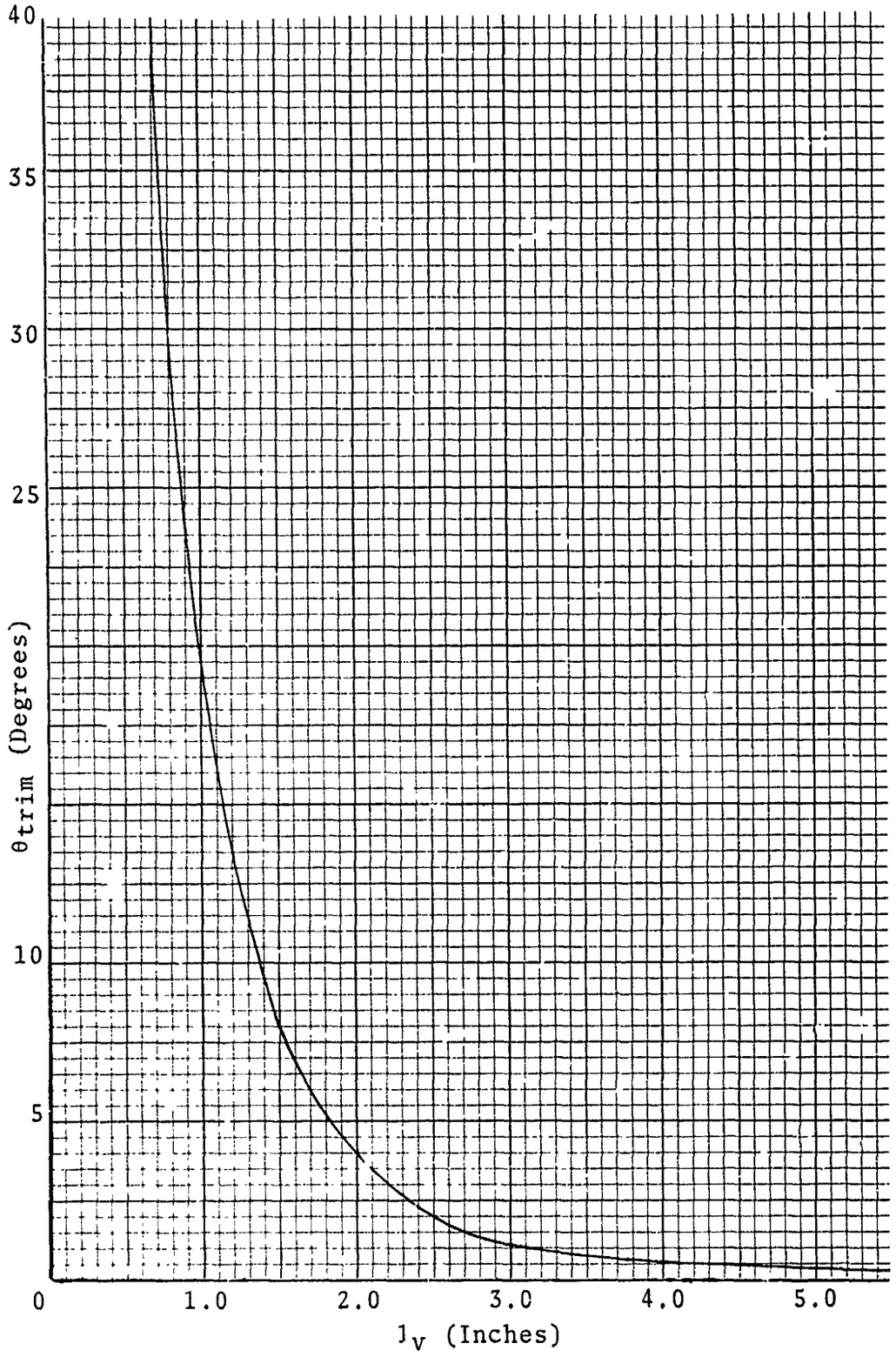

Figure 16. l_V Versus θ_{trim}

limit cycle vibrations persist for $d_V < 0.8d_C$. For larger variations, wind tunnel testing should be conducted to determine if the limit cycles are severe enough to warrant redesign of the volute. If the diameters cannot be brought close enough, a longer volute can be used. This has the effect of forcing the volute into the windstream early, reducing the amplitude of the limit cycle.

The damping derivative can be obtained from Equation (9) or Equation (42)

$$-(C_{m_q} + C_{m_{\dot{\alpha}}}) = \frac{C_{n_{v_o}} h_t' S_v \hat{x}_{v_t}}{d^2 S}\left[1 + \frac{C_{n_{b_o}} S_b h_b \hat{x}_b}{C_{n_{v_o}} S_v h_t' \hat{x}_{v_t}} + \frac{C_{n_{b_o}} S_b' h_b' \hat{x}_b'}{C_{n_{v_o}} S_v h_t' \hat{x}_{v_t}}\right] \hat{\theta} \qquad (42)$$

Using Equation (9) is less accurate because of the triangular area assumption but is quicker to use than Equation (42). Equation (9) yields the following results:

TABLE III. $(C_{m_q} + C_{m_{\dot{\alpha}}})$/Rad(THEORETICAL)

1+1	-0.298	2+1	-0.348	3+1	-0.506
1+2	-0.590	2+2	-0.654	3+2	-0.844
1+3	-1.124	2+3	-1.210	3+3	-1.434
1+4	-1.666	2+4	-1.688	3+4	-1.950
1+5	-2.476	2+5	-2.528	3+5	-2.862
1+6	-8.048	2+6	-8.234	3+6	-8.714

These are plotted in Figure 17.

As indicated by Table III, the damping coefficient increases dramatically with increase in tail length. Some experimental data was obtained for Models 3+1, 3+2, 3+3, 3+5 and 3+6.

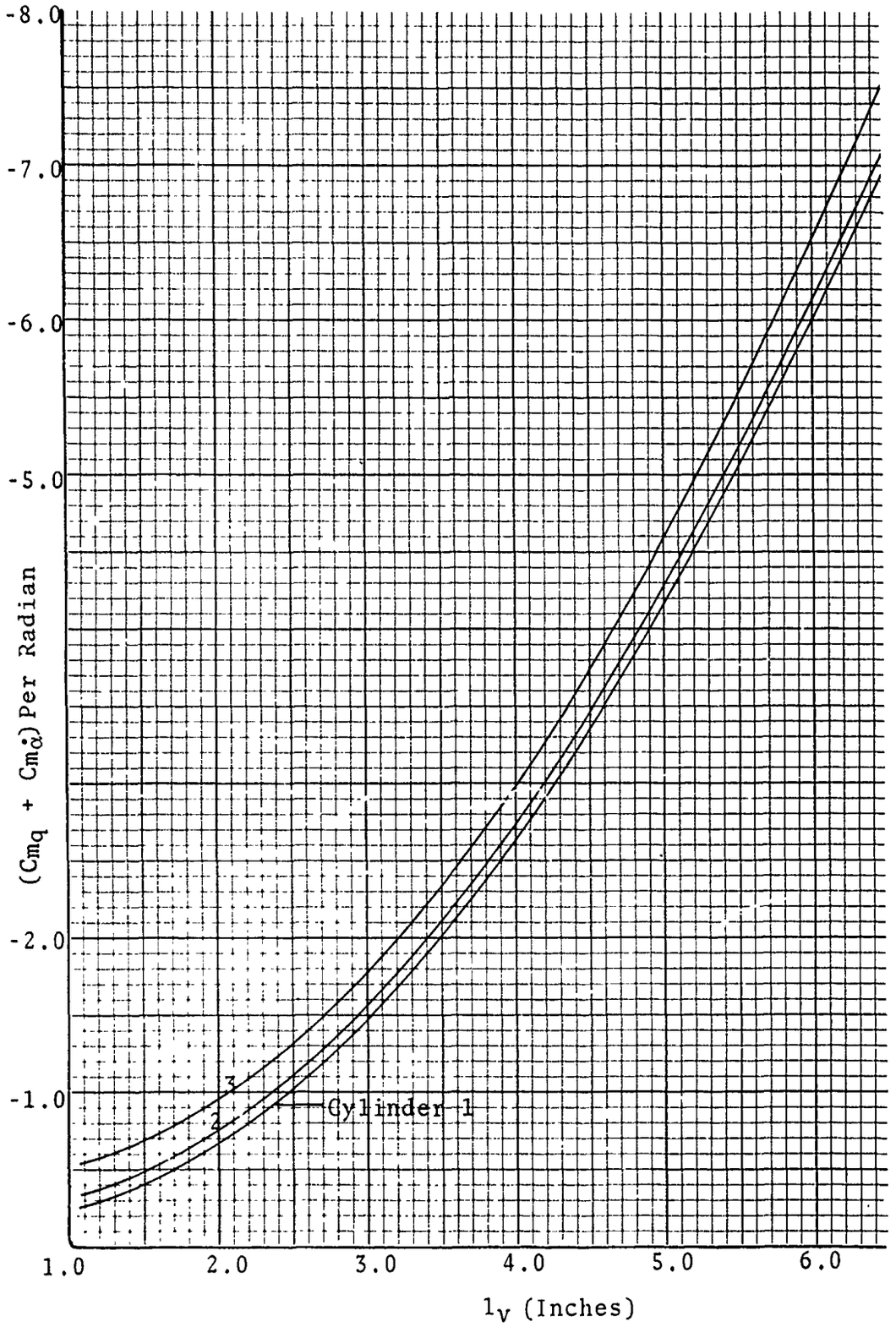

Figure 17. l_v Versus $(C_{m_q} + C_{m_{\dot{\alpha}}})$

TABLE IV $(C_{m_q} + C_{m_{\dot{\alpha}}})$/Rad.

Model	l_v/d_v	$(C_{m_q} + C_{m_{\dot{\alpha}}})$	$(C_{m_q} + C_{m_{\dot{\alpha}}})$ data
3+1	0.785	-0.506	-2.370
3+2	0.313	-0.844	-2.518
3+3	1.871	-1.434	-3.410
3+5	2.637	-2.863	-4.876
3+6	4.795	-8.714	-10.215

The theory consistently predicts low values for $(C_{m_q} + C_{m_{\dot{\alpha}}})$. As the volute becomes longer, agreement is better. Short volutes are the greatest problem because forebody turbulence is a prominent factor in determining the flow pattern about the majority of the volute length. Longer volutes operate at greater distances and consequently are able to act in a more uniform flow field of the type the theory is based upon. A second reason for the large difference in predicted versus actual data deals with $\hat{x}_t$. In the calculation of C_{m_α}, h_t had to be averaged and represented the only parameter that had to be approximated with average values. $(C_{m_q} + C_{m_{\dot{\alpha}}})$ depends upon h_t and $\hat{x}_t$ so that averaging errors in both are amplified when they are multiplied. $(C_{m_q} + C_{m_{\dot{\alpha}}})$ will have about twice the error as that in $C_{m_{\dot{\alpha}}}$. $(C_{m_q} + C_{m_{\dot{\alpha}}})$ were obtained only for Models 3+1, 3+2, 3+3, 3+5, and 3+6. These data points are plotted along with the theoretical values for cylinder 3 models in Figure 18.

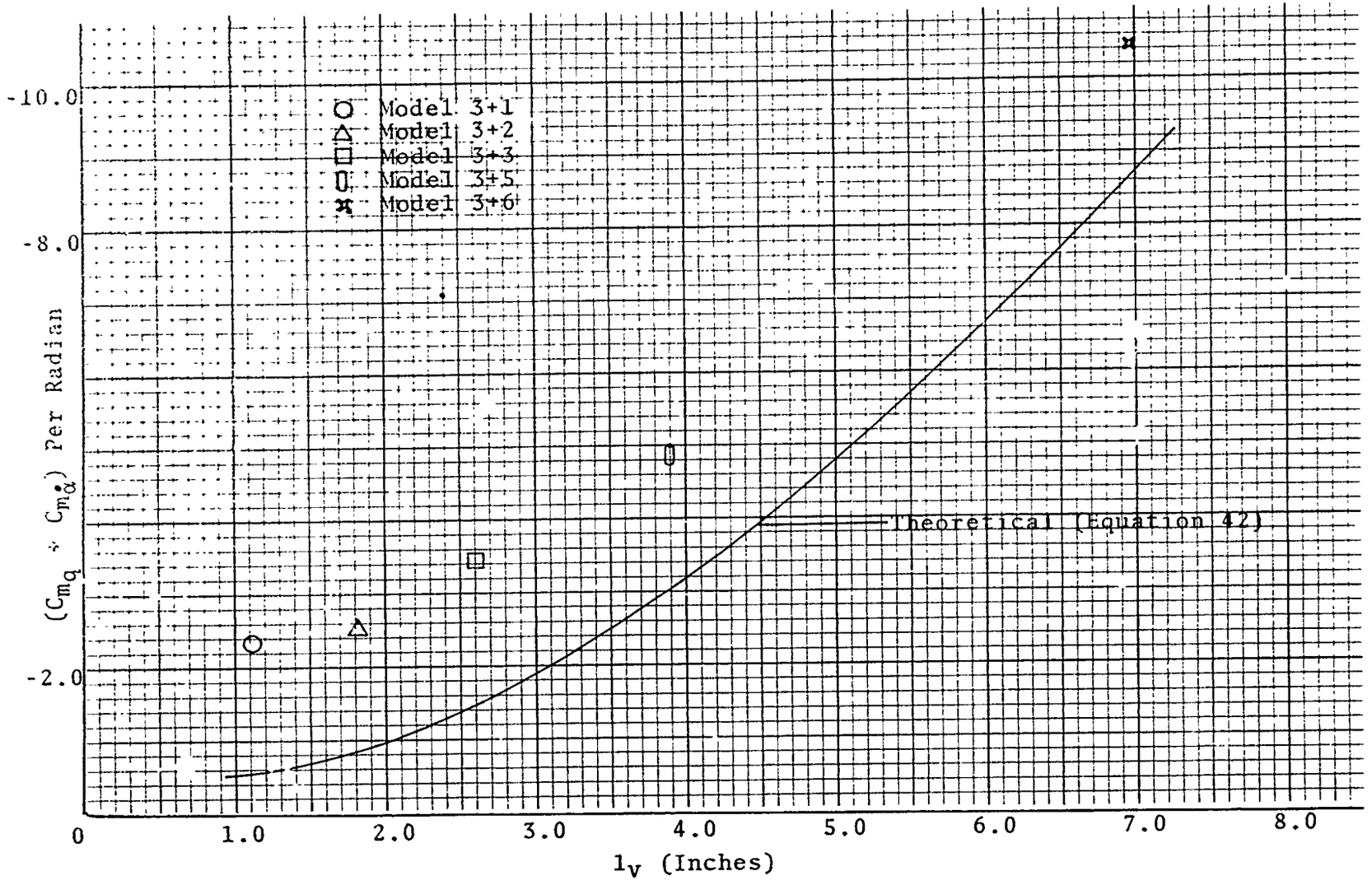

Figure 18. l_v Versus $(C_{m_q} + C_{m_{\dot{\alpha}}})$

SECTION III

FLEXIBLE BODY ANALYSIS

The various important geometrical parameters which affect dynamic and static stability discussed in Section II provided answers sufficient for preliminary design work and, in some cases (long volutes), good enough for final design.

Flexible volutes are not as efficient in stabilizing forebodies since they tend to bend out of the windstream. In addition, some configurations may be dynamically unstable depending upon the cg and the center of pressure location. Static stability is easily examined with slight modification to the rigid body analysis. Dynamic stability requires examining the characteristic equation of the model. If the model is idealized and allowed to have only two degrees of angular freedom, a fourth degree equation results which can be investigated with the Routh Hurwitz criteria. One simple approximation can be made to the two equations of motion which effectively uncouple the system and allow a single equation to be solved. This case will be dealt with presently.

Most volutes will be light in relation to the forebody. This fact can be put to use in simplifying the complex equations of motion. If it is also assumed that damping provided by volute motion relative to the forebody is small compared to the normal force set up by the freestream velocity, the following relation must hold:

$$\delta = - \frac{qC_{n_{V_o}} 0.661 l_V S_V \Phi}{k_V \dot{} + qC_{n_{V_o}} 0.661 l_V S_V \Phi} \quad \theta = -J\theta \tag{43}$$

The method using Equation (43) will be referred to as the "J" method. With Equation (43), δ can be replaced and the equation of motion reduced to one variable, θ, and the associated derivatives. The solution is not quite straightforward, however, because of the proportionality constant Φ. Φ is found by inserting Equation(43) into the Φ equation. This gives:

for, $\Phi = (\hat{\theta} + \hat{\delta})$ average

$$\Phi = \hat{\theta}(1 - J) \tag{44}$$

J, however, is a function of Φ so that the above can be written:

$$V\Phi^2 + k_V\Phi - \hat{\theta}k_V = 0 \tag{45}$$

where $$V = qC_{n_{V_o}}0.661_V S_V$$

Note that V can be a function of θ depending on whether tail interference is taken into consideration. If it is not, Equation (45) can be solved directly for a given V and k_V. With this value, J is known and the problem is nearly solved. Since there are no inertia effects, the aerodynamic coefficients are changed by a constant value, the new form for each being approximately:

$$C_{m_{\alpha_f}} = \left(C_{m_{\alpha/rigid}}\right)\frac{\Phi}{\hat{\theta}} - C_{m_{\delta/rigid}} J \tag{46}$$

$$\left(C_{m_q} + C_{m_{\dot{\alpha}}}\right)_f = \left(\left[C_{m_q} + C_{m_{\dot{\alpha}}}\right]_{/rigid}\right)\frac{\Phi}{\hat{\theta}} - C_{m_{\dot{\delta}/rigid}} J \tag{47}$$

The two forms above indicate that for flexible volutes, the overall static and dynamic stability decrease with increases in C_{m_δ} and $C_{m_{\dot{\delta}}}$. This assumes that the lateral spring constant remains constant. Note that for a given spring constant, increases in the volute size cause an increase in J along with C_{m_α}, C_{m_q}, $C_{m_{\dot{\alpha}}}$ changing the overall stability quickly. The conditions for dynamic and static stability are:

$$\Delta B + h_t' S_V C_{n_{V_o}}(1 - J) > 0 \tag{48}$$

$$\Delta B' + h_t' \hat{x}_{V_t} S_V C_{n_{V_o}}(1 - J) > 0 \tag{49}$$

The stabilizing effectiveness of many cylinders is small so that in some cases stability can be inferred by requiring that $J < 1$. If the cylinder has positive ΔB and $\Delta B'$, then the combination will never be dynamically or statically unstable, since $J < 1$ for $k_V > 0$.

Thus far, the flexible analysis has not considered forebody blanking. The first flexible forms are analogous to the first forms derived under the linear rigid body analysis. As was shown, forebody interference is important and gives rise to a trim angle. Returning to Equation (45), V is a function of θ because S_V is. S_V was derived earlier and plotted as a

function of θ. To use the results of this work for flexible models, it is necessary to enter the S_V curves with the angle $(\theta - \delta)$. The effective area is a function of the angle of attack measured relative to the volute axis which moves relative to the forebody for flexible volutes. To find the resulting pitching moment and its slope, it is first necessary to find J as before. For a given θ, the deflection angle δ of the volute is unknown since this is the problem. However, it is not possible to specify S_V without knowing δ. The calculation must be an iterative process. Choose θ and assume δ to be zero. Solve Equation (45) for θ to give the second approximation for S_V and the procedure repeats until δ approaches its limit value and a second angle chosen. An alternate method is to assume what the angle of attack $(\theta - \delta)$ is, solve the equations directly and compute what cylinder pitch angle will cause the specified deflection. Several examples will illustrate the linear and nonlinear flexible calculations.

(4) Example: Find the pitching moment slope coefficient and damping coefficient for Model (3 + 6)', using the linear method. Model (3 + 6) was characterized in Example 1. The rigid C_{m_α} is from Table I:

$$C_{m_\alpha} = -0.926/\text{rad}$$

A small leaf spring was inserted between the cylinder and volute, thus converting the rigid Model (3 + 6) to a flexible Model (3 + 6)'. The lateral spring constant was found to be $k_V = 0.27$ lbs/rad. With this new value, V can be found:

$$V = 1.124 \text{ ft-lbs}$$

This form of V assumes no interference effects. With V, Φ can be found, using Equation (45).

$$\Phi = 0.188$$

J can now be found

$$J = 0.439$$

C_{m_δ} and $C_{m_{\dot{\delta}}}$ are defined to be (Appendix I):

$$-C_{m_\delta} = \left[\frac{C_{n_{V_o}} S_V h_t'}{d_c S}\right]\Phi \tag{50}$$

$$-C_{m_{\dot\delta}} = \left[\frac{C_{n_{V_o}} S_V h_t \hat{x}_V}{d_c^2 S}\right]\Phi \tag{51}$$

Which compute:

$$C_{m_\delta} = -0.510/\text{rad.}$$

$$C_{m_{\dot\delta}} = -1.614/\text{rad.}$$

The aerodynamic coefficients follow from Equations (46)and (47):

$$C_{m_{\alpha f}} = -0.296/\text{rad.}$$

$$\left(C_{m_q} + C_{m_{\dot\alpha}}\right)_f = -4.183/\text{rad.}$$

(5) Example: Suppose that the volute changes in length in Example 4, what is the effect on $C_{m_{\alpha f}}$? Table V lists the problem variables for l_v = 0, 1.118, 1.825, 2.62, 3.89, 7 and ∞.

TABLE V. $C_{m_{\alpha f}}$/Rad

l_v	V	Φ	J	C_{m_α}	C_{m_δ}	$C_{m_{\alpha f}}$
0	0	$\hat{\theta}$	0	-0.0558	0	-0.0558
1.118	0.0281	0.324	0.0326	-0.126	-0.103	-0.119
1.825	0.0721	0.309	0.0763	-0.196	-0.167	-0.168
2.62	0.1512	0.288	0.1403	-0.275	-0.230	-0.2024
3.89	0.343	0.253	0.245	-0.470	-0.344	-0.2707
7.00	1.124	0.188	0.439	-0.926	-0.510	-0.2958
∞	∞	0	1	$-\infty$	0	$\sim$0

As indicated by Table V, there is a limit to the effectiveness of a flexible volute beyond which little is gained with further increase because of the tendency to bend out of the windstream. This is distinct from the rigid case where increase in volute length is manifest in greater C_{m_α} without limit. Larger flexible volutes provide greater righting moments than smaller volutes; however, their efficiency decreases as indicated by a falling off of $C_{m_{\alpha f}}$ beyond a certain best length l_v. If nothing else mattered, Equation (46) would be maximized and that value of l_v used. As l_v = 5.5 inches, C_{m_α} reaches about -0.290 and an increase of l_v by 1.5 to 7 inches increases $C_{m_{\alpha f}}$ by 1.8 percent. In the limit, $l_v \to \infty$, J goes to 1, Φ to 0 and $C_{m_{\alpha f}}$ to approximately 0. To find the best design length, the following example furnishes complete calculations.

(6) Example: Show the effect of increasing l_v for a cylinder with $l_c/d_c = 2$ where x_{cg} = 1.46 inches and d_c = 1.46 inches. Table VI shows the problem values. A plot of Table VI gives $C_{m_{\alpha f}}$ a maximum value of $C_{m_{\alpha f}}$ = -0.3007 at l_v = 7.5 inches. Beyond this, a larger volute would reduce in effectiveness. The curve approaches its maximum value rapidly and this value is nearly attained with smaller volutes. If the best design value is defined to be 90 percent (x) $l_{v_{max}}$ (maximum), a more reasonable length volute can be used. In this case, the best design value is -0.2764, which occurs at about l_v = 4.5 inches and represents a 77 percent reduction over the maximum value volute length (Figure 19).

All of the foregoing deal with the linear form of the flexible equations; no account was made for forebody interference. Thus, the area S_v used for all calculations was the entire volute planform area. To account for interference and find the value of θ_{trim}, it is necessary to invoke the results of Equation (29). As suggested earlier, the procedure is iterative.

(7) Example: Find C_{m_α} for Flexible Model 1, using iteration. The calculation will be carried out for θ = 0°, 5°, 10°, 15°, 20°, 25°, 30°, 35° and 40°. Assume δ = 0 and θ = 5°.
For the ratio l_v/d_c = 2.915, Equation (29) gives $S_v/\bar{d}^2/$ = 0.868 and S_v = 1.1487 in.^{2} With this number, the problem can be solved as in Example 4. This gives J = 0.1012. Thus, δ was not zero but is:

$$\delta = - J\theta = -(0.1012)5° = 0.506°$$

TABLE VI. BEST DESIGN LENGTH COMPUTATIONS

l_v	h_t'	B	B'	S_v	d_cS	C_{m_α}	C_{m_δ}	V	Φ	J	$C_{m_{\alpha_f}}$
0	1.46	1.2962	1.2962	0	6.224	0	0	0	0.335	0	0
0.5	1.76	1.2962	1.2962	0.365	6.757	-0.0350	-0.3048	0.0046	0.333	0.0056	-0.0345
1.5	2.45	1.2962	1.2962	1.095	7.823	-0.1263	-0.1204	0.0414	0.3193	0.0468	-0.1147
2.0	2.78	1.2962	1.2962	0.460	8.356	-0.1789	-0.1650	0.0736	0.3089	0.0779	-0.1521
2.5	3.11	1.2962	1.2962	1.825	8.888	-0.2353	-0.2088	0.1150	0.2973	0.1125	-0.1853
3.0	3.44	1.2962	1.2962	2.19	9.422	-0.2946	-0.2507	0.1656	0.2851	0.1488	-0.2134
3.5	3.77	1.2962	1.2962	2.555	9.947	-0.3568	-0.2905	0.2254	0.2728	0.1855	-0.2367
4.0	4.10	1.2962	1.2962	2.92	10.487	-0.4207	-0.3275	0.2944	0.2608	0.2210	-0.2551
4.5	4.43	1.2962	1.2962	3.285	11.020	-0.4866	-0.3619	0.3726	0.2492	0.2561	-0.2693
5.0	4.76	1.2962	1.2962	3.650	11.553	-0.5542	-0.3940	0.4600	0.2382	0.2890	-0.2802
5.5	5.09	1.2962	1.2962	4.015	12.086	-0.6231	-0.4239	0.5566	0.2279	0.3196	-0.2884
6.0	5.42	1.2962	1.2962	4.380	12.619	-0.6932	-0.4513	0.6625	0.2181	0.3487	-0.2939
6.5	5.75	1.2962	1.2962	4.745	13.152	-0.7645	-0.4772	0.7775	0.2091	0.3758	-0.2978
7.0	6.08	1.2962	1.2962	5.110	13.685	-0.8366	-0.5009	0.9017	0.2006	0.4012	-0.2999
7.5	6.41	1.2962	1.2962	5.47	14.210	-0.9093	-0.5230	1.034	0.1927	0.425	-0.3007
8.0	6.74	1.2962	1.2962	5.84	14.751	-0.9833	-0.5436	1.1787	0.1852	0.4472	-0.3005
8.5	7.07	1.2962	1.2962	6.205	15.284	-0.0577	-0.4520	1.329	0.178	0.4686	-0.2986

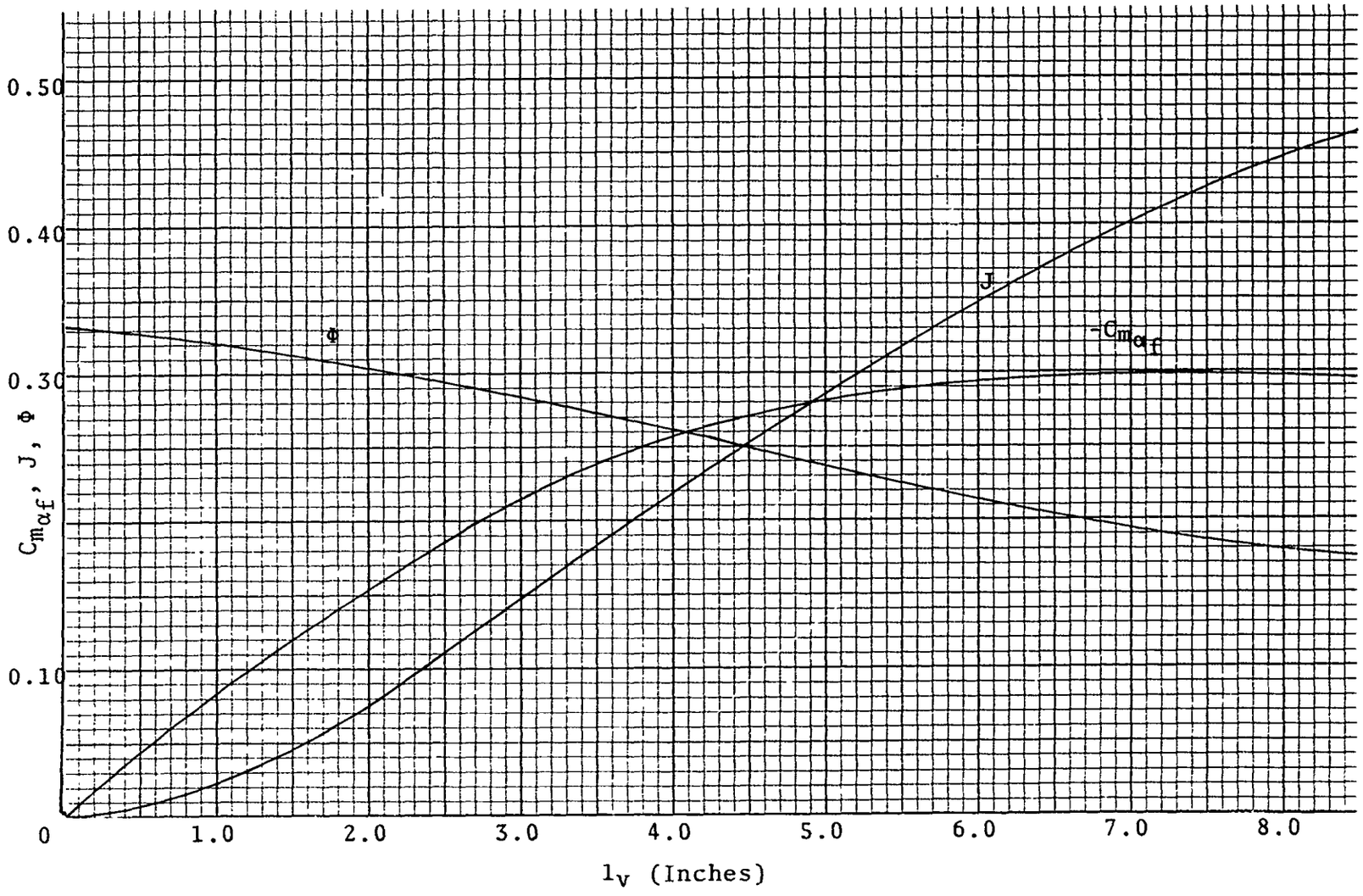

Figure 19. l_v Versus $C_{m_{\alpha f}}$

The net angle of attack is:

$\theta_{volute} = \theta_{cyl.} - \delta = 5° - 0.506° = 4.494°$
Enter Equation (29) with this new angle and find $S_V = 1.081$ in.^{2} Repeat the procedure. The following table of values results:

TABLE VII. Cm_{α_f}/Rad.

θ	S_V	Φ	J	δ	Cm_δ	Cm_α	Cm_{α_f}
0°	0	0.335	0	0	0	0	0
5°	1.0889	0.3026	0.0968	-0.4413	-0.1642	-0.1799	-0.1466
10°	1.484	0.2938	0.1238	-1.102	-0.2172	-0.2492	-0.1917
15°	1.677	0.2894	0.1361	-1.797	-0.2418	-0.2856	-0.2139
20°	1.786	0.2871	0.1430	-2.502	-0.2555	-0.3055	-0.2236
25°	1.855	0.2857	0.1475	-3.204	-0.2640	-0.3195	-0.2336
30°	1.903	0.2848	0.1498	-3.890	-0.2700	-0.3266	-0.2372
35°	1.936	0.2844	0.1517	-4.592	-0.2743	-0.3363	-0.2439
40°	1.959	0.2837	0.1531	-5.308	-0.3048	-0.3397	-0.2410

The results of the flexible test work for flexible Models 1 and 2 are plotted and the predicted values are plotted (Figures 20 and 21). As was done in the rigid analysis, Cm_δ was chosen to represent the pitching moment data and the three analytical curves represent the same three theories outlined in the rigid work. The first is the most linear flexible theory (i.e., Equation (46) - no forebody blanking) and the second and third take into account $\Phi\sin(\theta + \delta)$ and $\sin^2(\theta + \delta)$ variations of pitching moment plus forebody blanking.

As previously stated, the flexible volute operating behind the cylindrical forebody will have a trim angle different from zero if the cg of the model is located aft of the cg of the cylinder. Returning to Example 4, if the volute is imagined to have elasticity with $k_V = 0.27$, the following example can be solved for the trim angle:

(8) Example: For this a trapezoidal area will be used. The rigid body analysis provided two equations which can be used for this purpose. The total area into the windstream at a given angle of attack is the sum of the following two expressions:

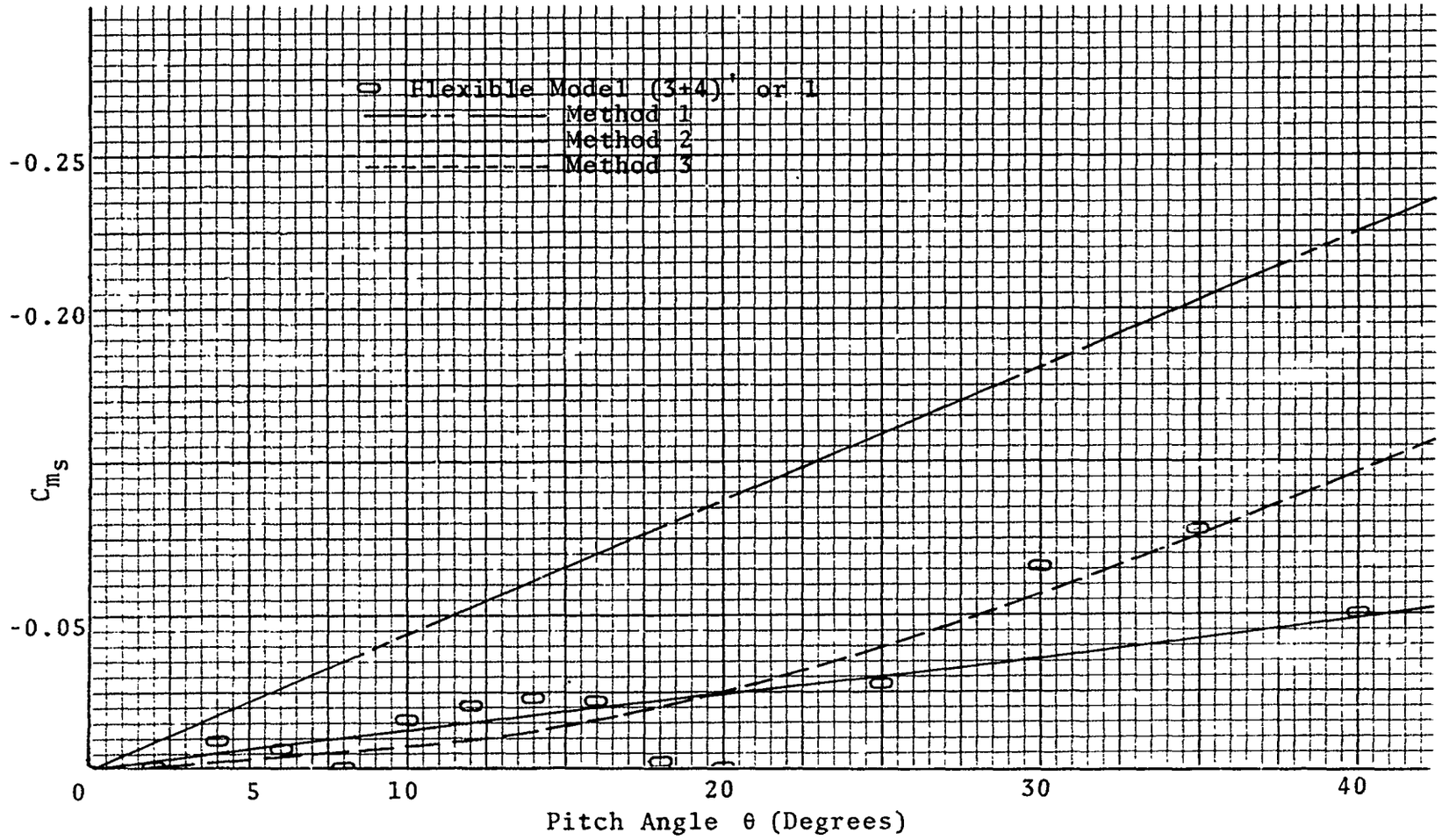

Figure 20. θ Versus C_{m_s}

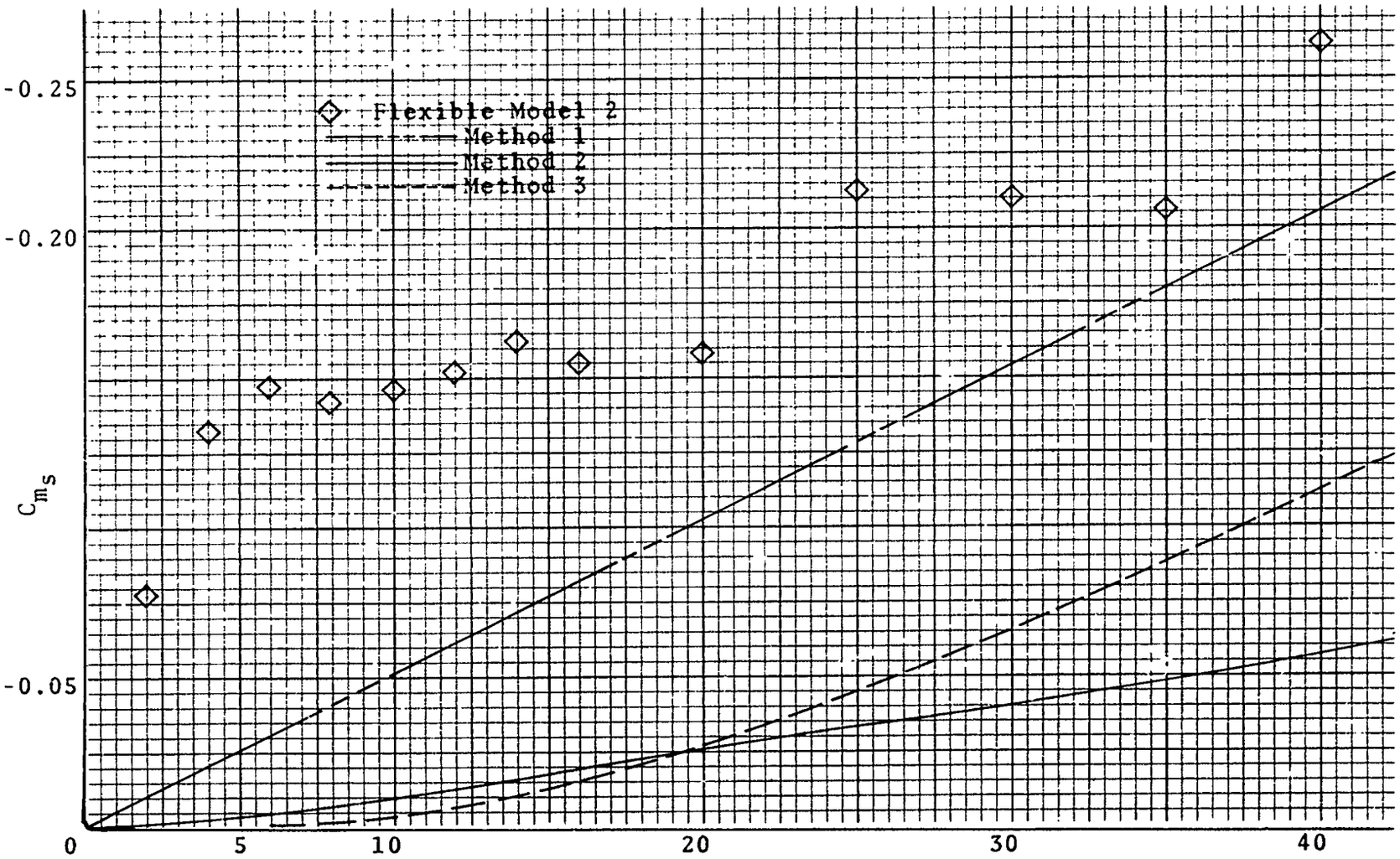

Figure 21. θ Versus C_{m_s} Flexible Model 1

$$S_V' = d l_V/2 - d^3/8 l_V \left[\frac{1}{(\tan\theta + \frac{\bar{d}}{2 l_V})^2} \right]$$

$$S_V'' = d_V (l_V - x')$$

Thus $$S_V = S_V' + S_V''$$

The condition for finding the trim angle is found by setting Equation (48) to zero.

$$\Delta B + h_t S_V C_{n_{V_o}} (1 - J) = 0$$

Recalling the values of the constant terms from Example 4, the above can be written as:

$$1.568 - \frac{0.186}{\tan\theta + 0.291} - \frac{0.0818}{(\tan\theta + 0.2907)^2} = \frac{0.4046}{1 - J}$$

An iterative procedure may be used. The following table gives intermediate answers and the final value for the trim angle.

TABLE VIII. TRIM ANGLE

θ_{trim}	S_V	V	Φ	J	Left Side	Right Side
0	0	0	0	0	-0.039	0.4046
30'	0.057	0.005	0.333	0.006	0.037	0.4070
1°	0.109	0.009	0.332	0.009	0.108	0.4083
2°	0.197	0.017	0.328	0.020	0.226	0.4129
4°	0.336	0.029	0.324	0.034	0.419	0.419

It remains to look into the damping derivatives, using the J method. These calculations are quite simple and can be carried out quickly, using Equations (47) and (51). This was done for the models listed in Example 5 and are tabulated below:

TABLE IX. $(C_{m_q} + C_{m_{\dot{\alpha}}})_f$/Rad. (THEORETICAL)

Model	l_v	$(C_{m_q} + C_{m_{\dot{\alpha}}})$	$\Phi/\hat{\theta}$	$C_{m_{\dot{\delta}}}$	$(C_{m_q} + C_{m_{\dot{\alpha}}})_f$
3+1	1.118	-0.506	0.967	-0.169	-0.484
3+4	1.805	-0.844	0.922	-0.315	-0.754
3+3	2.62	-1.434	0.859	-0.519	-1.159
3+5	3.89	-2.862	0.755	-0.891	-1.904
3+6	7.00	-8.714	0.561	-1.871	-4.067

The J method represented a good first approximation for determining the effects of volute flexing upon the basic stability derivatives. The greatest shortcoming deals in the area of dynamic stability; such instability cannot be predicted since the volute is assumed massless. Wind tunnel testing shows, however, that even for light volutes of the type which would probably be used, dynamic instability is a serious problem.

A coning motion which persists after the initial transients have damped out is apparently caused by turbulence and coupling between the pitching, yawing and stretching motions of the volute. The three motions seem to enhance each other, periodically damping out only to be revived to the same or greater amplitude motion. For speeds lower than Mach 0.19, the motion was less violent. The following theory deals only with two dimensional motion and allows for only two-degree angular freedom motion in one plane.

Equations (1) and (2) represent the backbone of this theory. To fully grasp the meaning of each leading coefficient, the two equations will be broken down to the individual parts and discussed separately. The basic equations for reference are again:

$$a_{11}\ddot{\theta} + a_{12}\ddot{\delta} = - a_{13}\dot{\theta} - a_{14}\theta - a_{15}\dot{\delta} - a_{16}\delta \qquad (52)$$

$$a_{21}\ddot{\theta} + a_{22}\ddot{\delta} = - a_{23}\dot{\theta} - a_{24}\theta - a_{25}\dot{\delta} - a_{26}\delta \qquad (53)$$

a_{11} - The inertia of the forebody and volute are accounted for with a_{11}. This term is the same as that which would appear with $\ddot{\theta}$ for a rigid model.

$$a_{11} = I_b + I_V + 2 M_V R_V \bar{r}_V + M_V R_V^2 = I \qquad (54)$$

a_{12} - Allowing the volute to oscillate and giving it mass and, hence, inertia, gives rise to an inertia force which is transmitted to the forebody through the elastic coupling. This inertia force must be included on the inertia side of the moment summation equation. For $\ddot{\delta} = 0$. The a_{12} inertia term drops out of the equation and the left side of Equation (52) reduces to the rigid form.

$$a_{12} = I_V + M_V R_V \bar{r}_V = K_V \tag{55}$$

a_{13} - This term represents the damping moment set up by a rigid body model having the same tail and forebody as the flexible one. The term is relatively large and represents a major contribution to the overall damping of the model. The term has an order of magnitude of about 10^{-3}. It can be written as:

$$\tfrac{1}{2}\rho V_\infty{}^2 S d_c \left[\frac{2C_{n_{b_o}} S_b \hat{x}_b h_b}{d_c{}^2 S} + \frac{2C_{n_{b_o}} S_b' \hat{x}_b' h_b'}{\Delta B' \; d_c{}^2 S} + \frac{2C_{n_{v_o}} S_v \hat{x}_{v_t} h_t'}{d_c{}^2 S} \right] \frac{dc\Phi}{2V_\infty} \tag{56}$$

or, using linear aerodynamic notation:

$$-qd_c S \; (C_{m_q} + C_{m_{\dot{\alpha}}}) \frac{d_c}{2V_\infty} \tag{57}$$

$(C_{m_q} + C_{m_{\dot{\alpha}}})$ is the same as that defined for the rigid models. An important fact yet to be shown is that a_{13} must be large in relation to a_{15} [its complimentary term in Equation (52)]to aid in insuring dynamic stability. The terms in Equation (56) indicate how to make a_{13} large. This can be accomplished without increasing a_{15} by increasing the forebody size or by moving the cg forward which increases $\hat{x}_{v_t}$. This latter point will be examined more thoroughly since the same adjustment will provide better static stability. $\hat{x}_{v_t}$ plays a critical role in determining whether the model will have tendencies toward dynamic instability.

a_{14} - This is simply the rigid expression for static pitching moment. It is one of the largest terms in Equation (52), having an order of magnitude of about 10^{-1}. The term must be positive if the model is to be statically stable. It can be written two ways as:

$$\tfrac{1}{2}\rho V_\infty^2 \, d_c \left[-\frac{C_{n_{b_o}} S_b h_b}{d_c S} + \frac{C_{n_{b_o}} S_{b'} h_{b'}}{d_c S} + \frac{C_{n_{v_o}} S_v h_t'}{d_c S} \right] \Phi \qquad (58)$$

or

$$-q d_c S \, C_{m_\alpha} \qquad (59)$$

a_{15} - This term does not show up favorably since it causes trouble in the characteristic equation of the model. A sign reversal on one coefficient of the characteristic equation will occur if a_{15} is too large which, according to the Routh-Hurwitz criteria, guarantees dynamic instability. Unfortunately, a_{15} cannot be indiscriminately reduced since several of the constituent terms are required to be large for large a_{13} and a_{14} which are considered to be favorable quantities (i.e., the larger, the better). a_{15} is written two ways as:

$$\tfrac{1}{2}\rho V_\infty^2 S d_c \left[\frac{2 C_{n_{v_o}} S_v \hat{x}_v h_t'}{d^2 c S} \right] \frac{d_c \Phi}{2V_\infty} \qquad (60)$$

and, by using linear aerodynamic notation, as:

$$-q d_c S \left(C_{m_{\dot{\delta}}} \right) \frac{d_c}{2V_\infty} \qquad (61)$$

It would be difficult to have large a_{13} and small a_{15} if not for the subtle difference between $\hat{x}_V$ and $\hat{x}_{V_t}$ because the forebody $\Lambda B'$ is usually small. $\hat{x}_{V_t}$ can be written as a function of the volute length and the cg location. For a given volute, $\hat{x}_{V_t}$ is controlled by the cg location. Movement forward will be manifest in greater $\hat{x}_{V_t}$ which helps to insure dynamic stability. $\hat{x}_V$ is not affected by cg location and, hence, does not change. If the cg were to shift backwards and longer volutes were added to the same forebody, a_{15} would increase at a faster rate than a_{13} which is undesirable. $\hat{x}_V$ and $\hat{x}_{V_t}$ are both related to center of pressure and their definition carefully takes into account the volute planform shape. Thus, the above indicates how the center of pressure and the cg location need to be related.

a_{16} - This term is analogous to a_{14} and represents the static moment set up by deflection of the volute into the wind. Note that this deflection is measured relative to the forebody. Depending on whether the volute bends into the wind or away from it, a_{16} can add or detract from

static stability. Like a_{15}, a_{16} does not show up favorably in the dynamic stability criteria. If the forebody has the cg location in its geometrical center, then a_{16} is equal to a_{14}. This is evident from the defining equation:

$$\tfrac{1}{2}\rho V_\infty{}^2 S d_c \left[\frac{C_{n_{V_o}} S_V h_t'}{d_c S}\Phi\right] \tag{62}$$

or as:

$$-q d_c S\, C_{m_\delta} \tag{63}$$

Thus a_{16} has the same order of magnitude as a_{14}. There is no way to increase a_{14} without also increasing ΔB if h_t' is measured from the model cg and is the same for both coefficients.

a_{21} - The second equation of motion was found through a moment summation about the tail hinge point. Because of this, it was necessary to alter the normal expression for the inertia terms and include the effects of a linearly accelerating coordinate system. When the inertia side of the moment summation is written out, a_{21} appears as the lead coefficient. In terms of the physical constraints:

$$J_V + M_V R_V \bar{r}_V \tag{64}$$

a_{22} - This is the second portion of the inertia expression. It is defined to be:

$$I_V \tag{65}$$

a_{23} - When a_{13} has been determined, a_{23} can be found by subtracting the forebody contribution to a_{13} and multiplying by $0.661_V/h_t'$. a_{23} represents a damping moment set up by forebody pitching. Note here that the moment arm is only 0.661_V, since the moment summation center was located at the hinge line. a_{23} can be defined in several alternate ways, as follows:

$$\tfrac{1}{2}\rho V_\infty{}^2 S d_c \left[\frac{2 C_{n_{V_o}} S_V \hat{x}_{V_t} 0.661_V}{d_c{}^2 S}\right] \frac{d_c \Phi}{2V_\infty} \tag{66}$$

$$-qd_cS\ (C_{m_{\dot{\delta}}})\frac{0.661_V}{h'_t}\ \frac{\hat{x}_{V_t}}{\hat{x}_V}\ \ \frac{d_c}{2V_\infty} \tag{67}$$

$$\left(a_{13}\ -\ (\text{forebody contribution})\right)\frac{0.661_V}{h'_t} \tag{68}$$

a_{23} has a destabilizing effect on the dynamics of the model. The same conclusion previously reached concerning cg versus center of pressure location can be arrived at here by examining the moment arm 0.661_V. Note that a_{13}, which serves the same variable in Equation (52) as does a_{23} in Equation (53), depends upon h'_t which itself relies on cg location for a fixed volute. Increasing rearward location of the cg must be done with some care if dynamic stability is to be maintained.

a_{24} - This term is the static pitching contribution due to excursions of θ in Equation (53). It has a similar form, as does a_{14}, and can be written in several ways:

$$\tfrac{1}{2}\rho V_\infty{}^2Sd_c\left[\frac{C_{n_{V_o}}S_V\,\frac{2}{3}l_V\,\Phi}{d_cS}\right] \tag{69}$$

$$-qd_cS\,(C_{m_{\dot{\delta}}})\ 0.661v/h'_t \tag{70}$$

$$\left(a_{14}\ -\ (\text{forebody contribution})\right)\frac{0.661_V}{h'_t} \tag{71}$$

a_{25} Dynamic stability is aided if a_{25} is large. One finds here that a compromise must be made among the variables since the previous findings concerning cg location versus large l_V are not manifest in a_{25}. That is, a_{25} can be made large regardless of cg location. By increasing l_V, however, to enlarge a_{25}, destabilizing elements are at work through a_{15} and a_{23}, both of which are growing with increases in l_V. a_{13} also increases with l_V. The relation between these coefficients to determine whether such changes in the model geometry cause instability is the subject of the Routh Hurwitz criteria. a_{25} may be written as:

$$\tfrac{1}{2}\rho V_\infty{}^2Sd_c\left[\frac{2C_{n_{V_o}}S_V\hat{x}_V 0.661_V}{d^2{}_cS}\right]\frac{d_c\Phi}{2V_\infty} \tag{72}$$

$$-qd_cS\left(C_{m_{\dot{\delta}}}\right)\frac{0.661_V}{h'_t}\ \frac{d_c}{2V_\infty} \tag{73}$$

$$(a_{13} \text{ - forebody contribution})\ \frac{\hat{x}_V 0.661_V}{\hat{x}_{V_t} h'_t} \tag{74}$$

a_{26} - This is a unique coefficient and includes the effects of the elastic coupling. It is the only coefficient that includes the spring constant k_V. It has already been shown that the value of the spring constant is important in determining the value of pitching and damping moments set up by the model's motion. The dynamic criteria shows that large k_V helps to provide a dynamically stable model. a_{26} is a function of a_{24} which can be typified as an unfavorable value if too large. For a_{26} to be large without compromising stability through a_{24}, k_V must be large. This stands to reason since, in the limit as k_V approaches infinity, the system reduces to its rigid body form. a_{26} is easiest to use defined as below:

$$a_{24} + k_V \tag{75}$$

All of the preceding comments regarding dynamic stability result from the Routh Hurwitz criteria. An absolute stability criteria involving the model constraints was not obtained because of the great amount of algebraic work and the practically impossible task of using the results. Thus, the volute equipped body has not been proven to be unstable for a given type of configuration. To prove that volute equipped models cannot be unstable requires writing the coefficients of the characteristic equation in the stability criteria scheme and insuring that the proper terms will not change sign by relating the constraints back to the original a_{ij}'s.

It was found by computing many examples for a variety of different volute and forebody combinations that a good indicator of impending dynamic instability was the coefficient C_{12} of the s^3 term of the fourth degree characteristic polynomial. This term will be the first one to change sign, thus indicating dynamic instability. That is not to say that no change is reason not to invoke the remainder of the stability criteria. If the mentioned coefficient is much smaller than the other coefficients but does not change sign (all coefficients would then have the same sign), there is a good chance the model will still have two unstable roots and two stable roots. The Routh Hurwitz criteria is discussed more fully in Appendix I. From that discussion the following observations are made which tie

the preceding to the a_{ij}'s. The fourth degree characteristic equation can be written as:

$$C_{11}s^4 + C_{12}s^3 + C_{13}s^2 + C_{14}s + C_{15} = 0 \qquad (76)$$

The coefficient of interest is C_{12}. C_{12} can be written in terms of the a_{ij}'s as follows:

$$C_{12} = (a_{11}a_{25} + a_{22}a_{13}) - (a_{21}a_{15} + a_{12}a_{23}) \qquad (77)$$

Since C_{12} may be the first of the C_{ij}'s to go negative, a necessary but not sufficient condition for dynamic stability is:

$$a_{11}a_{25} + a_{22}a_{13} > a_{21}a_{15} + a_{12}a_{23} \qquad (78)$$

This inequality constraint is a relation between the inertia of the cylinder and volute and the damping properties of the cylinder and volute combination. Note that the spring constant does not appear in Equation (78). The small mass assumption used in the J method will reduce Equation (78) to:

$$a_{11}a_{25} > 0 \ , \ a_{11} > 0, \ a_{25} > 0 \text{ (always)} \qquad (79)$$

Thus massless volutes will probably be stable. Giving the volute mass requires matching the a_{ij}'s so that C_{12} cannot change sign. Note that C_{11} will usually be positive which requires that C_{12} be greater than zero.

Equation (78) is useful in finding out if a given configuration will have an obvious dynamic stability problem. Substituting for the volute and cylinder geometrical and inertia properties for the a_{ij}'s, the following equation results:

$$\left|C_{m_{\dot{\delta}}}\right|_{\text{rigid}} \left[K_V + \frac{0.661_V}{h_t'}\left(\frac{K_V \hat{x}_{Vt}}{\hat{x}_V} - 1\right)\right] < I_V \left|C_{m_q} + C_{m_{\dot{\alpha}}}\right|_{\text{rigid}} \qquad (80)$$

Note that K_V, h_t' I_V, $\hat{x}_{Vt}$, 1_V are all interdependent and changing any one changes the others. Increasing 1_V causes the remaining parameters to increase. I, however, can be changed without affecting the other variables by increasing S_b.

This is a favorable trend, since Equation (80) shows that I reduces the left side and enhances the inequality. Having a large cylinder in relation to the volute tends to produce greater dynamic stability, holding all other parameters the same. Equation (80) can be used to examine the stability of several cylinder volute combinations.

Table X lists the a_{ij}s for several models. These values were calculated using $\hat{x}_V = 0.661_V$ and $\hat{x}_{Vt} = l_O + 0.500l_V$. Note that here an approximation was made since the earlier rigid work indicated that these variables h_t' and h_V will be functions of θ and $\dot{\theta}$. h_t' was set equal to $l_O + \frac{2}{3}l_V$ and $h_V = 0.661_V$. The a_{ij}s were multiplied by 1000 which gave the following set of equations:

Model (3+1)'

$$0.204\ddot{\theta} + 0.036\ddot{\delta} + 0.043\dot{\theta} + 38\theta + 0.0092\dot{\delta} + 33\delta = 0$$
$$0.036\ddot{\theta} + 0.011\ddot{\delta} + 0.009\dot{\theta} + 9.60\theta + 0.0027\dot{\delta} + 279.6\delta = 0$$

Model (3+2)'

$$0.343\ddot{\theta} + 0.112\ddot{\delta} + 0.077\dot{\theta} + 66\theta + 0.028\dot{\delta} + 61\delta = 0$$
$$0.112\ddot{\theta} + 0.058\ddot{\delta} + 0.025\dot{\theta} + 24.4\theta + 0.011\dot{\delta} + 294.4\delta = 0$$

Model (3+3)'

$$0.605\ddot{\theta} + 0.272\ddot{\delta} + 0.124\dot{\theta} + 103\theta + 0.064\dot{\delta} + 98\delta = 0$$
$$0.272\ddot{\theta} + 0.156\ddot{\delta} + 0.061\dot{\theta} + 51.5\theta + 0.034\dot{\delta} + 321.5\delta = 0$$

Model (3+5)'

$$1.296\ddot{\theta} + 0.737\ddot{\delta} + 0.291\dot{\theta} + 203\theta + 0.193\dot{\delta} + 198\delta = 0$$
$$0.735\ddot{\theta} + 0.460\ddot{\delta} + 0.166\dot{\theta} + 116.4\theta + 0.115\dot{\delta} + 386.4\delta = 0$$

Model (3+6)'

$$5.760\ddot{\theta} + 4.222\ddot{\delta} + 1.078\dot{\theta} + 535\theta + 0.929\dot{\delta} + 530\delta = 0$$
$$4.222\ddot{\theta} + 3.183\ddot{\delta} + 0.769\dot{\theta} + 381.4\theta + 0.675\dot{\delta} + 651.4\delta = 0$$

From these equations, the characteristic equation can be derived by noting that the initial values for θ and δ will not be zero. Substituting for the variables according to the scheme in Appendix I, the following set of equations can be written:

Model (3+1)'

$$s^4 + 0.295s^3 + 25{,}850s^2 + 5{,}400s + 4{,}746{,}000 = 0$$

Model (3+2)'

$$s^4 + 0.313s^3 + 12{,}960s^2 + 2{,}800s + 2{,}440{,}000 = 0$$

TABLE X. A_{ij}

$\ddot{\theta}$ a_{11}	$\ddot{\delta}$ a_{12}	$\dot{\theta}$ a_{13}	θ a_{14}	$\dot{\delta}$ a_{15}	δ a_{16}
0.0002044	0.00003636	0.0000434	0.038	0.0092	0.033
0.0003428	0.00011210	0.0000765	0.066	0.0280	0.061
0.0006050	0.00027150	0.0001242	0.103	0.0640	0.098
0.0012960	0.00073500	0.0002909	0.203	0.1930	0.198
0.0057600	0.00422200	0.0010779	0.535	0.9290	0.530

$\ddot{\theta}$ a_{21}	$\ddot{\delta}$ a_{22}	$\dot{\theta}$ a_{23}	θ a_{24}	$\dot{\delta}$ a_{25}	δ a_{26}
0.00003636	0.00001698	0.00000855	0.0096	0.00000268	0.2796
0.00011210	0.00005823	0.00002530	0.0244	0.00001127	0.2944
0.00027150	0.00015554	0.00006095	0.0515	0.00003402	0.3215
0.00073500	0.00046210	0.00016640	0.1164	0.00011459	0.3864
0.00422200	0.00318320	0.00076900	0.3814	0.00067500	0.6514

Model (3+3)'

$$s^4 + 0.289s^3 + 8{,}330s^2 + 1600s + 1{,}376{,}000 = 0$$

Model (3+5)'

$$s^4 + 0.335s^3 + 6{,}200s^2 + 1400s + 947{,}000 = 0$$

Model (3+6)'

$$s^4 + 0.278s^3 + 3{,}050s^2 + 570s + 278{,}000 = 0$$

To find the roots of these equations, it is necessary to use the results of Appendix I which outline a graphical scheme. It is helpful and also time saving if the characteristic equations are examined with the Routh Hurwitz criteria before attempting to factor them. The values of the criteria terms are:

Model (3+1)'

1	25,850	4,746,000
0.0 95	5,400	
0.011	6.607	
0.125		

Model (3+2)'

1	12,960	2,440.000
0.313	2,800	
0.067	41.32	
1.295		

Model (3+3)'

1	8,330	1,376,000
0.289	1600	
0.335	165.991	
10.026		

Model (3+5)'

1	6,200	947,000
0.335	1400	
7.038	2,443.452	
458.451		

Model (3+6)'

1	3,050	278,000
0.278	570	
65.074	12,392.047	
18,542.087		

Since the first column of each scheme does not change sign, all given models are dynamically stable. Thus, the quadratic factors of the fourth degree polynomials will all have positive coefficients and will factor into negative real and ± imaginary parts. Thus each polynomial will appear as:

$$(s^2 + d_1 s + d_2)\ (s^2 + d_3 s + d_4) \tag{81}$$

The graphical technique requires solution of two simultaneous equations: (Reference 1)

$$d_1 = \frac{C_{12}}{2C_{11}} \pm \left[\left(\frac{C_{12}}{2C_{11}}\right)^2 - \frac{C_{13}}{C_{11}} + d_2 + \frac{C_{15}}{C_{11} d_2}\right]^{\frac{1}{2}} \tag{82}$$

$$d_1 = \frac{C_{14}/C_{11}(d_2) - C_{12}/C_{11}(d_2^2)}{C_{15}/C_{11} - d_2^2} \tag{83}$$

Either equation is rather complicated to solve by plugging in arbitrary numbers. For stable motion it is known that values for d_1 must be positive. d_1 and d_3 will be much smaller than d_2 and d_4. The latter two are related to the oscillating frequency of the model. The above type of characteristic equation is similar to the linearized equation frequently encountered in studying pitching motion of low speed aircraft. In these equations the important angular quantities are pitch angle and angle of attack. The angle of attack differs from the aircraft pitch angle in a similar manner that the volute angle of attack differs from the cylinder pitch angle. The mechanics of the two systems are different since the volute angle of attack is the result of aeroelasticity, whereas, the aircraft wing angle of attack is purely an aerodynamic phenomenon (excluding aeroelasticity). These comparisons mean that the volute model will probably have a short period mode and a long period mode, as do aircraft. The frequencies of the two modes should be quite different, one being high, the other being low, analogous to an aircraft's short period and phygoid mode of vibrations. d_2 was chosen as the parameter easiest to estimate since it represents a frequency quantity. If the low frequency vibration is estimated to be about 2 cycles/second, $d_2 = 157.75$. This is a good approximation to begin with in solving Equation (82). The following illustrates the technique:

(9) Example: Solve for the roots of Model (3+3).

(83)		(82)	
d_1	d_2	d_1	d_2
0.193	168	174	165
0.195	169	28.49	168
		4.69	168.5
		1.846	168.56
		1.372	168.57
		0.898	168.58
		0.796	168.59
		0.577	168.595
		neg	169.000

The right-hand side shows that increasing d_2 causes d_1 to drop in value and to continue dropping until it becomes negative. Inserting 168 into Equation (83) gives 0.193, which compares to 28.49, indicating that the solution is still off a good bit. At 169, d_1 computes to be 0.195, a minor change from 168; however, the right columns show d_1 passing through zero which would indicate that the solution must lie between 168 and 169. Both of the above sets of columns plot out as straight lines and no further points are needed. Figure 22 is a plot of the above, the intersection being the value of d_1 and d_2. Direct division yields d_3 and d_4. The factors are:

$$d_1 = 0.194 \qquad d_3 = 0.095$$

$$d_2 = 168.582 \qquad d_4 = 8{,}161.4$$

With these values for the factors, the quadratic roots follow directly.

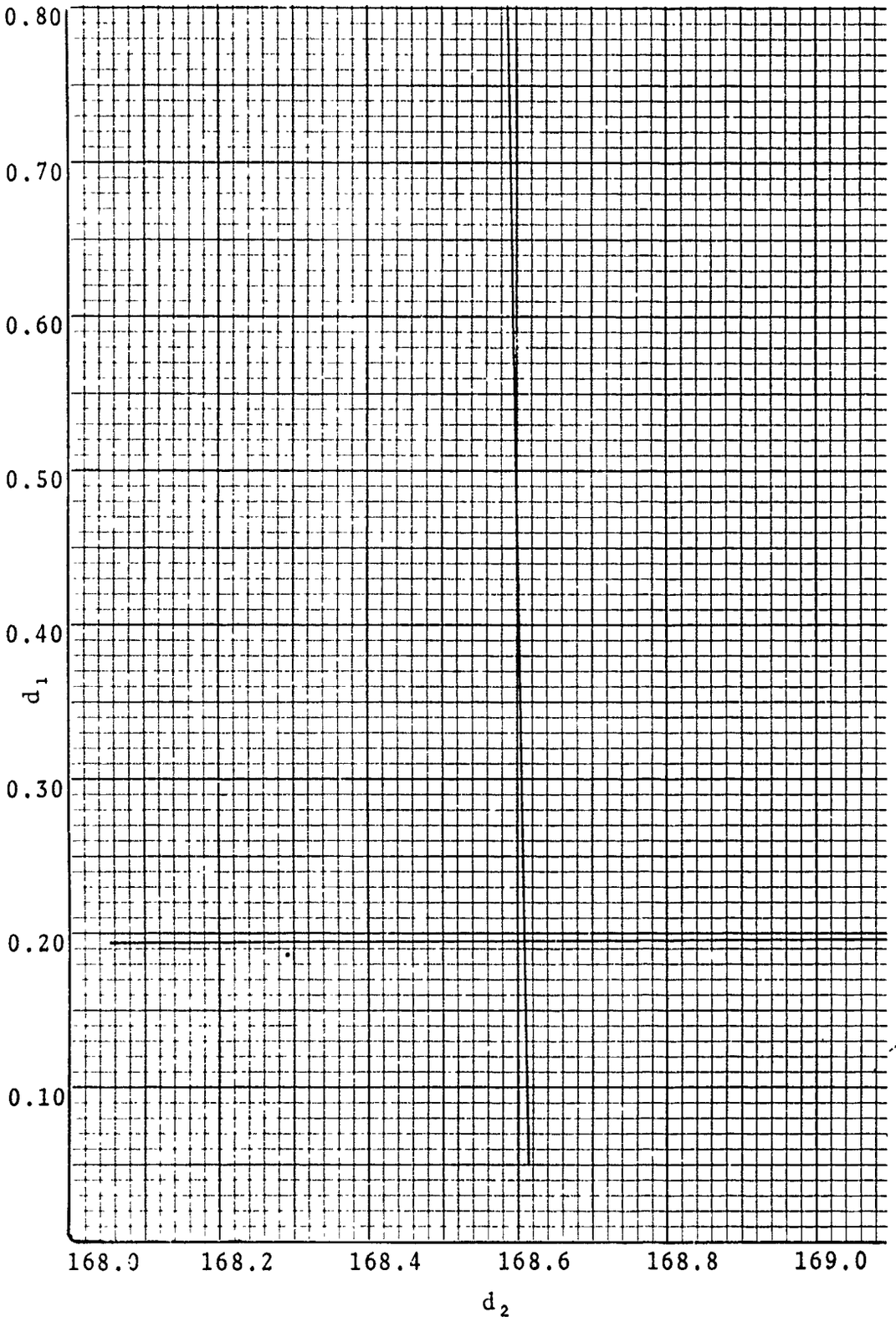

Figure 22. d_2 Versus d_1

$$s_1 = -0.097 + 2.067i, \quad i = \sqrt{-1}$$

$$s_2 = -0.097 - 2.067i$$

$$s_3 = -0.048 + 14.41i$$

$$s_4 = -0.048 - 14.41i$$

The particular solution for the two equations of motion is:

$$\theta = A_1 e^{-0.097t} (\sin 2.067t + \psi_1) + A_2 e^{-0.048t} (\sin 14.41t + \psi_2)$$

$$\delta = A_3 e^{-0.097t} (\sin 2.067t + \psi_3) + A_4 e^{-0.048t} (\sin 14.41t + \psi_4)$$

At first glance it would appear that there are eight arbitrary constants. There actually are only four, however, since the A_i and ψ_i are functions of four independent constants found from the initial conditions θ, $\dot{\theta}$ and δ,$\dot{\delta}$. The technique for finding the A_i and ψ_i terms whereby the complete expressions can be written is outlined in Reference 2. Since stability is the prime concern of this program, the technique is not included in this report. The equation is composed of two angular quantities damped at different rates. The mass of the volute drastically changes the motion of the forebody. This is manifest through the additional high frequency term in the θ equation. If the mass of the volute was sufficiently small, this term would have negligible effect on θ . The motion would be determined primarily by the leading term. At t = 10 seconds the long period mode has damped to 38 percent of its initial value and the short period mode has damped to 62 percent of its initial value. Wind tunnel testing showed that the model did indeed have the kind of motion indicated by the solution equation. The short period mode was easiest to follow with the eye and damped out first. The remaining high speed motion was then evident. Unfortunately, this high speed vibration only damped out partially and continued to vibrate. This limit cycle cannot be predicted by the simple linear theory. At this point in the two-year effort it is safe to say that the residual motion results from interaction among the pitch, yaw and stretch motion of the spring. It was somewhat surprising to see large amplitude second harmonics appearing in the bending of flexible helix volute. These waves in the spring were quite evident. The spring motion was unsteady and appeared very complex. An approximate analytical method will have to include two dimensional oscillations (coning) and possible second harmonic effects (three degrees of angular freedom). This type of analysis

is beyond the scope of the first year study but may be the subject of the second year study.

The remaining roots of the flexible models were solved for the method of the preceding example. The roots of these models are:

Model (3+2)'

$$s_1 = -0.104 + 2.164i$$
$$s_2 = -0.104 - 2.164i$$
$$s_3 = -0.043 + 25.549i$$
$$s_4 = -0.043 - 25.549i$$

Model (3+3)'

$$s_1 = -0.109 + 2.201i$$
$$s_2 = -0.109 - 2.201i$$
$$s_3 = -0.048 + 17.998i$$
$$s_4 = -0.048 - 17.998i$$

Model (3+5)'

$$s_1 = -0.115 + 2.040i$$
$$s_2 = -0.115 - 2.040i$$
$$s_3 = -0.053 + 12.380i$$
$$s_4 = -0.053 - 12.380i$$

Model (3+6)'

$$s_1 = -0.095 + 1.550i$$
$$s_2 = -0.095 - 1.550i$$
$$s_3 = -0.044 + 8.660i$$
$$s_4 = -0.044 - 8.660i$$

With this analytical information it is possible to construct a curve relating the damping power of the tail along with its stability power to the volute length l_V. (Figure 23 through 26) These can be used with caution to predict the frequency and damping characteristics of volute cylinder combinations different from the samples. Caution must be exercised because of the vast number of assumptions used to derive the analytical expressions. Also, the forebody in a particular problem must have about the same ΔB as the plotted values, which was about 0.440. It is best to refer back to the theory and begin with

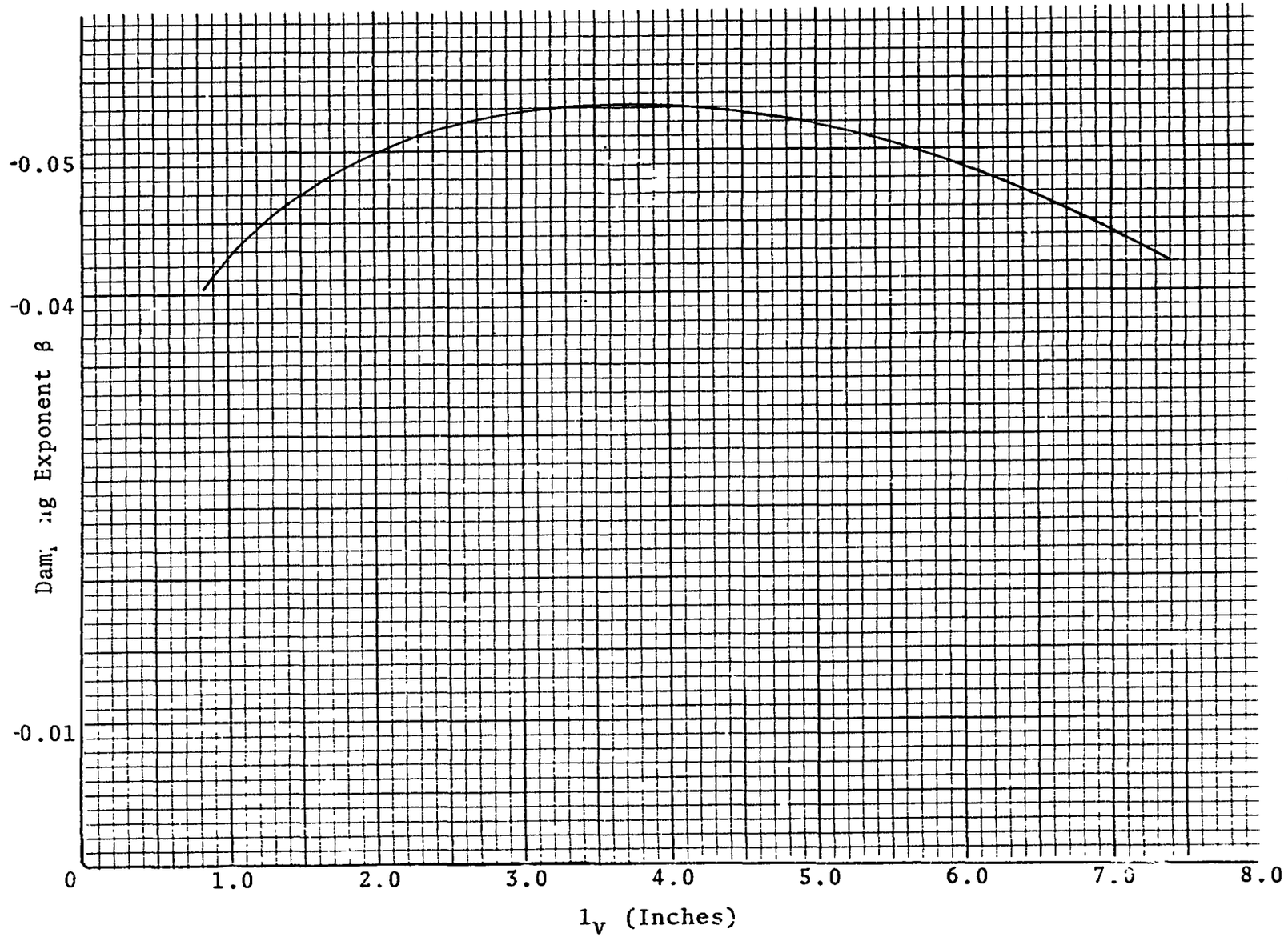

Figure 23. l_v Versus β

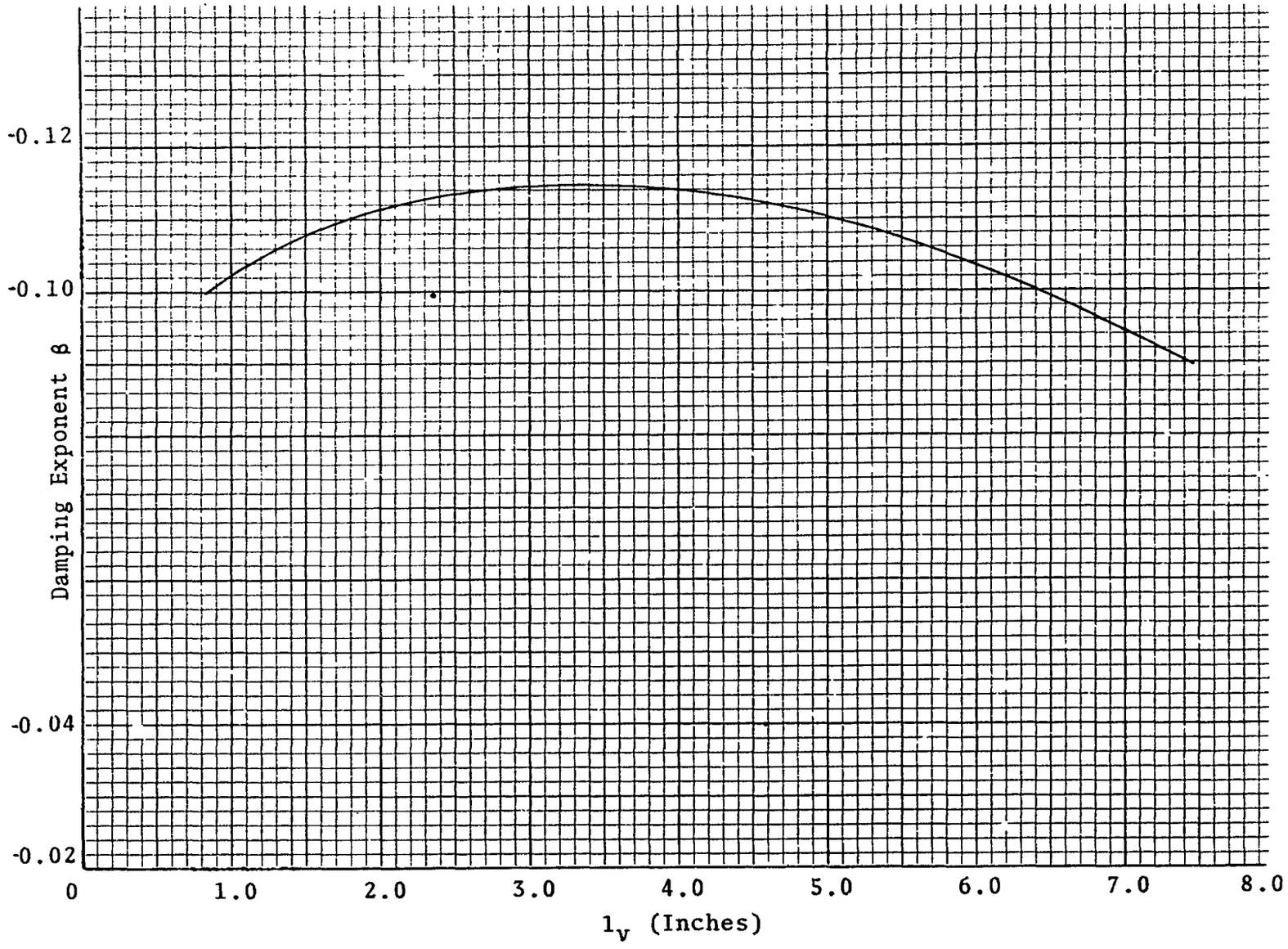

Figure 24. l_v Versus β

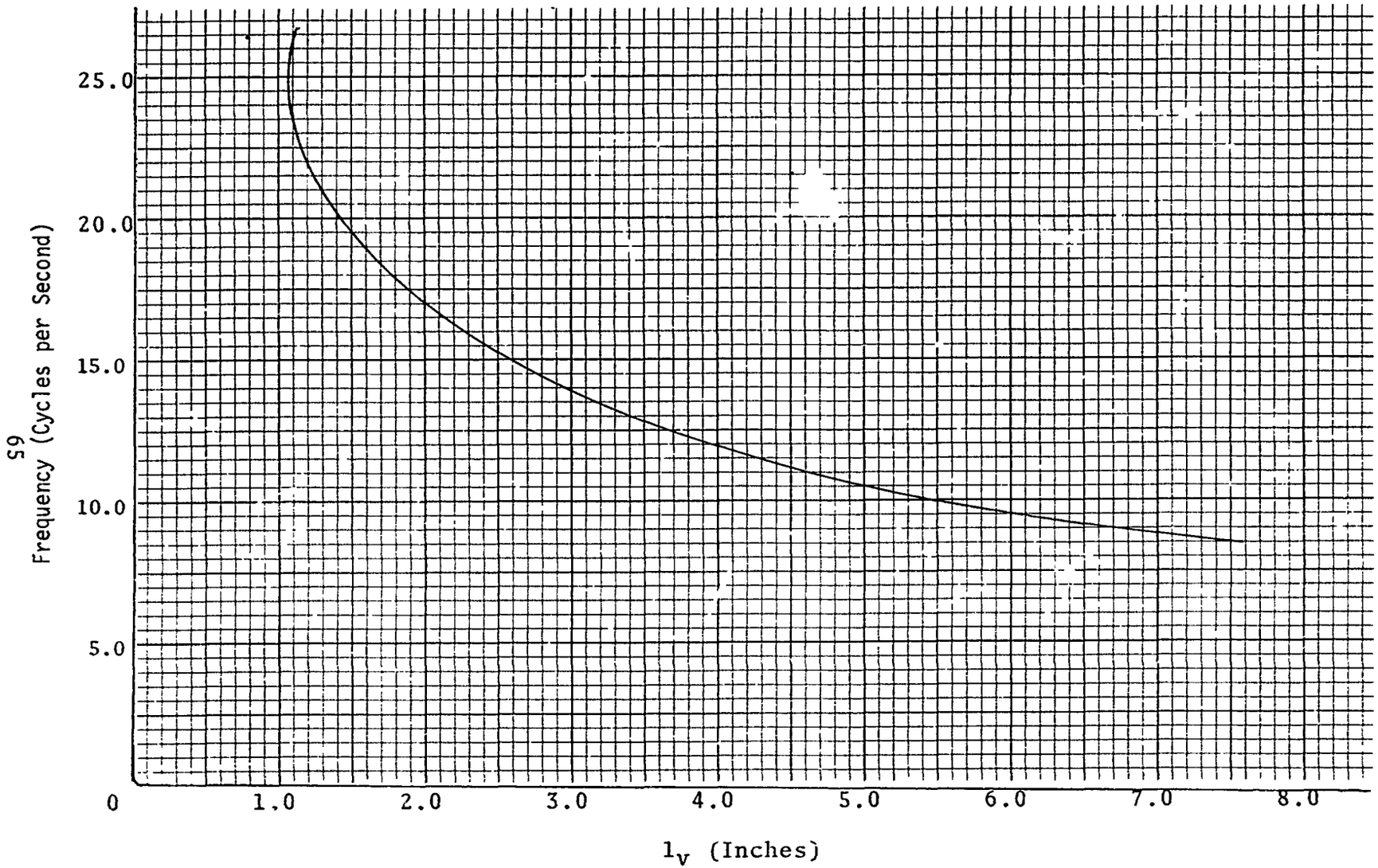

Figure 25. l_V Versus Frequency

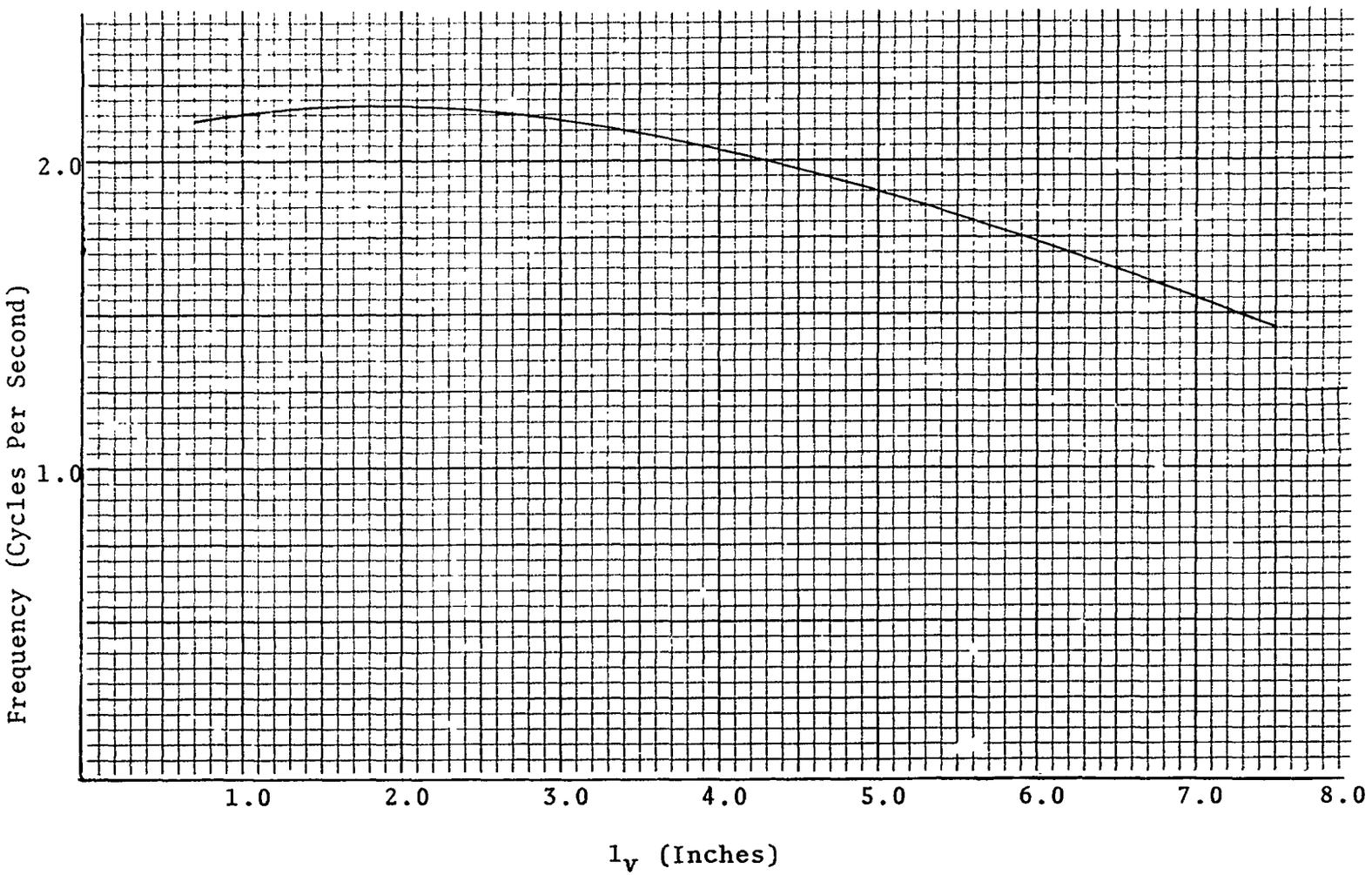

Figure 26. l_v Versus Frequency

the basic expressions for the a_{ij}'s and derive the stability margins for each case. Even when this is done, the answers represent only a first indication of the model stability characteristics and should be interpreted as necessary but not sufficient conditions for dynamic stability.

SECTION IV

FINAL DESIGN

The preceding sections served to outline two methods for finding the static and dynamic stability of volute equipped cylinders. The first method for rigid volutes only showed which of the volute parameters entered into the stability criteria and provided a base for the more complex flexible analysis which followed. Because of the anticipated complexity of the flexible analysis, the first approach there assumed a small mass volute but allowed bending. This method took into account bending by altering the rigid expression for C_{m_α} and $(C_{m_q} + C_{m_{\dot{\alpha}}})$ by a constant factor dependent upon the geometrical and structural constraints of the volute tail. The final analysis examined the dynamic stability of several models through characteristic equations extracted from the two angular equations of motion. It remains now to tie the preceding work together so that a systematic method can be used for a given problem. One more piece of information must be provided along with the aerodynamic analysis to allow this.

All aerodynamic work derived points to a best design length volute for a given cylinder; however, it may not be feasible to fit the optimum length into the cylinder cavity (Section I). The maximum length of the volute here is determined by the spring thickness and the cavity diameter. In some cases the design length obtained in the J method may be larger than the maximum length capable of being stored in the cylinder. To make matters more complicated, the spring constant k_V appears to be inversly proportional to the volute length for a given cross sectional inertia which changes the optimum l_V. This latter fact represents one of the most difficult parameters to estimate. That is, for a given material wound in a spiral to a length l_V, what is k_V?

During the study program it was discovered that k_V varies inversely with l_V. Only a limited number of volutes were tested, but these followed Equation (84):

$$k_V = (\text{Constant}) / l_V^z \qquad (84)$$

The spring used on Model (3+4)' was taken as the center point to evaluate (Constant). If $z = \frac{1}{2}$ the proportionality constant was found to be 0.501. If a given spring is close to the mentioned spring (Appendix II) in cross section material and

length, Equation (84) will give good answers. Large excursions must be dealt with separately.

For a volute to have maximum efficiency, it must be wound as lightly as possible. That is, viewed from the side, there should be no space between successive coils. To determine whether such a spring will fit into a given cylinder cavity, Equation (85) can be used.

$$nt_1 < R \tag{85}$$

To find the length of uncoiled wire needed to construct a volute with given l_V, use Equation (86):

$$l_V = 2\pi (R - (n - 1) t_1) \tag{86}$$

The volute length l_V is approximately,

$$l_V = nt_2 \tag{87}$$

Spring steel is recommended as the volute structural material; specifying the cross section would be at the discretion of the designer. The key flexible volute [(3 + 4)'] test model material, cross section was 0.020 x 0.200. For this material, Equation (84) can be used to find k_V. Using the J method to maximize C_{m_α} with respect to volute length l_V, variable $k_V = f(l_V)$ should be used if Equation (84) can be used or an alternate derived, based on different material than 0.020 x 0.200 spring steel. Variable k_V has a profound effect upon C_{m_α}. C_{m_α} falls off with l_V faster for $k_V = f(l_V)$ than k_V = constant. This fact adjusts the design l_V to a smaller value. Example 6 was carried out for k_V = constant. If Equation (84) is used instead, Table XI results:

TABLE XI. $C_{m_{\alpha_f}}$/Rad.

Let $k_V = \frac{0.501}{\sqrt{l_V}}$				
l_V	k_V	Φ	J	$C_{m_{\alpha_f}}$
0				
0.5	0.708	0.3343	0.0021	-0.03485
1.5	0.4090	0.3237	0.0337	-0.11798
2.0	0.3543	0.3145	0.0612	-0.15786
2.5	0.3168	0.3019	0.0988	-0.19142
3.0	0.2892	0.2876	0.1415	-0.21744
3.5	0.2678	0.2725	0.1866	-0.23600
4.0	0.2505	0.2572	0.2322	-0.24695
4.5	0.2362	0.2423	0.2767	-0.25180
5.0	0.2241	0.2281	0.3191	-0.25162
5.5	0.2136	0.2148	0.3588	-0.24740
6.0	0.2045	0.2023	0.3959	-0.24000
6.5	0.1965	0.1906	0.4310	-0.22929
7.0	0.1890	0.1802	0.4621	-0.21855
7.5	0.1829	0.1705	0.4910	-0.20599
8.0	0.1771	0.1614	0.5182	-0.18911
8.5	0.1718	0.1533	0.5424	-0.17919

These values were plotted in Figure 27 and compared to the results of Example 6. If k_V cannot be found as a function of l_V, use the best constant value (from elastic testing if possible).

It is likely that the first step in designing a volute stabilizer will be to insure rigid static stability. The approximate dimensions of the best design volute are obtainable from the simple rigid analysis if the spring constant is very large (2 pounds/radian), or if the volute is short. Generally, the volute stabilizer will not have k_V as large as 2 pounds/radian, probably closer to 0.300 or 0.400 pounds/radian. In these cases, the J method should be used to follow up the first order approximate rigid analysis and the tail length altered according to the results. Dynamic stability can be checked for this configuration best in a wind tunnel. However, the two-dimensional angular freedom analysis will provide at least a first approximation to what the dynamic stability characteristics will be like. Since the observed limit cycle motion referred to in the text appeared to result from pitch-yaw coupling, a more precise analysis will have to wait until completion of the second year study.

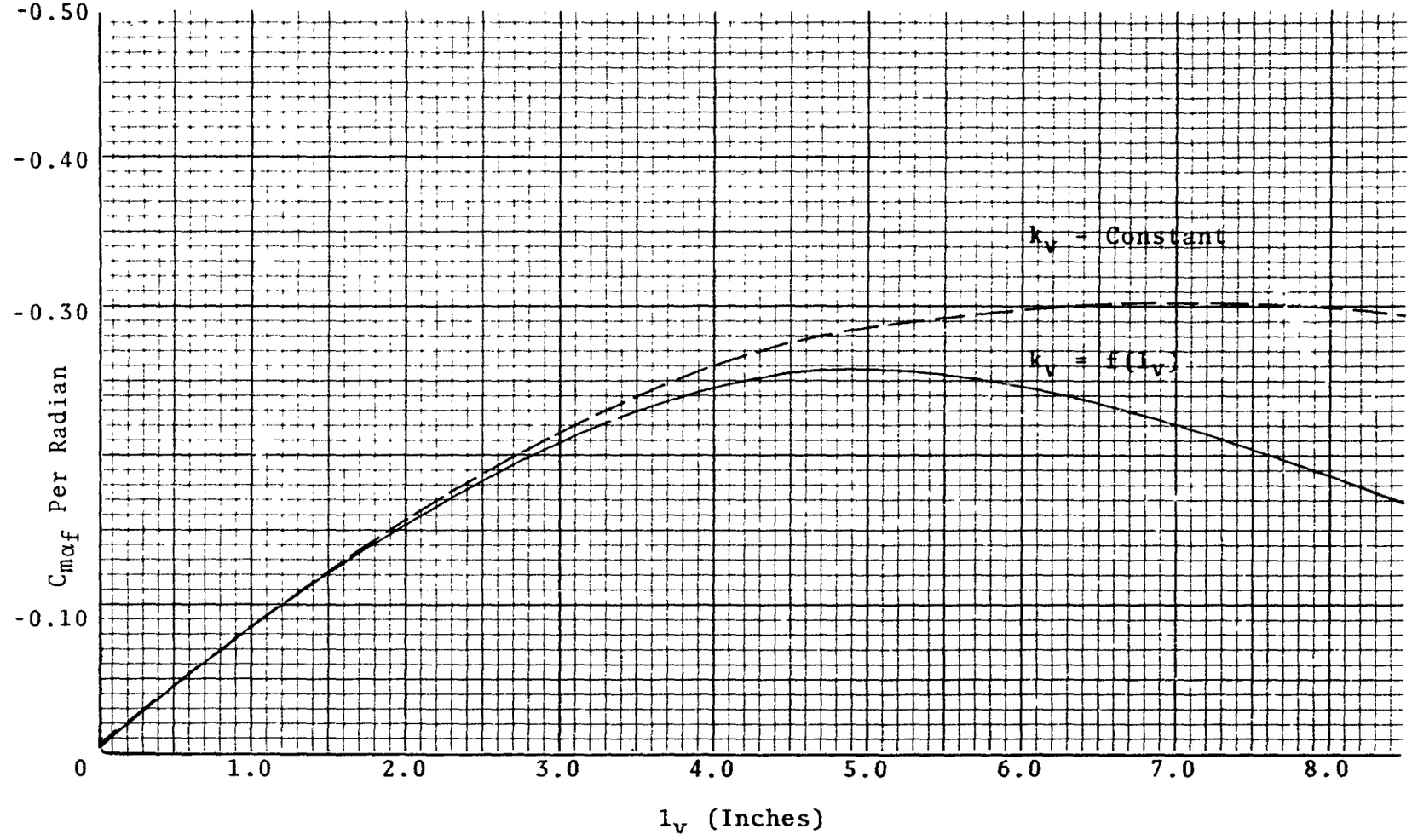

Figure 27. l_v Versus $C_{m_{\alpha f}}$

SECTION V

CONCLUSIONS

The preceding analysis, together with data collected at the Eglin Air Force Base low speed wind tunnel and free flight data collected at the Von Karman Gas Dynamic Facility, proved that the volute stabilizer is a feasible and practical approach to providing a compact stabilizer for cylindrical forebodies. The rigid and flexible body analysis yielded a convenient method of estimating the effects on both static and dynamic stability when the various geometrical constraints of the volute shape are altered. For each case, the analysis provides the necessary and sufficient conditions to insure static stability and thereby proved that properly designed and matched volute tails insure absolute static stability.

The extensive amount of wind tunnel testing conducted at the two facilities clearly indicated that all test volutes constructed of coiled spring steel operating at M = 0.2 to 0.6 and R_n = 1 x 10^5 to 1 x 10^6 suffer a certain amount of residual vibrations which apparently never damp out. This, as shown in the analysis, can be offset through proper volute design; however, it appears that these limit cycles can never be removed entirely. The effect on stability can be reduced to a point where the forebody wanders through ± 5 degrees arc. The amplitude of the limit cycle motion is sensitive to the lateral spring constant of a given spring tail and under some conditions will produce $(C_{m_q} + C_{m_{\dot{\alpha}}}) > 0$ causing divergence up to a certain maximum amplitude, the largest observed to be about ± 30 degrees.

Under nearly steady state conditions, the cylinder equipped with a volute stabilizer will trim out at a trim angle which is controlled by the volute length and the cg location. This trim angle can be reduced to nearly zero if the cylinder-volute combination is carefully matched. If this is not done, the combination can be expected to trim out at an angle different from 0.

(The reverse of this page is blank)

APPENDIX I

ANALYSIS

The 1-d rigid volute model is analyzed in detail below. Because this particular model is more amenable to analytical treatment than the remaining flexible models, this section identifies and treats the basic volute parameters which affect aerodynamic damping and pitching moment. The effects of cg movement and forebody induced tail blanking are included separately.

At the outset of the analysis, the following assumptions are made:

(1) The volute is attached rigidly to the forebody

(2) The volute is a complete cone

(3) All area behind the cg acts as a tail, all area in front of the cg acts against the tail

(4) Normal force coefficients are based upon cone-cylinder combinations and strictly cones or cylinders

Volute and forebody geometry will be identified according to the following diagram:

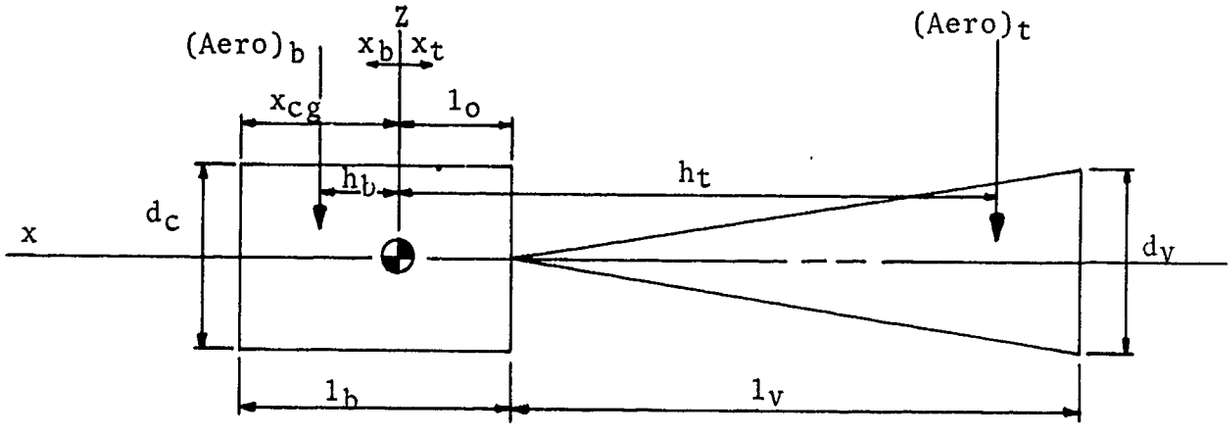

A stabilizing pitching moment is set up primarily because of a normal component of velocity relative to the volute forebody axis. By finding this component of velocity and an appropriate normal force coefficient evaluated at $\pi/_2$, the normal force can be calculated.

Relative Velocity

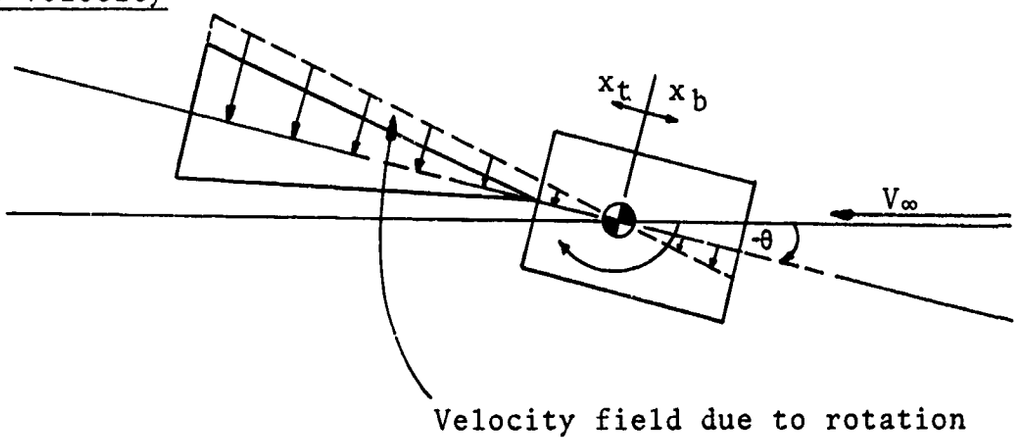

Moving out to a point on the forebody, the relative velocity there can be found with the aid of the vector diagram below.

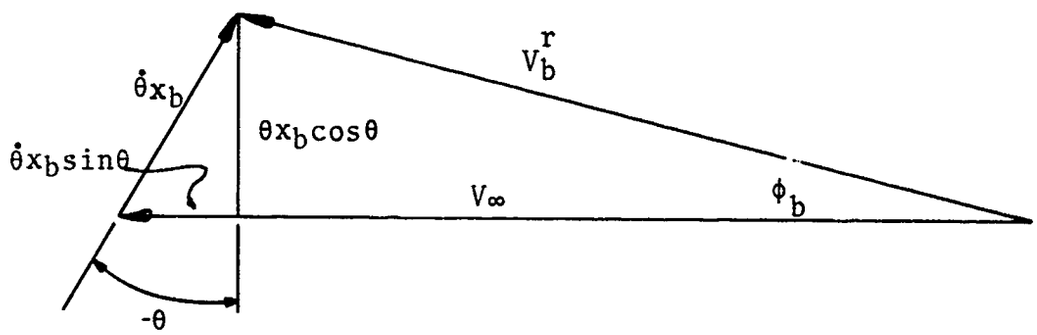

$$V_b^r = \left[(V_\infty - \dot{\theta}x_b\sin\theta)^2 + (\dot{\theta}x_b\cos\theta)^2\right]^{\frac{1}{2}}$$

The angle between the free stream velocity and the relative velocity obtained from the diagram is:

$$\phi_b = \tan^{-1}\left[\frac{\dot{\theta}x_b\cos\theta}{V_\infty - \theta x_b\sin\theta}\right]$$

Tail quantities are obtained in a similar manner. The rotation induced field adds to the free stream field to give:

$$V_t^r = \left[(V_\infty + \dot{\theta} x_t \sin\theta)^2 + (\dot{\theta} x_t \cos\theta)^2 \right]^{1/2}$$

$$\phi_t = \tan^{-1} \left[\frac{\dot{\theta} x_t \cos\theta}{V_\infty + \dot{\theta} x_t \sin\theta} \right]$$

Assumptions:

(5) Approximate x_b and x_t with the average values $\hat{x}_b$ and $\hat{x}_t$.

(6) $V_\infty >> \dot{\theta}\hat{x}$ so that $\phi_b \cong \dot{\theta}\hat{x}b/V_\infty$, $\phi_t \cong \dot{\theta}\hat{x}t/V_\infty$

To find the normal component of velocity, the angle of attack α must be found. This is done with the following diagram:

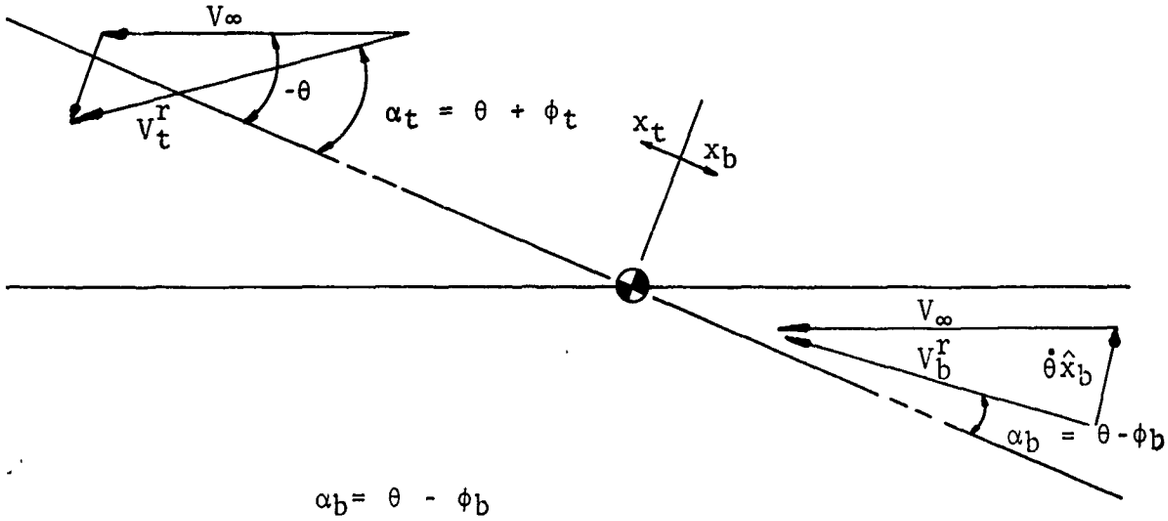

$$\alpha_b = \theta - \phi_b$$

$$\alpha_t = \theta + \phi_t$$

With the angle of attack for both the "b" and "t" sections known, the normal component of velocity is expressed as:

$$V_b^n = V_b^r \sin\alpha_b$$

$$V_t^n = V_t^r \sin\alpha_t$$

$$V_b^n = V_\infty \sin\theta - \dot{\theta}\hat{x}_b$$

$$V_t^n = V_\infty \sin\theta + \dot{\theta}\hat{x}_t$$

Moment Balance

To find the total aerodynamic moment acting on the total body, moments are summed about the center of gravity.

Assumptions:

(7) Use average moment arms h_b and h_t

(8) Use $C_{n_{t_o}}$ based on cone-cylinder values evaluated for $\pi/_2$ radians.

(9) $\sin\theta \cong \theta$

(10) There is no tail forebody interference

Then,

$$-I\ddot{\theta} = \tfrac{1}{2}\rho C_{n_{t_o}} h_t (V_\infty\theta + \hat{x}_t\dot{\theta}) |V_\infty\theta + \hat{x}_t\dot{\theta}| S_t$$

$$- \tfrac{1}{2}\rho C_{n_{b_o}} h_b (V_\infty\theta - \hat{x}_b\dot{\theta}) |V_\infty\theta - \hat{x}_b\dot{\theta}| S_b$$

Assumption:

(11) The ratio $\left|\theta - \frac{\hat{x}_b}{V_\infty}\dot{\theta}\right| / \left|\theta + \frac{\hat{x}_t}{V_\infty}\dot{\theta}\right| \cong 1$

Then,

$$-I\ddot{\theta} = \tfrac{1}{2}\rho C_{n_{t_o}} h_t \hat{x}_t S_t V^2_\infty \left[\dot{\theta}\left|\theta + \frac{\hat{x}_t}{V_\infty}\dot{\theta}\right|\right]\left[1 + \frac{C_{n_{b_o}} h_b S_b \hat{x}_b}{C_{n_{t_o}} h_t S_t \hat{x}_t}\right]$$

$$+ \tfrac{1}{2}\rho C_{n_{t_o}} h_t S_t V^2_\infty \left[\theta\left|\theta + \frac{\hat{x}_t}{V_\infty}\dot{\theta}\right|\right]\left[1 - \frac{C_{n_{b_o}} h_b S_b}{C_{n_{t_o}} h_t S_t}\right]$$

Let

$$V_h = h_b S_b / h_t S_t \quad , \quad \tilde{\theta} = \theta + \hat{x}_t / V_\infty \dot{\theta}$$

Assumption:

(12) $$C_{n_{t_o}} h_t \hat{x}_t S_t \left[1 + \frac{C_{n_{b_o}} \hat{x}_b}{C_{n_{t_o}} \hat{x}_t} V_h\right] |\tilde{\theta}| \cong$$

$$C_{n_{t_o}} h_t \hat{x}_t S_t \left[1 + \frac{C_{n_{b_o}} \hat{x}_b}{C_{n_{t_o}} \hat{x}_t} V_h\right] |\theta|$$

and $$C_{n_{t_o}} h_t S_t \left[1 - \frac{C_{n_{b_o}}}{C_{n_{t_o}}} V_h\right] |\tilde{\theta}| \cong$$

$$C_{n_{t_o}} h_t S_t \left[1 - \frac{C_{n_{b_o}}}{C_{n_{t_o}}} V_h\right] |\theta|$$

(13) Let $C_{nt_o}|\theta| \cong C_{nt_o}\hat{\theta}$. Static normal force coefficients can be expressed as $C_{nt} = C_{nt_\alpha}\,\alpha + C\sin^2\alpha$. Thus $C_{nt_o} = C_{nt_\alpha}(\pi/2) + C$. This assumption averages $C_{nt_o}|\theta|$ over θ, and requires that $C_{n_{\dot{\theta}}}$ be small.

$$-I\ddot{\theta} = \tfrac{1}{2}\rho V^2_\infty dS\left[\dot{\theta}\,\frac{S_t C_{nt_o} h_t \hat{x}_t}{d_c^2 S}\left[1 + \frac{C_{nb_o}\hat{x}_b}{C_{nt_o}\hat{x}_t}V_h\right]\frac{d_c\hat{\theta}}{V_\infty} + \theta\,\frac{C_{nt_o}h_t S_t}{d_c S}\left[1 - \frac{C_{nb_o}V_h}{C_{nt_o}}\right]\hat{\theta}\right]$$

From linear aerodynamics:

$$I\ddot{\theta} = \tfrac{1}{2}\rho V^2_\infty dS\left[\dot{\theta}\frac{d}{2V_\infty}\,(C_{mq} + C_{m_{\dot{\alpha}}}) + C_{m_\alpha}\theta\right]$$

By identification of common terms:

$$(C_{mq} + C_{m_{\dot{\alpha}}}) = -\frac{2S_t C_{nt_o} h_t \hat{x}_t}{d_c^2 S}\left[1 + \frac{C_{nb_o}\hat{x}_b}{C_{nt_o}\hat{x}_t}V_h\right]\hat{\theta}$$

$$C_{m_\alpha} = -\frac{S_t C_{nt_o} h_t}{d_c S}\left[1 - \frac{C_{nb_o}V_h}{C_{nt_o}}\right]\hat{\theta}$$

$$\text{If,} \qquad V_h' = h_t S_t/d_c S$$

$$(C_{mq} + C_{m_{\dot{\alpha}}}) = -C_{nt_o}V_h'\frac{\hat{x}_t}{d_c}\left[1 + \frac{C_{nb_o}\hat{x}_b}{C_{nt_o}\hat{x}_t}V_h\right]\hat{\theta}$$

$$C_{m_\alpha} = -C_{nt_o}V_h'\left[1 - \frac{C_{nb_o}V_h}{C_{nt_o}}\right]\hat{\theta}$$

The effects of cg movement can best be determined by relating the movement to pitching and damping derivatives through the above equations. Taking the pitching moment slope coefficient first:

$$C_{m_\alpha} = - C_{n_{t_o}} V_{h'} \left[1 - \frac{C_{n_b} h_b S_b}{C_{n_{t_o}} h_t S_t} \hat{\theta} \right]$$

for, $$\frac{C_{n_{b_o}} h_b S_b}{C_{n_{t_o}} h_t S_t} < 1, \; C_{m_\alpha} < 0$$

This constraint can be related to the cg location by expressing the individual terms as functions of x_{cg}. When this is done:

$$-C_{m_\alpha} = \frac{1}{d_c S} \left(\tfrac{1}{2} \tilde{C}_{n_{b_o}} (S_f - d_c x_{cg})(l_b - x_{cg}) + \right.$$

$$\left. \tilde{C}_{n_{v_o}} S_v (l_b - x_{cg} + a l_v) - \tilde{C}_{n_{b_o}} \frac{x_{cg}}{2} (x_{cg} d_c) \right)$$

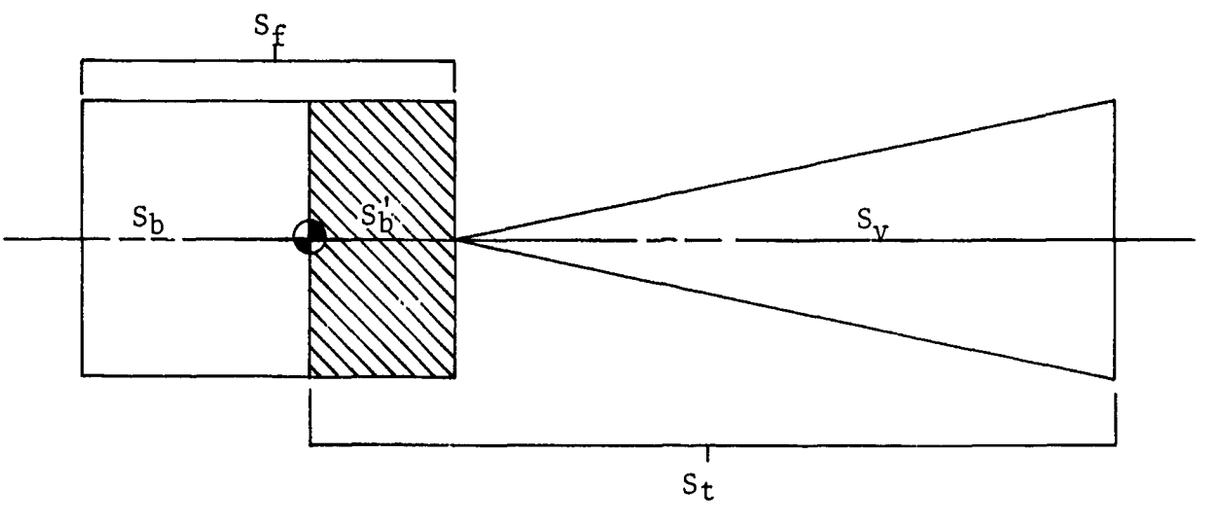

The individual terms as functions of x_{cg} are:

$$\tilde{C}_{nb_o} = C_{nb_o}\,\hat{\theta}$$

$$h_b = \frac{x_{cg}}{2}$$

$$S_b = d_c x_{cg}$$

$$C_{nt_o} = \frac{1}{S_t}\left(C_{nb_o}S_b + C_{n_{v_o}}S_v\right)\hat{\theta}$$

$$C_{nt_o}S_t h_t = C_{nb_o}S_b\,(l_b - x_{cg})\tfrac{1}{2} + C_{n_{v_o}}S_v(l_b - x_{cg} + al_v)$$

$$S_b' = S_f - d_c x_{cg}$$

Note, that because C_{nt_o} is made up of normal force coefficients of both the cylinder and cone portions aft of the rotational axis, it is a function of cg location.

After some reduction:

$$-C_{m_\alpha} = \tilde{x}_{cg}\left(\tilde{S}_f(\tilde{C}_{nb_o} + \tilde{C}_{n_{v_o}}) - \tilde{C}_{n_{v_o}}\right) +$$

$$\tilde{C}_{n_{v_o}}(1 - \tilde{S}_f)\left(a\tilde{l}_v + \tilde{l}_b\right) + \tfrac{1}{2}\tilde{C}_{nb_o}\tilde{S}_f\tilde{l}_b$$

Where

$$\tilde{x}_{cg} = x_{cg}/d_c,\ \tilde{S}_f = S_f/S,\ \tilde{l}_v = l_v/d_c,\ \tilde{l}_b = l_b/d_c$$

A more convenient form of the above was obtained from Reference 3 wherein a method is derived which allows prediction of C_{m_α} about any axis, if C_{m_α}' is known about any other axis in the forebody. The transfer equation is:

$$C_{m_\alpha} = C_{m_\alpha}' + \frac{x_{cg}}{d_c} C_{n_\alpha}$$

C_{n_α} has to be determined for each volute-forebody configuration. C_{m_α}' can be obtained by setting x_{cg} to zero in the cg equation or, directly, from the definition of C_{m_α}. When this is done:

$$-C_{m_\alpha}' = C_{n_{v_o}} \hat{\theta}\left(1 - \frac{S_f}{S}\right)\left(a \frac{l_v}{d_c} + \frac{l_b}{d_c}\right) + \frac{1}{2} C_{n_{b_o}} \hat{\theta} \frac{S_f}{S} \frac{l_b}{d_c}$$

$$= \frac{h_t C_{n_{t_o}}}{d_c} \hat{\theta}, \quad h_t C_{n_{t_o}} = l_b\left(\frac{C_{n_{b_o}}}{2} - \frac{C_{n_{b_o}} S_v}{2S} + \frac{C_{n_{v_o}} S_v}{S}\right)$$

$$+ a\, C_{n_{v_o}} \frac{S_v}{S} l_v$$

The damping derivative turns out to be a quadratic function of the cg location. The equation is too unwieldy for general usage but is duplicated below for completeness:

$$C_{m_q} + C_{m_{\dot{\alpha}}} = \frac{1}{d_c \overline{S}}\left[x^2_{cg}\left(\frac{3}{4}\tilde{C}_{n_{b_o}} l_b + \frac{1}{2} l_v\left[\tilde{C}_{n_{v_o/2}} + a\,\tilde{C}_{n_{b_o}}\right]\right)\right.$$

$$+ x_{c.g.}\left(-\frac{3}{4}\tilde{C}_{n_{b_o}} l_b^2 - \frac{3}{4}\tilde{C}_{n_{v_o}} a l_v^2 - l_v l_b\left[\tilde{C}_{n_{v_o/2}} - a\,\tilde{C}_{n_{b_o}}\right]\right)$$

$$+ \frac{1}{4}\tilde{C}_{n_{b_o}} l_b^3 + l_b^2\, l_{v/2}\left[\tilde{C}_{n_{v_o/2}} + a\,\tilde{C}_{n_{b_o}}\right] + \tilde{C}_{n_v} l_v^2 l_b$$

$$\left. + \tilde{C}_{n_v} \frac{1}{2} l_v^3 a^2\right]$$

The derivation follows that used for C_{m_α} as a function of cg. $\hat{x}_t$ is defined to be:

$$\hat{x}_t = (l_b - x_{cg})/2 + al_v$$

$$\hat{x}_b = x_{cg}/2$$

Since C'_{m_α} was found, it is possible to use parallel axis transfer equations to find the effect of cg movement of the damping derivative. This equation is extracted from Reference 3 and appears as:

$$(C_{m_q} + C_{m_{\dot{\alpha}}}) = (C_{m_q} + C_{m_{\dot{\alpha}}})' + \frac{x_{cg}}{d_c}\left(C'_{n_q}\right)$$

$$- \frac{x_{cg}}{d_c}\left(C_{m_\alpha}\right) - \left(\frac{x_{cg}}{d_c}\right)^2 C_{n_\alpha}$$

It is much easier to use than the one derived directly from the definition. If the primed parameters are measured from the nose of the forebody (consistent with the definition of x_{cg}) and C_{n_q} is small, the damping derivative as a function of cg location is:

for, $$C_{m_\alpha}' = - \frac{h_t C_{n_{t_o}}}{d_c}\hat{\theta}$$

and, $$x_{cg} > 0 \quad (C_{m_q} + C_{m_{\dot{\alpha}}}) = - x^2_{cg}\left(\frac{C_{n_\alpha}}{d_c^2}\right)$$

$$+ x_{cg}\left(\frac{h_t C_{n_{t_o}}}{d_c^2}\right)\hat{\theta} + (C_{m_q} + C_{m_{\dot{\alpha}}})\Big|_{x_{cg} = 0}$$

$$= - x^2_{cg} \left(\frac{C_{n_\alpha}}{d_c^2}\right) + x_{cg} \left(\frac{h_t C_{n_{to}}}{d_c^2}\hat{\theta}\right) - \frac{h_t C_{n_{to}}}{d_c^2}\hat{x}_t\ \hat{\theta}$$

The cg location for maximum damping will occur at:

$$x_{cg} = \tfrac{1}{2} h_t \frac{C_{n_{to}}}{C_{n_\alpha}}\hat{\theta}$$

In the derivation of the above formulas, an average moment arm and average value for the rotary velocity field was assumed. The average value was introduced with the constant multiplied by l_v (i.e., al_v). "a" was used both in the expression for average moment arm and average rotary velocity. The value will be taken as $\frac{2}{3}$. The expressions for $\hat{x}_t$, h_t, and later $\hat{x}_{v_t}$ are complex and depend upon θ and $\dot{\theta}$. The following analysis is devoted to this subject:

$$\underline{\hat{x}}_t \qquad \iint_{S_b' + S_v} V^2 d\ S = V^2_{ave}\ S$$

Plugging in the necessary values and reducing,

$$\int_0^{l_o} (V^2_\infty \sin^2\theta + 2V_\infty x \sin\theta\dot{\theta} + \dot{\theta}^2 x^2) d_c dx$$

$$+$$

$$\int_{l_o}^{l_o + l_v} (V^2_\infty \sin^2\theta + 2V_\infty x \sin\theta\dot{\theta} + \dot{\theta}^2 x^2)\ \frac{d_v}{l_v}\ (x - l_o)\ dx =$$

$$= \left(\tfrac{1}{2}\, d_V l_V + d_C l_O\right)\left(V^2_\infty \sin^2\theta + 2V_\infty \sin\theta\, \dot{\theta}\, \hat{x}_t + \dot{\theta}^{\,2}\hat{x}_t^{\,2}\right)$$

$$\hat{x}_t^{\,2} = \frac{\tfrac{2}{3}\, l_O^{\,3} + \tfrac{4}{3}\, l_O l_V^{\,2} + l_V l_O^{\,2} + \tfrac{1}{2}\, l_V^{\,3}}{2l_O + l_V}, \theta = 0$$

$$\hat{x}_t = \frac{l_O^{\,2} + l_V l_O + \tfrac{2}{3}\, l_V^{\,2}}{2l_O + l_V}, \dot{\theta} = 0$$

$\underline{\hat{x}}_{V_t}$

$\hat{x}_{V_t}$ is found from the following identity:

$$\int_0^{l_V} V^2 \left(\frac{d_V}{l_V}\right) x \, dx = V^2 \text{ ave } S$$

Inserting the necessary values and reducing,

$$\int_0^{l_V} \left[V^2_\infty \sin^2\theta + 2V_\infty \sin\theta (x + l_O)\dot{\theta} + \dot{\theta}^2 (x^2 + 2xl_O + l_O^{\,2})\right]\frac{d_V}{l_V}\, x \, dx$$

$$= \tfrac{1}{2}\, d_V l_V \left(V^2_\infty \sin^2\theta + 2V_\infty \sin\theta\, \dot{\theta}\hat{x}_{V_t} + \dot{\theta}^2 \hat{x}_{V_t}^{\,2}\right)$$

$$\hat{x}_{V_t}^{\,2} = l_V^2/2 + 4l_V l_O/3 + l_O^{\,2}, \theta = 0$$

$$\hat{x}_{V_t} = l_O + \tfrac{2}{3} l_V, \dot{\theta} = 0$$

$\underline{h_t}$

h_t is found with the following identity:

$$\iint_{S_V} V^2 x \, dS = V^2 \text{ave } h_t' S_V$$

Inserting the necessary values and reducing,

$$\int_0^{l_V} (x + l_o)\left[(V^2_\infty \sin^2\theta + 2V_\infty \sin\theta\dot{\theta}(x + l_o) + \dot{\theta}^2(x + l_o)^2\right]\frac{d_V}{l_V}\, x\, dx =$$

$$\frac{1}{2}\, d_V l_V (V^2_\infty \sin^2\theta + 2V_\infty \sin\theta\dot{\theta}\hat{x}_{Vt} + \dot{\theta}^2\hat{x}^2_{Vt})h'_t$$

$$h'_t = \frac{1}{\hat{x}^2_{Vt}}\left(\frac{3}{2}\, l_o l_V^2 + 2l_o^2 l_V + \frac{2}{5}\, l_V^3 + l_o^3\right),\ \theta = 0$$

$$h'_t = l_o + \frac{2}{3}\, l_V, \dot{\theta} = 0$$

The above forms are gotten by carrying out the integrations and alternately setting θ then $\dot{\theta}$ equal to zero. The three variables span a range of values which can be considered to be the upper and lower bounds of each during one cycle of oscillation. It was found that using $\hat{x}_t = l_o/2 + \frac{2}{3}l_V$ gives reasonable answers and is easier to use than the derived expressions which themselves are only approximate. h'_t and $\hat{x}_{Vt}$ give good answers defined as $h'_t = (l_o + \frac{2}{3}l_V)$ and $\hat{x}_{Vt} = (l_o + \frac{1}{2}l_V)$. Note that in the expression for h'_t at $\theta = 0$, h'_t is inversely proportional to the square of $\hat{x}_{Vt}$. A plot of h'_t shows that for certain values of l_V, h'_t actually decreases for increase in l_V up to a point and then increases.

The preceding forms do not consider forebody interference. Because the forebody interrupts the air flow over the volute tail, the effectiveness of any volute is lowered. To find what percentage of the tail is blanked out by the forebody, the following approximate analysis is offered. Note that here a trapezoidal area for the volute is used instead of the typical triangular planform. This is done because at low angles of attack this additional area has a significant effect on the volute performance if d'_V is large or about $d_V 5$. The following diagram is useful:

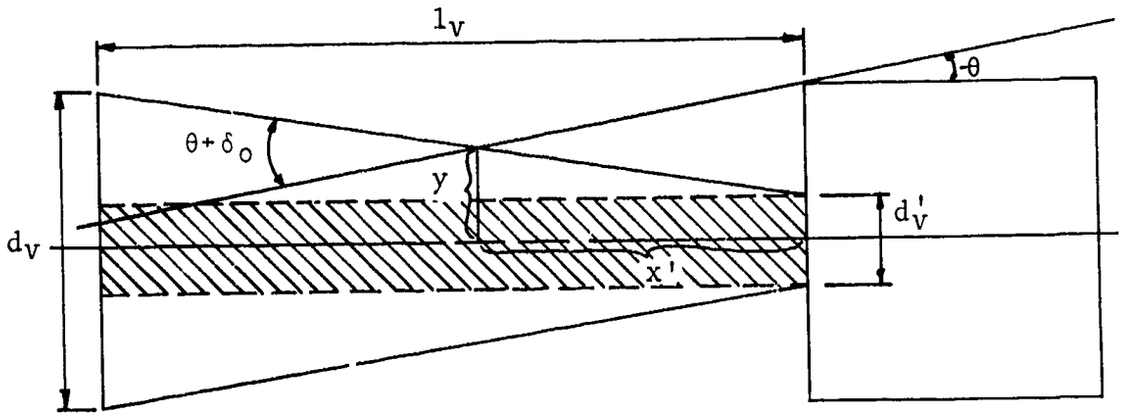

$$\tan\delta_o = \frac{(y - d_v\frac{1}{2})}{x}, \quad (y - d_v\,\tfrac{1}{2}) = x\tan\delta_o$$

$$S_v \text{ (two trapezoidal pieces)} = \int_{x'}^{l_v} 2x\tan\delta_o dx$$

$$S_v' = \tan\delta_o(l_v^2 - x'^2), \quad x' = \frac{d_v - d_v'}{2(\tan\theta + \tan\delta_o)} = \frac{\bar{d}_v}{2(\tan\theta + \tan\delta_o)}$$

$$S_v' = \tan\delta_o\left(\frac{-\bar{d}_v^{\,2}}{4(\tan\theta + \tan\delta_o)^2}\right) + \tan\delta_o l_v^2$$

$$\frac{S_v'}{\bar{d}_v^{\,2}} = \frac{l_v}{2\bar{d}_v} - \frac{\bar{d}_v}{l_v 8}\,\frac{1}{(\tan\theta + \frac{\bar{d}_v}{2l_v})^2}$$

$$S_v'' \text{ (shaded portion)} = d_v'(l_v - x')$$

$$S \text{ (total area)} = S_v' + S_v''$$

Overshadowing the previous analysis is the obvious fact that the volute is not rigid, but flexible. This fact alters the previous expressions for damping and pitching derivatives. To make the analysis as tenable as possible, the first flexible volutes considered will have small masses and moments of inertia.

Using the following diagram, basic flexible volute formulas can be derived.

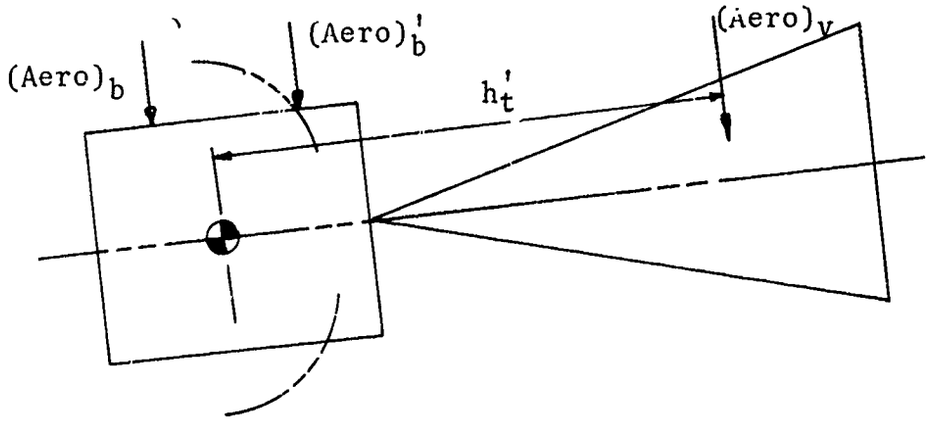

The stability equation for the flexible combination can be written as was the rigid form if the volute contribution contains the pitch angle and the volute angle in the aerodynamic force expression. Symbolically this is:

$$\circlearrowleft \sum M_{cg} \cong -(\text{aero})_b \frac{x_{cg}}{2} + (\text{aero})_b' \frac{l_o}{2} + (\text{aero})_v h_t'$$

The inertia torque of the masses can be shown (Reference 4) to be:

$$I\ddot{\theta} + K_v\ddot{\delta}$$

where,

$$I = M_v R_v^2 + 2M_v R_v \bar{r}_v + I_v + I_b$$

$$K_v = M_v R_v \bar{r}_v + I_v$$

Written out the whole expression is:

$$I\ddot{\theta} + K_v\ddot{\delta} = -\tfrac{1}{2}\rho V_\infty^2 S d_c \left[\left[-\frac{C_{n_{b_o}} S_b h_b}{d_c S} + \frac{C_{n_{b_o}} S_b' h_b'}{d_c S} + \frac{C_{n_{v_o}} S_v h_t'}{d_c S} \right] \theta \Phi \right.$$

$$+ \left[\frac{2C_{n_{b_o}} S_b \hat{x}_b h_b}{d_c^2 S} + \frac{2C_{n_{b_o}} S_b' \hat{x}_b' h_b'}{d_c^2 S} + \frac{2C_{n_{v_o}} S_v \hat{x}_{v_t} h_t'}{d_c^2 S} \right] \dot{\theta} \frac{d_c}{2V_\infty} \Phi$$

$$\left. + \left(\frac{C_{n_{v_o}} S_v h_t'}{d_c S} \right) \delta \Phi + \left(\frac{2C_{n_{v_o}} S_v \hat{x}_v h_t'}{d_c^2 S} \right) \dot{\delta} \frac{d_c}{2V_\infty} \Phi \right], \quad \Phi = |\theta + \delta|_{\text{average}}$$

To take a closer look at the tail reaction, a free body diagram is drawn and moments summed relative to a nonrotating but linearly accelerating observer. To account for this, the inertia term is written according to:

$$\sum M_{\text{external}} = \frac{d}{dt}\left(\int_m \vec{R} \times (\vec{\omega} \times \vec{R})\, dm \right) + M_v (\vec{R}_{c.m.} \times \vec{a}_o)$$

Which yields in terms of problem variables:

$$I\ddot{\xi} + M_V R_V \bar{r}_V \ddot{\theta} \quad , \xi = \theta + \delta$$

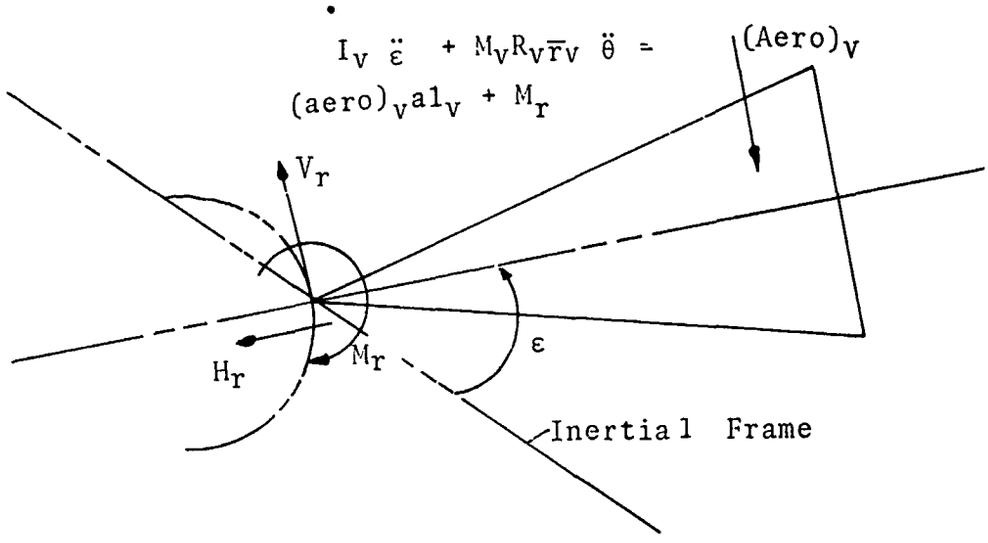

If the volute is idealized to have negligible mass and moment of inertia, the above reduces to:

$$- k_V \delta = (aero)_V \; a \; l_V \simeq \tfrac{1}{2}\rho V^2{}_\infty C_{n_{V_O}} \; \Phi \; (\theta + \delta) \; a \; l_V S_V$$

This is a constraint on δ expressible as:

$$\delta = - \frac{\tfrac{1}{2}\rho V_\infty^2 \; C_{n_{V_O}} \; \Phi \; a \; l_V S_V}{k_V + \tfrac{1}{2}\rho V^2{}_\infty C_{n_{V_O}} \; \Phi \; a \; l_V S_V} \; \theta$$

$$\delta = - J\theta$$

Note that the damping force was assumed small compared to $C_{nV_O} V_\infty^2 S$.

The inclusion of this expression into the basic flexible form equation reduces the expression to the familiar rigid form with variables $\ddot{\theta}$, $\dot{\theta}$, θ. The coefficients of θ and $\dot{\theta}$ respectively are:

$$I\ddot{\theta} + K_V\ddot{\delta} = \tfrac{1}{2}\rho V^2{}_\infty S d_c \left[\left[\left(\frac{C_{n_{b_o}} S_b' h_b'}{d_c S} + \frac{C_{n_{b_o}} S_V h_t'}{d_c S} \right) \Phi - \left(\frac{C_{n_{b_o}} S_b h_b}{d_c S} + \frac{J C_{n_{v_o}} S_V h_t'}{d_c S} \right) \Phi \right] \frac{\theta}{\equiv} \right]$$

$$+ \tfrac{1}{2}\rho V^2{}_\infty S d_c \left[\left(\frac{2C_{n_{b_o}} S_b \hat{x}_b h_b}{d_c{}^2 S} + \frac{2C_{n_{b_o}} S_b' \hat{x}_b' h_b'}{d_c{}^2 S} \right.\right.$$

$$\left.\left. + \frac{2C_{n_{VO}} S_V \hat{x}_{V_t} h_t'}{d_c{}^2 S} - \frac{2JC_{n_{v_o}} S_V \hat{x}_V h_t'}{d_c{}^2 S} \right) \Phi \frac{\dot{\theta} d_c}{2V_\infty} \right]$$

For J = 1 the volute is totally ineffective and its contribution in both damping and stability are nullified. For J = 0 the equation reduces to its rigid body form. The effects on the values of $(C_{m_q} + C_{m_{\dot{\alpha}}})$ and C_{m_α} can be inferred by reducing the effectiveness of the volute by (1-J) and including this value instead of the full value into the rigid body equations. By doing this, the tail effectiveness will be reduced and the overall stability of the combination will be reduced. Similarly, the damping effectiveness of the volute suffers by the same factor. Note that since the whole tail (as defined in the rigid analysis) is not affected by the volute flexing, the aft portion of the forebody which helps in stability is not affected. In terms of J, the new flexible body damping and stability coefficients are:

$$C_{m_\alpha}/_{\text{flexible}} = \left[\frac{C_{m_\alpha}}{\hat{\theta}} \Big/_{\text{rigid}} \right] \Phi - \frac{J C_{n_{v_o}} h_t' S_V}{d_c S} \Phi$$

$$\left(C_{m_q} + C_{m_{\dot{\alpha}}}\right)_f = \left[\frac{\left(C_{m_q} + C_{m_{\dot{\alpha}}}\right)}{\hat{\theta}}\Bigg/_{\text{rigid}}\right]\Phi - \frac{2JC_{n_{v_o}}h_t' S_v \hat{x}_v}{d_c^2 S}\Phi$$

If the volute is not light or has negligible inertia, the derived forms will not be accurate. A complete dynamic analysis is somewhat frustrating since the results are so complicated as to be almost useless for general design purposes unless a convenient means of interpreting the equations is provided. Here, an attempt will be made to present the complete equations so that useful design information can be obtained.

The analysis begins with the general equation derived for the forebody volute combination, and the equation derived for just the volute without the small mass assumption. The two equations have the general forms shown below:

$$I\ddot{\theta} + K_t\ddot{\delta} = -a_{13}\dot{\theta} - a_{14}\theta - a_{15}\dot{\delta} - a_{16}\delta$$

$$(I_V + M_V R_V \bar{r}_V)\ddot{\theta} + I_v\ddot{\delta} = -a_{23}\dot{\theta} - a_{24}\theta - a_{25}\dot{\delta} - a_{26}\delta$$

The coefficients are:

$$a_{13} = \tfrac{1}{2}\rho V^2{}_\infty S d_c \left[\frac{2C_{n_{b_o}} S_b \hat{x}_b h_b}{d_c{}^2 S} + \frac{2C_{n_{b_o}} S_b' \hat{x}_b' h_b'}{d_c{}^2 S} + \frac{2C_{n_{v_o}} S_v \hat{x}_{v_t} h_t'}{d_c{}^2 S}\right]\frac{d_c\Phi}{2V_\infty}$$

$$a_{14} = \tfrac{1}{2}\rho V^2{}_\infty S d_c \left[-\frac{C_{n_{b_o}} S_b h_b}{d_c S} + \frac{C_{n_{b_o}} S_b' h_b'}{d_c S} + \frac{C_{n_{v_o}} S_v h_t'}{d_c S}\right]\Phi$$

$$a_{15} = \tfrac{1}{2}\rho V^2{}_\infty S d_c \left(\frac{2C_{n_{v_o}} S_v \hat{x}_v h_t'}{d_c\, S}\right)\frac{d_c\Phi}{2V_\infty}, \quad a_{16} = \tfrac{1}{2}\rho V^2{}_\infty S d_c \left(\frac{C_{n_{v_o}} S_v h_t'}{d_c S}\right)\Phi$$

$$a_{23} = \tfrac{1}{2}\rho V^2{}_\infty S d_c \left(\frac{2C_{n_{V_o}} S_V \hat{x}_{V_t} a l_V}{d_c{}^2 S}\right)\frac{d_c \Phi}{2V_\infty},\quad a_{24} = \tfrac{1}{2}\rho V^2{}_\infty S d_c \left(\frac{C_{n_{V_o}} S_V a l_V}{d_c S}\right)\Phi$$

$$a_{25} = \tfrac{1}{2}\rho V^2{}_\infty S d_c \left(\frac{2C_{n_{V_o}} S_V \hat{x}_V a l_V}{d_c{}^2 S}\right)\frac{d_c \Phi}{2V_\infty},\quad a_{26} = \tfrac{1}{2}\rho V^2{}_\infty S d_c \left(\frac{C_{n_{V_o}} S_V a l_V}{d_c S}\right)\Phi + k_V$$

The two equations for which a solution is sought are:

$$a_{11}\ddot{\theta} + a_{12}\ddot{\delta} + a_{13}\dot{\theta} + a_{14}\theta + a_{15}\dot{\delta} + a_{16}\delta = 0$$

$$a_{21}\ddot{\theta} \quad a_{22}\ddot{\delta} \quad a_{23}\dot{\theta} \quad a_{24}\theta \quad a_{25}\dot{\delta} \quad a_{26}\delta = 0$$

To find a solution assume that:

$$\theta = \bar{\theta}\, e^{st},\quad \delta = \bar{\delta}\, e^{st}$$

Insertion into the equations of motion yields:

$$S^2(a_{11}\bar{\theta} + a_{12}\bar{\delta}) + S(a_{13}\bar{\theta} + a_{15}\bar{\delta}) + (a_{14}\bar{\theta} + a_{16}\bar{\delta}) = 0$$

$$S^2(a_{21}\bar{\theta} + a_{22}\bar{\delta}) + S(a_{23}\bar{\theta} + a_{25}\bar{\delta}) + (a_{24}\bar{\theta} + a_{26}\bar{\delta}) = 0$$

These equations for the assumed $\bar{\delta}$ and $\bar{\theta}$ will give solutions different from zero only if:

$$\begin{vmatrix} (a_{11}S^2 + a_{13}S + a_{14}) & (a_{12}S^2 + a_{15}S + a_{16}) \\ (a_{21}S^2 + a_{23}S + a_{24}) & (a_{22}S^2 + a_{25}S + a_{26}) \end{vmatrix} = [0] \text{ for } \bar{\delta} \;\&\; \bar{\theta} \neq 0$$

This requires that:

$$C_{11}S^4 + C_{12}S^3 + C_{13}S^2 + C_{14}S + C_{15} = 0$$

$$C_{11} = (a_{11}a_{22} - a_{12}a_{21}),\quad C_{15} = (a_{14}a_{26} - a_{16}a_{24}) \text{ etc.}$$

Solutions to the characteristic equation are:

$$S_1 = -n_1 + ip_1, \quad S_2 = -n_1 - ip_1$$

$$S_3 = -n_2 + ip_2 \quad S_4 = -n_2 - ip_2$$

In terms of trigonometric functions:

$$\theta = e^{-n_1 t}(A_1 \cos p_1 t + A_2 \sin p_1 t) + e^{-n_2 t}(A_3 \cos p_2 t + A_4 \sin p_2 t)$$

$$\delta = e^{-n_1 t}(B_1 \cos p_1 t + B_2 \sin p_1 t) + e^{-n_2 t}(B_3 \cos p_2 t + B_4 \sin p_2 t)$$

Before delving deeper into the solution equation, it is useful to examine the characteristic equation further since stability of the system can be found by examining its coefficients and factors. Static stability can be inferred immediately by examining the values of the constant portion (C_{15}) of the characteristic equation. It should be positive. If it is positive for one configuration and a single design parameter is varied so that C_{15} changes sign, then one divergence (static instability) appears in the solution (Reference 1). To find out what effect this change has on dynamic stability, the characteristic equation needs to be analyzed further. Routh's Criteria is a convenient means for finding whether the system is dynamically unstable. This method is outlined in Reference 1. Briefly, the technique is as follows:

The quartic is:

$$C_{11}s^4 + C_{12}s^3 + C_{13}s^2 + C_{14}s + C_{15} = 0$$

Form two rows as follows:

$$\begin{array}{ccc} C_{11} & C_{13} & C_{15} \\ C_{12} & C_{14} & 0 \end{array}$$

Construct additional rows:

$$P_{31} \quad P_{32} \quad 0$$

$$P_{41} \quad 0 \quad 0$$

where:

$$P_{31} = C_{12}C_{13} - C_{11}C_{14}, \; P_{32} = C_{12}C_{15}$$

$$P_{41} = P_{31}C_{14} - P_{32}C_{12}$$

For the system to be dynamically stable, each element in the first column must be positive. If the mentioned change in a single design parameter results in an element in the first column changing to a negative value, then the system will have one divergent oscillation.

Once the volute-forebody characteristic equation has been obtained, any of several root extraction methods can be applied to determine the degree of damping and the two free vibrations of the system. It is intuitive that the system will vibrate in both modes and will be lightly damped so that the solution roots will have negative real parts and imaginary parts. Since the equation is fourth degree, there must be two quadratic factors obtainable by the following method:

Rewrite the quartic as:

$$(s^2 + d_1 s + d_2)(s^2 + d_3 s + d_4) = 0$$

Expand this equation and equate coefficients to the original quartic:

$$\frac{C_{12}}{C_{11}} = d_1 + d_3, \; \frac{C_{13}}{C_{11}} = d_2 + d_1 d_3 + d_4$$

$$\frac{C_{14}}{C_{11}} = d_3 + d_2, \; \frac{C_{15}}{C_{11}} = d_2 \, d_4$$

These equations can be solved to yield:

$$d_1 = \frac{C_{12}}{2C_{11}} \pm \left[\frac{C_{12}}{2C_{11}}^2 - \frac{C_{13}}{C_{11}} + d_2 + \frac{C_{15}}{C_{11}} d_2 \right]^{\frac{1}{2}}$$

$$d_1 = \frac{C_{14}/C_{11}(d_2) - C_{12}/C_{11}(d_2^2)}{C_{15}/C_{11} - d_2^2}$$

A plot of these two equations will reveal the common points at one or two intersections. These are then the factors of one quadratic, the other two following directly. The equations are analyzed below:

$$d_1 = \frac{C_{14}/C_{11}(d_2) - C_{12}/C_{11} d_2^2}{C_{15}/C_{11} - d_2^2} \quad C_{11}, C_{12}, C_{13}, C_{14}, C_{15} > 0$$

$$d_2 \to \infty, \; d_1 \to C_{12}/C_{11}$$

$$d_1 \to \infty, d_2 \to \frac{C_{15}}{C_{11}}$$

$$d_1 < 0, d_2 \to C_{14}/C_{12}$$

Looking at the second,

$$d_1 = \frac{C_{12}}{2C_{11}} \pm \left[\left(\frac{C_{12}}{2C_{11}} \right)^2 - \frac{C_{13}}{C_{11}} + d_2 + \frac{C_{15}}{C_{11} d_2} \right]^{\frac{1}{2}}$$

$$\frac{Dd_1}{Dd_2} = \frac{1}{2} \left[\left(\frac{C_{12}}{2C_{11}} \right)^2 - \frac{C_{13}}{C_{11}} + d_2 + \frac{C_{15}}{C_{11} d_2} \right]^{-\frac{1}{2}} \left[1 - \frac{C_{15}}{C_{11}} d_2^{-2} \right]$$

Maximizing:

$$0 = 1 - \frac{C_{15}}{C_{11}} d_2^{-2}, \quad d_2 = \pm \sqrt{\frac{C_{15}}{C_{11}}}$$

APPENDIX II

DATA

The data portion of the program was conducted in two parts. The first consisted of free flight data obtained from the Von Karman Gas Dynamics Facility. Static and dynamic data was obtained at the Eglin Air Force Base low speed facility at Mach 0.19 for Rn = $5x10^5$. The free flight data is contained in the report "Volute Stabilization" project VA0086.

Since the volute is a coiled flexible spring, it was necessary to approximate the rigid model of a volute with a solid body grooved in a staircase fashion to represent the volute coils. Five aluminum and one epoxy models were constructed. Three cylinder forebodies were made to mate these volutes. The test bodies with complete geometrical and physical properties are shown in Figures II-1 through II-3. These models formed the core of the rigid body data bank. Several attempts were made to construct flexible models from these by inserting a leaf spring between the forebody and the volute, giving a two-degree angular freedom model. Unfortunately, the models generally failed structurally because the aluminum volute was too heavy. Some flexible data was obtained at Eglin Air Force Base for each flexible model. The coiled spring tails on models (1-2) are shown in Figure II-4.

Static data for the rigid models is plotted in Figures II-5 to II-10. Flexible data for flexible models is shown in Figures II-11 and II-12.

Two specialized pieces of equipment, an accelerometer stand and a dynamic shaker stand, were developed for the test program at Eglin to obtain dynamic derivatives. Neither of these items were fully tested during the program because of time constraints and may be used extensively during the second year's work. The operation of each is described below:

Accelerometer Stand

The accelerometer stand was developed for mounting in the Eglin low speed tunnel. Inside the strut are assorted electronics for transferring a voltage signal from an accelerometer model to a special discriminator. The output from the discriminator drives an oscillograph, giving a trace of the acceleration of the volute versus time. Diagrams of the strut and electric package are provided in Figures II-13 and II-14, respectively. With the various filter modifications, the strut may be used in flexible test work during the second year's work.

Dynamic Stand

The dynamic stand enables extraction of the basic aerodynamic derivatives of a given model by forcing it into resonance. Data is obtained with a high speed camera and reduced according to a scheme outlined in Reference 4 . The stand is illustrated is Figures II-15 and II-16.

A sample of the free flight data obtained from the Von Karman Gas Dynamic Facility is included as Figures II-17 through II-20. Reduced data for the aerodynamic coefficients has been extracted from "Volute Stabilization" report and included for completeness and comparison with the planar oscilatory data obtained at Eglin Air Force Base.

Models are formed by combining the cylinders with the volute tails. Their designation is provided by identifying each model by the cylinder forebody number and the volute tail number, such as 3+2, which is a model having cylinder 3 as its forebody and volute 2 as the tail. Some flexible tests were conducted by inserting a leaf spring between the cylinder and volute. These models are identified as above except that they are primed thus: (3+2)'. The physical properties used to obtain the basic inertia terms are shown in Table II-1.

TABLE II-1. VOLUTE MODEL MEASUREMENTS

Model	$\bar{r}_V$	R_V	K_V	I
3 + 1	0.05533	0.1516	0.00003636	0.0002044
3 + 2	0.10033	0.1516	0.00011210	0.0003428
3 + 3	0.14408	0.1516	0.00027150	0.0006050
3 + 5	0.21592	0.1516	0.00073500	0.0015090
3 + 6	0.38850	0.1516	0.00422200	0.0057600

The reduced data from the Von Karman test program can be used for design purposes as well as providing an extensive data bank. Various aerodynamic coefficients were reduced from the raw data for a number of models, distinct from the ones used at Eglin. Table II-3 lists the data from the Von Karman Gas Dynamic Facility. To assist in correlating that data with previous model configurations, Table II-2 is provided.

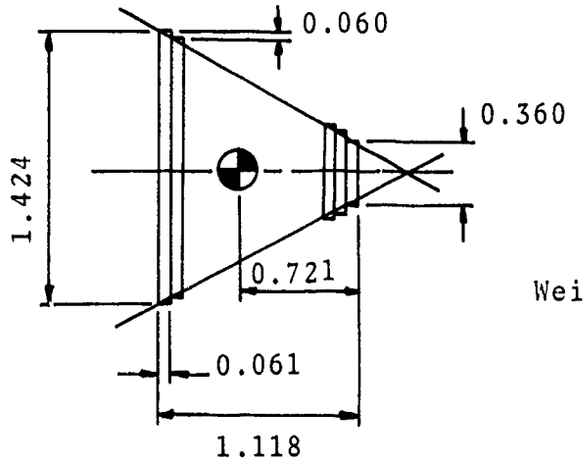

VOLUTE 1

Weight (Pounds)	I_V (Slugs-Ft^2)
0.0744	0.00001698

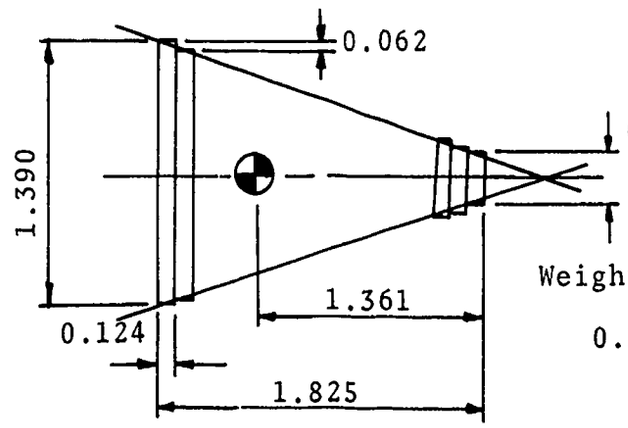

VOLUTE 2

Weight (Pounds)	I_V (Slugs-Ft^2)
0.114	0.00005823

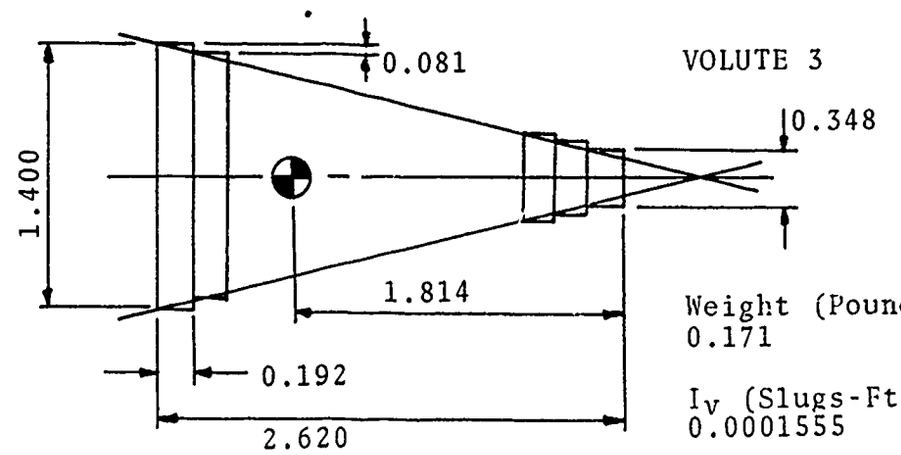

VOLUTE 3

Weight (Pounds)	I_V (Slugs-Ft^2)
0.171	0.0001555

Figure II-1. Rigid Volutes : 1, 2, and 3

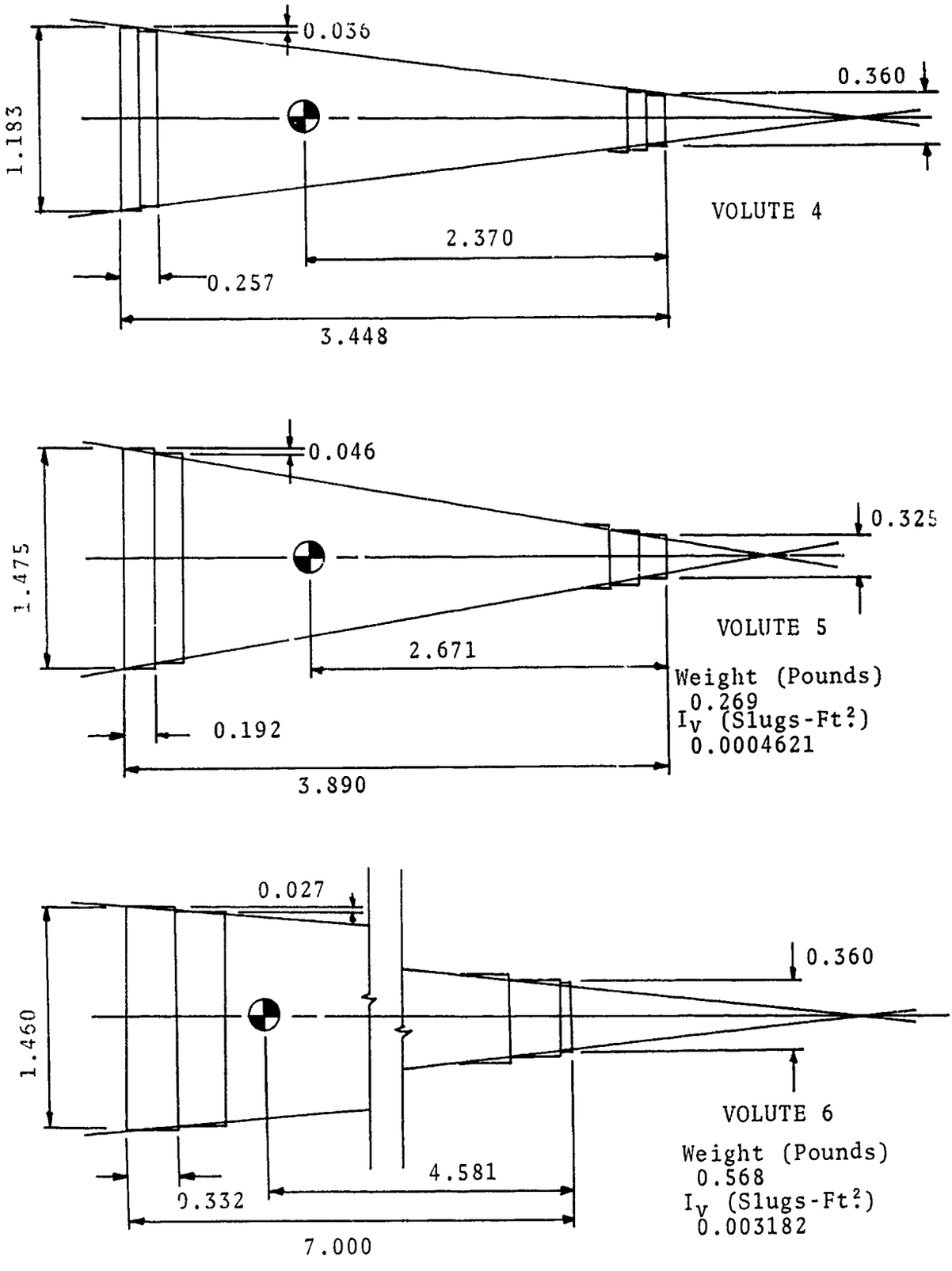

Figure II-2. Rigid Volutes : 4, 5, and 6

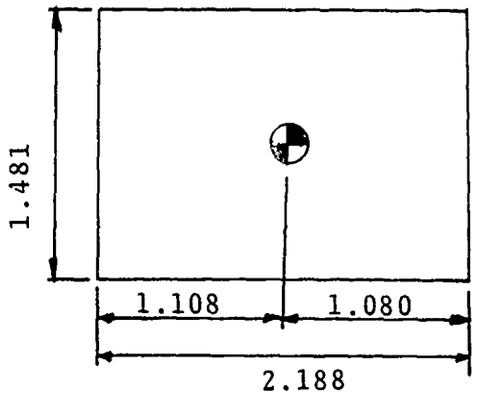

CYLINDER 1

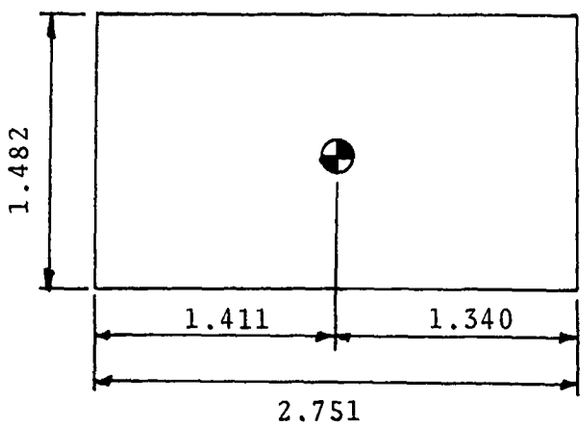

CYLINDER 2

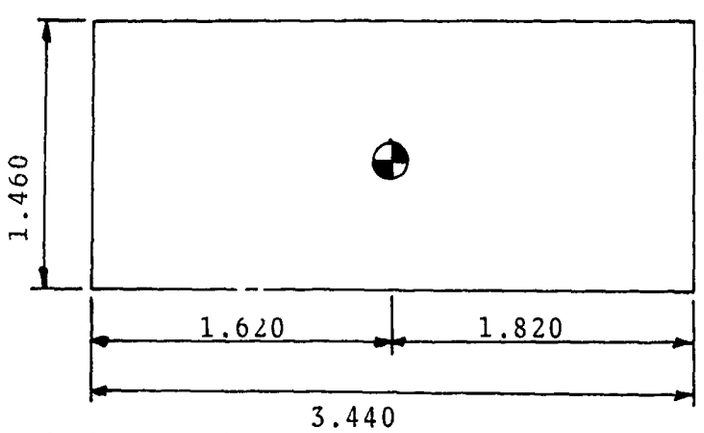

CYLINDER 3

Weight (Pounds)
0.434
I_B (Slugs-Ft^2)
0.00009558

Note: Model Pitch center locations are the same as the cylinders.

Figure II-3. Cylinder Models

Volute Elastic Model (3 + 4)' or 1

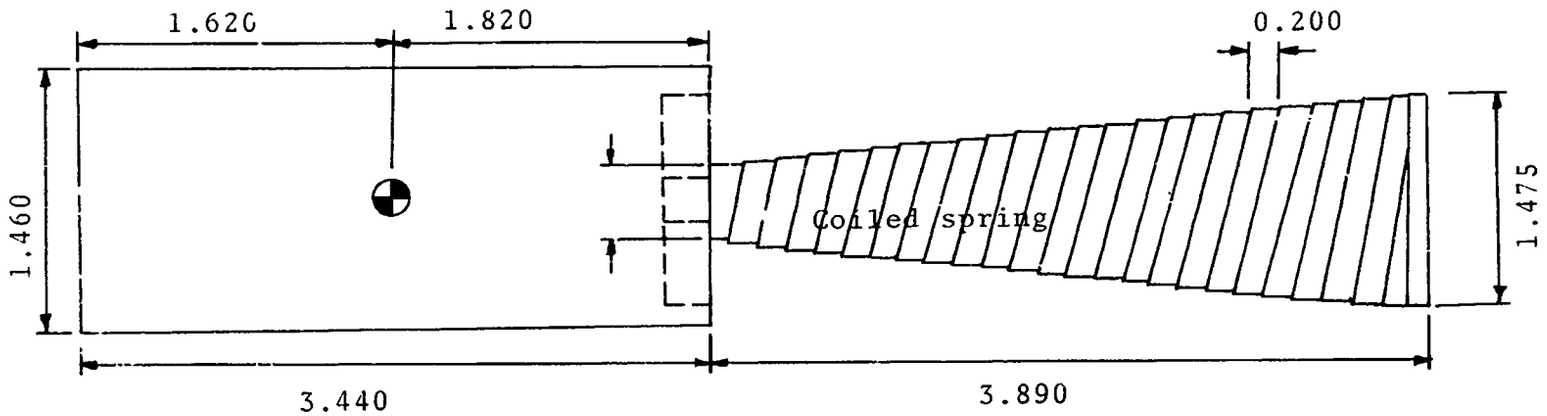

Volute Elastic Model 2

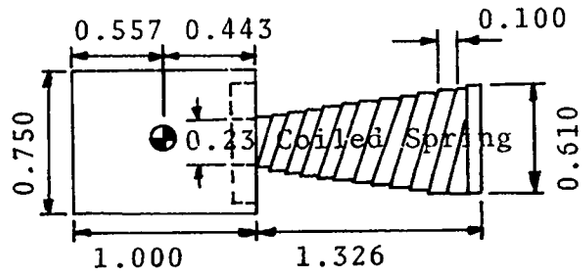

Figure II-4. Helical Coil Flexible Models

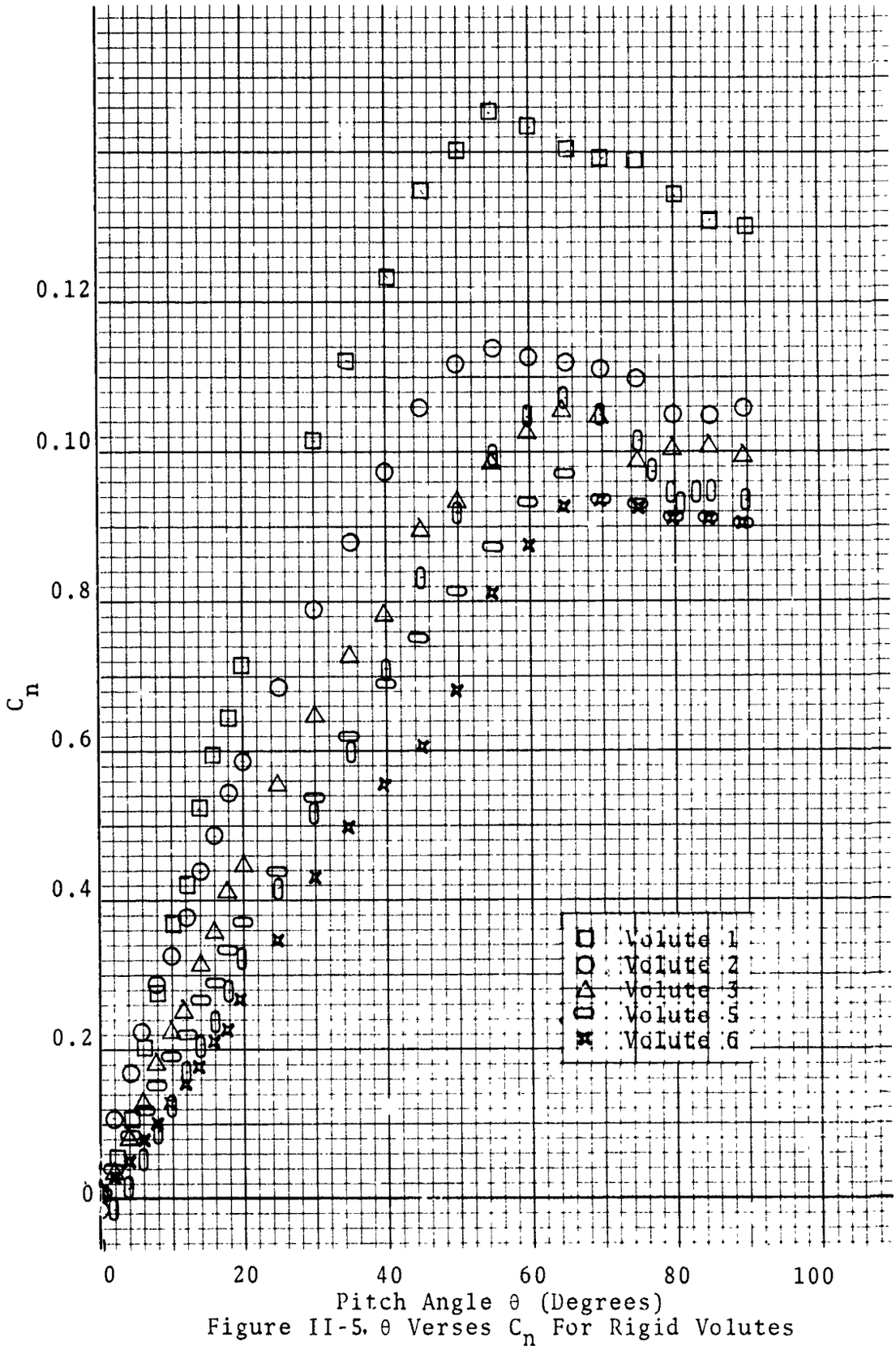

Figure II-5. θ Verses C_n For Rigid Volutes

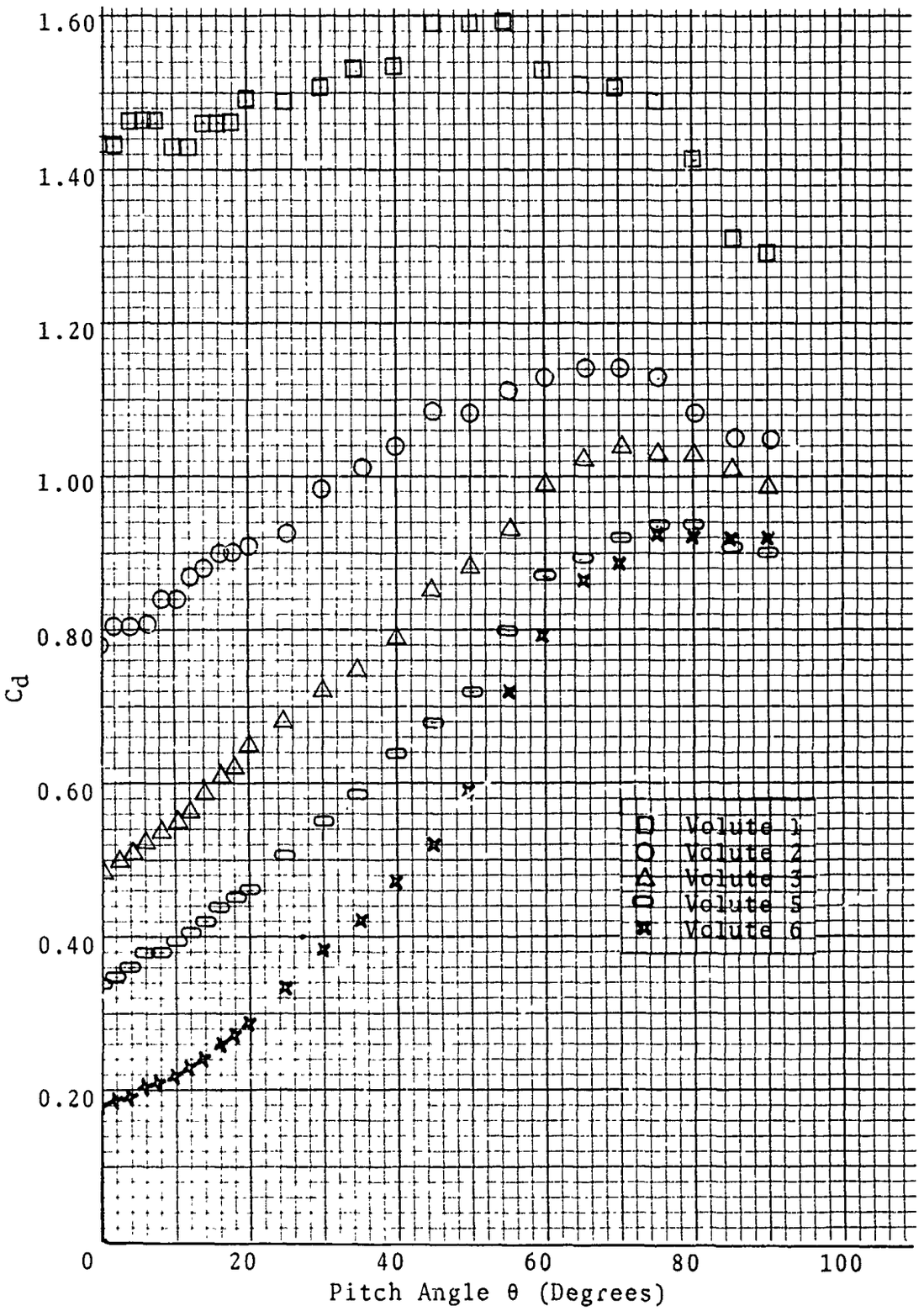

Figure II-6. θ Versus C_d For Rigid Volutes

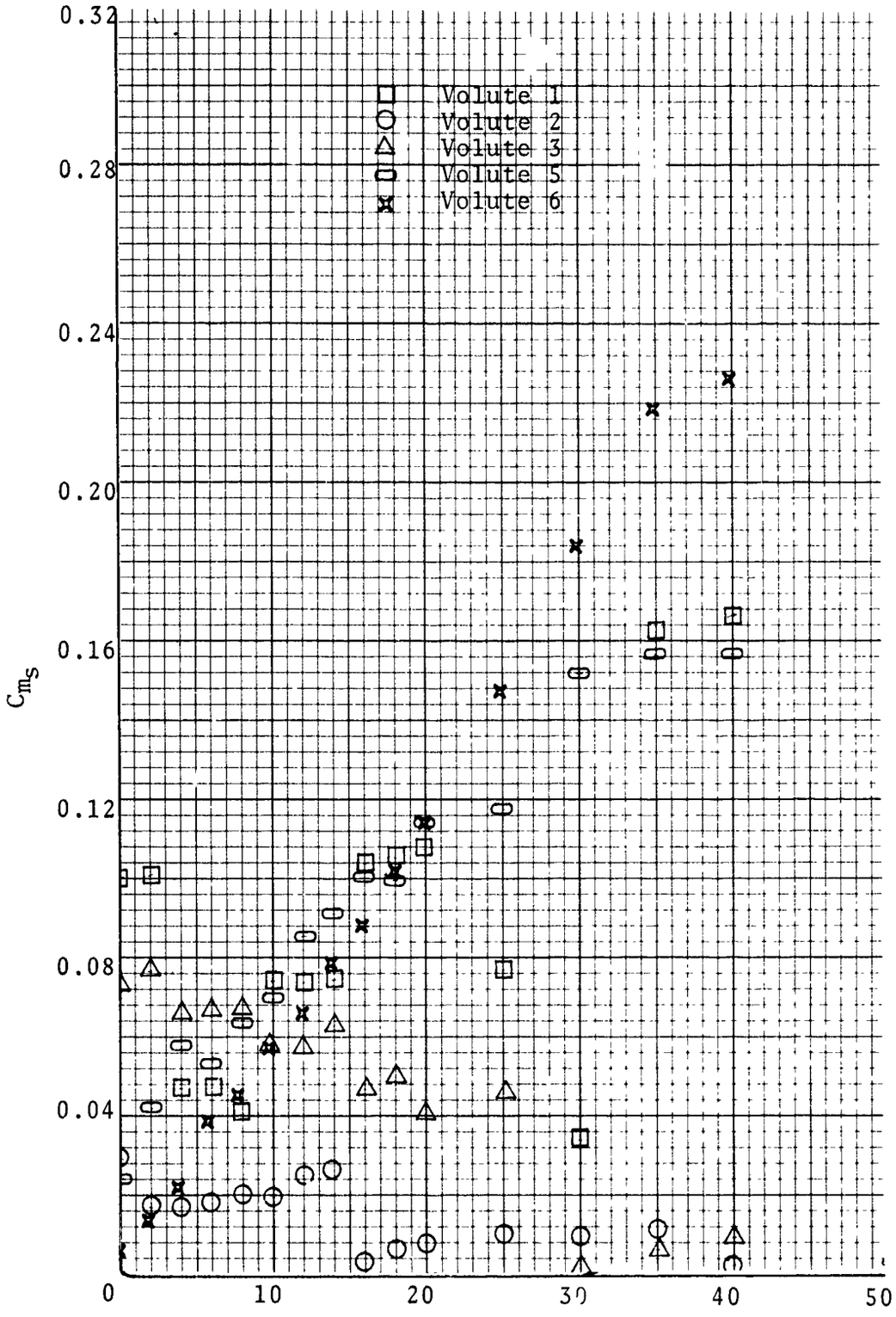

Figure II-7. θ Versus C_{m_s} For Rigid Volutes

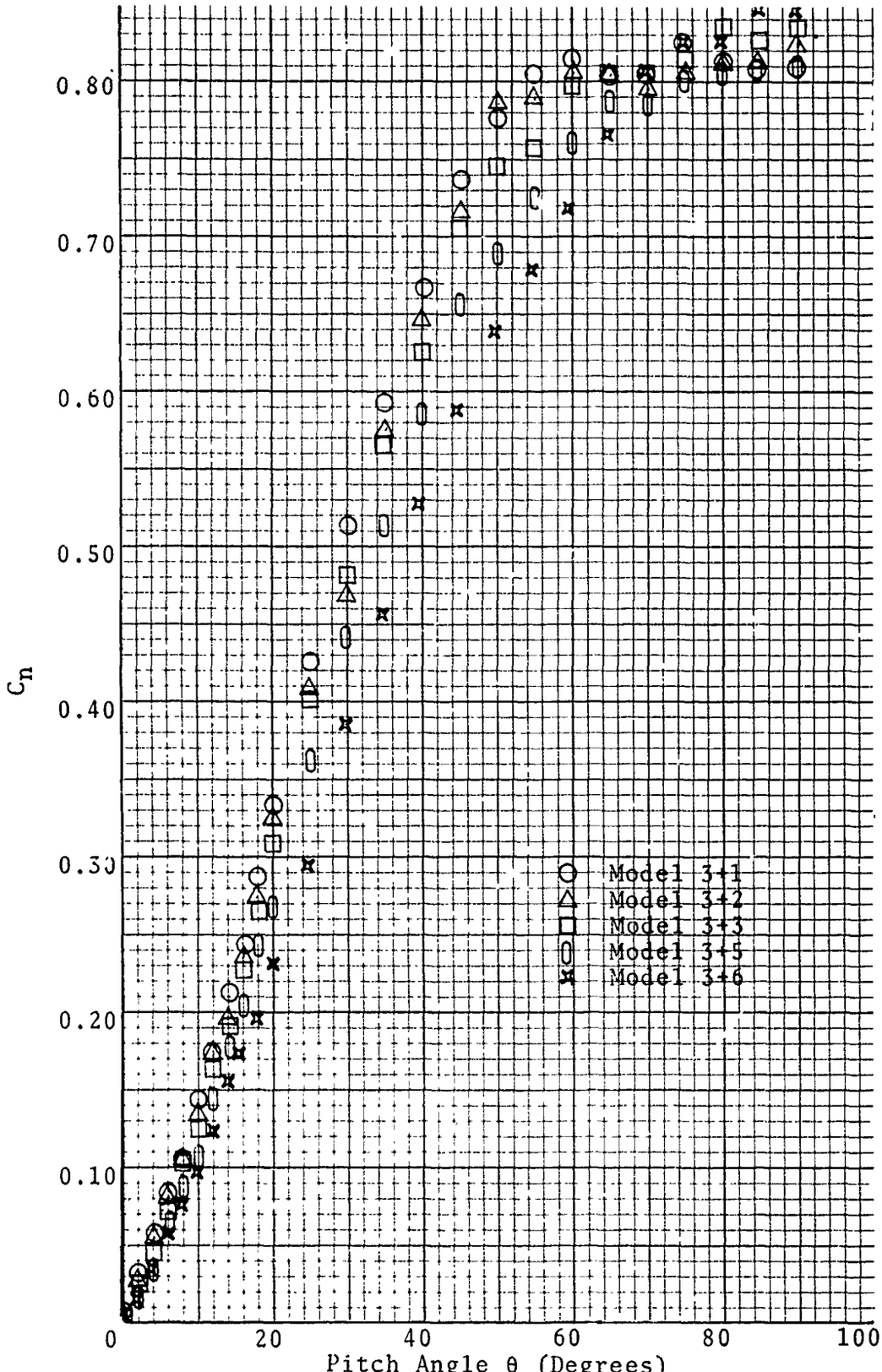

Figure II-8. θ Versus C_n For Rigid Models

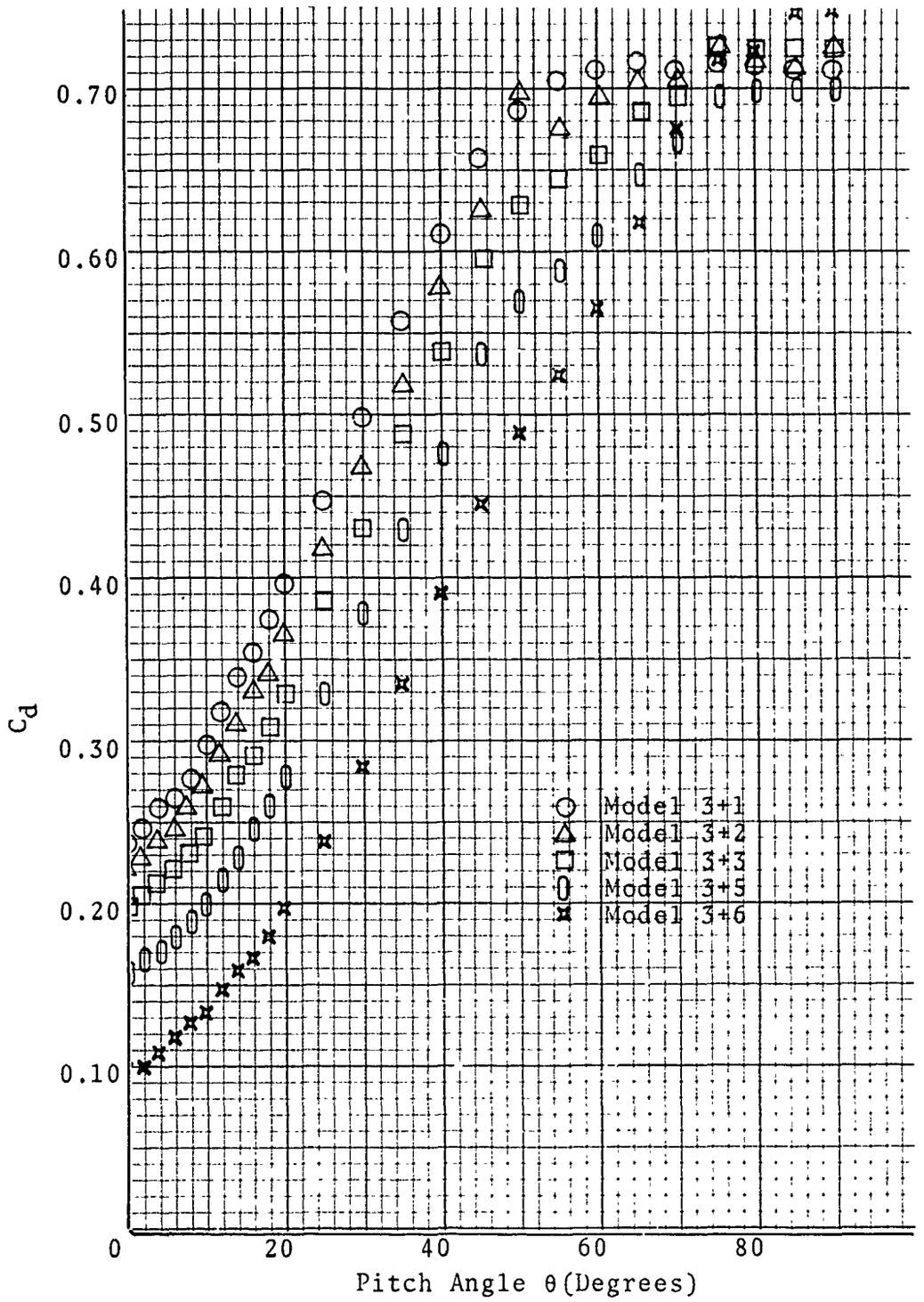

Figure II-9. θ Versus C_d For Rigid Models

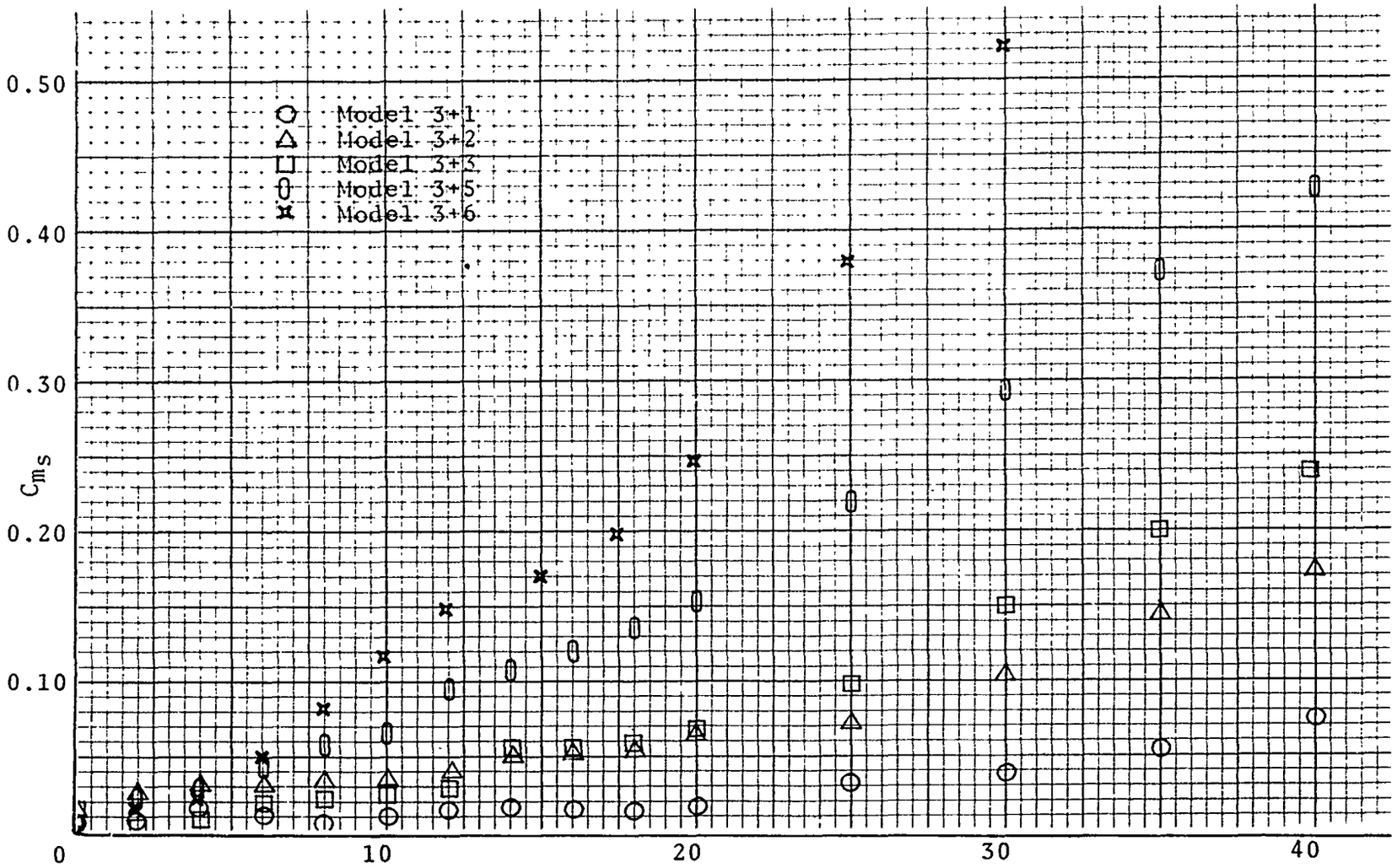

Figure II-10. θ Versus C_{m_s} Rigid Models

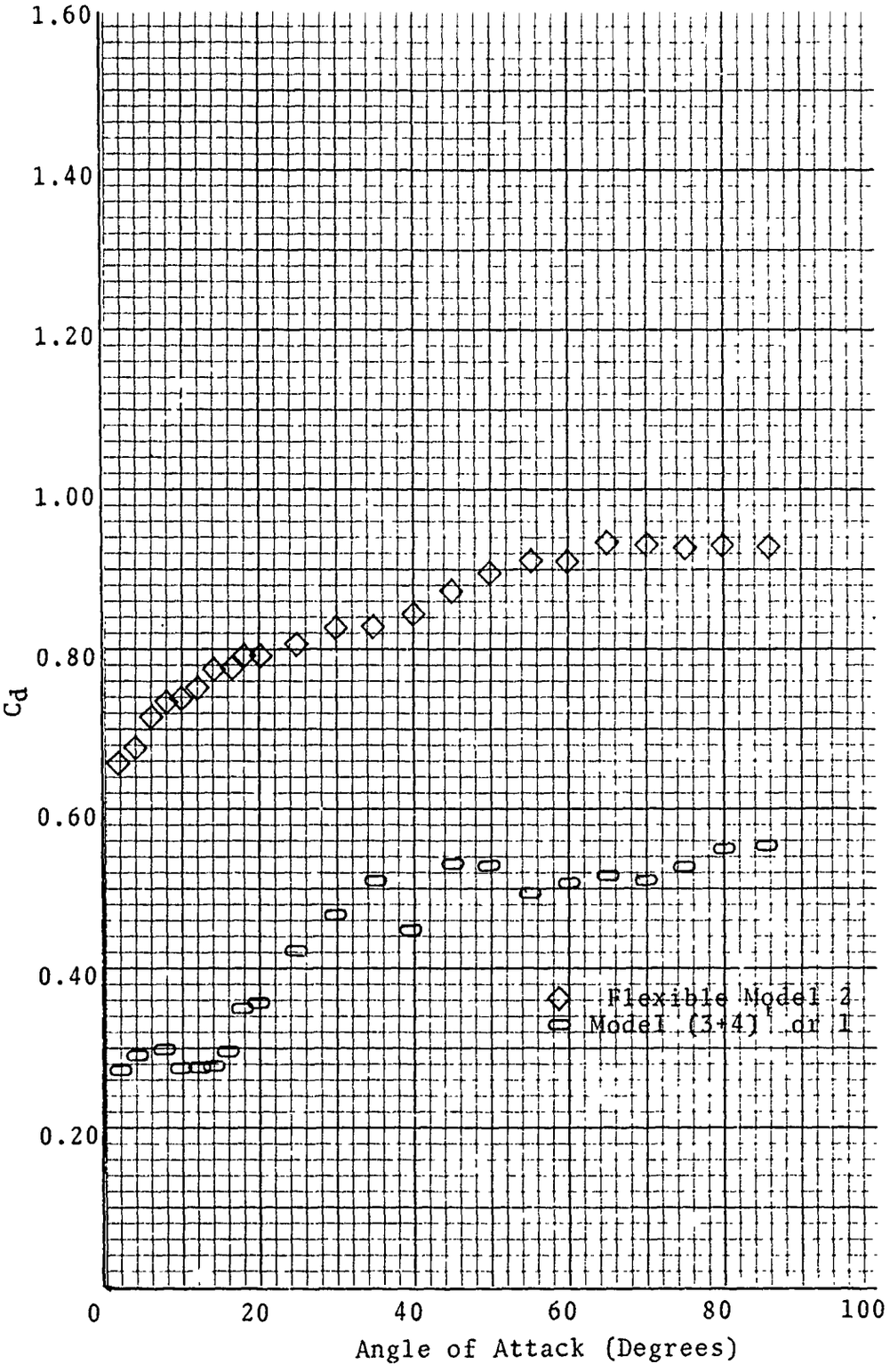

Figure II-12. θ Versus C_d Flexible Models

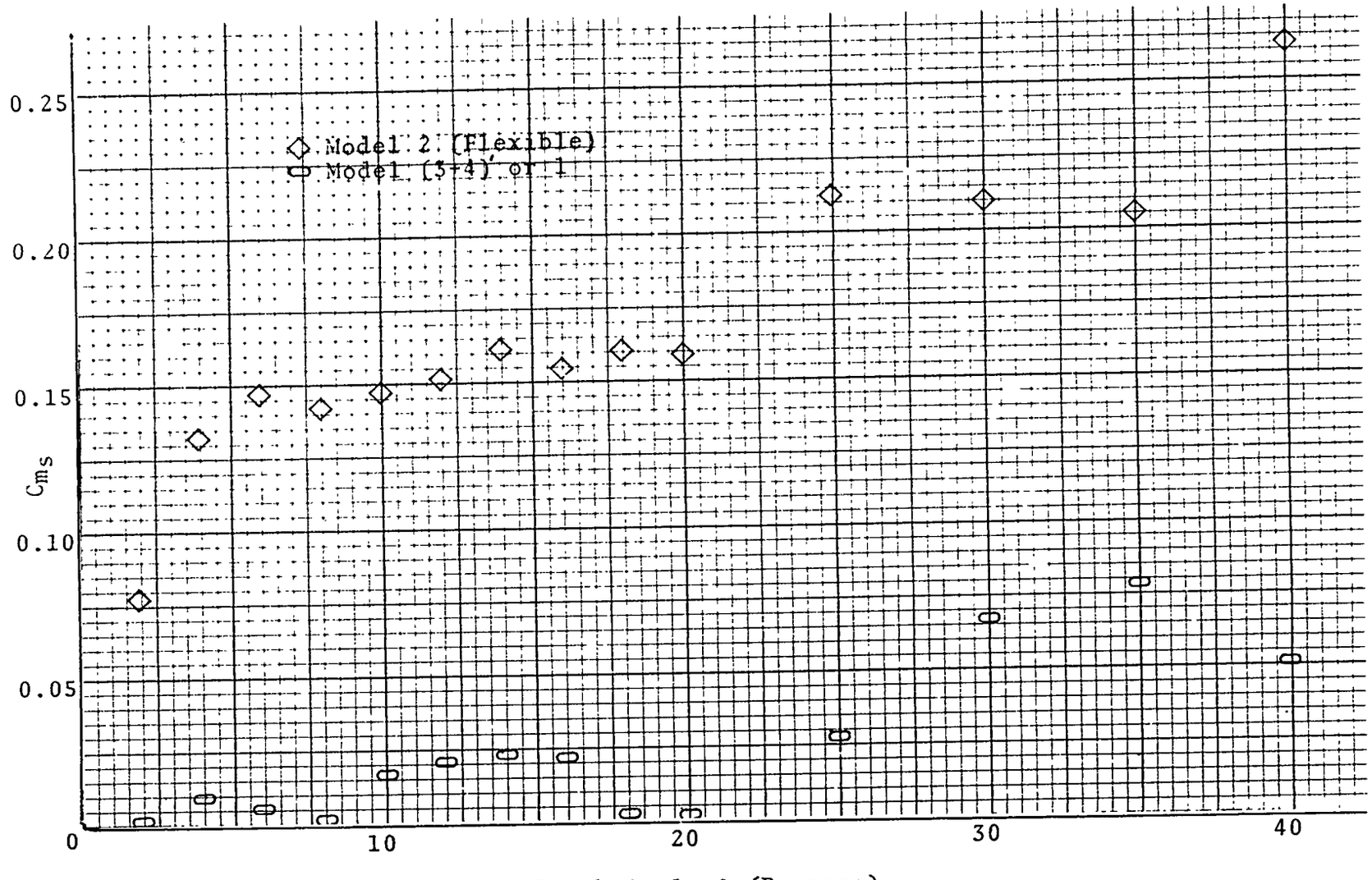

Figure II-11. θ Versus C_{m_s} Flexible Models

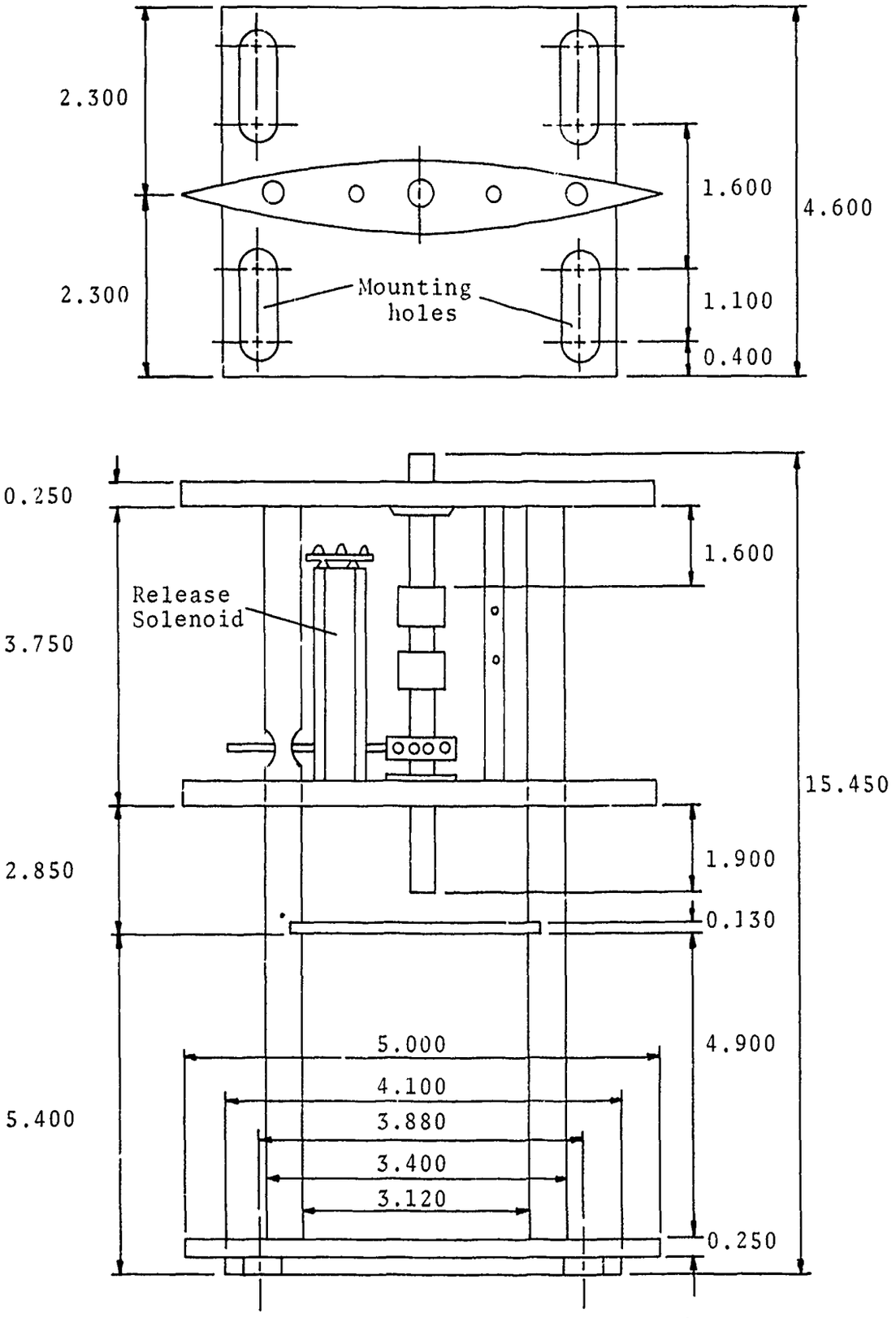

Figure II-13. Accelerometer Stand

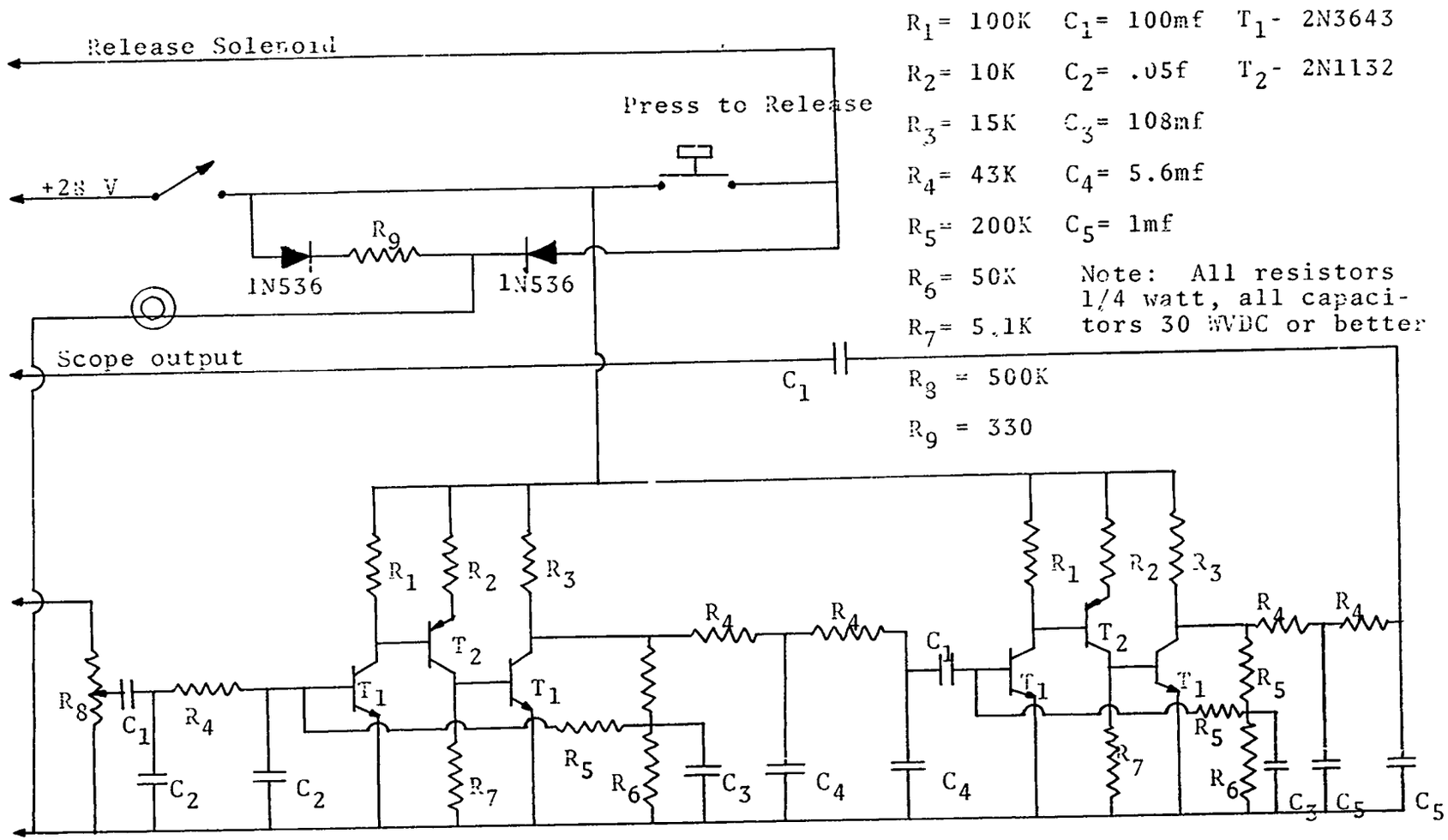

Figure II-14. Accelerometer Output Filter

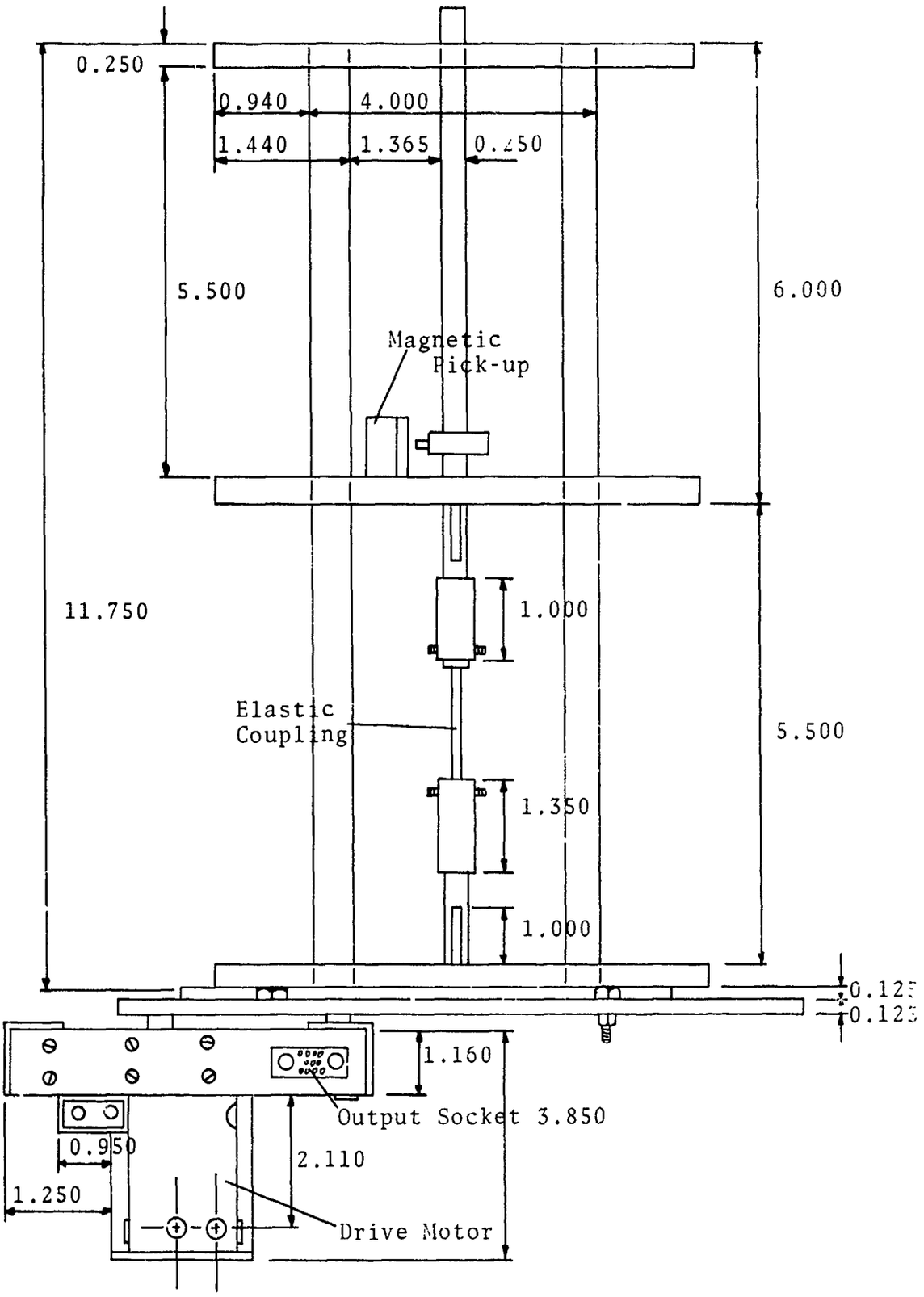

Figure II-15. Dynamic Shaker Stand (Side View)

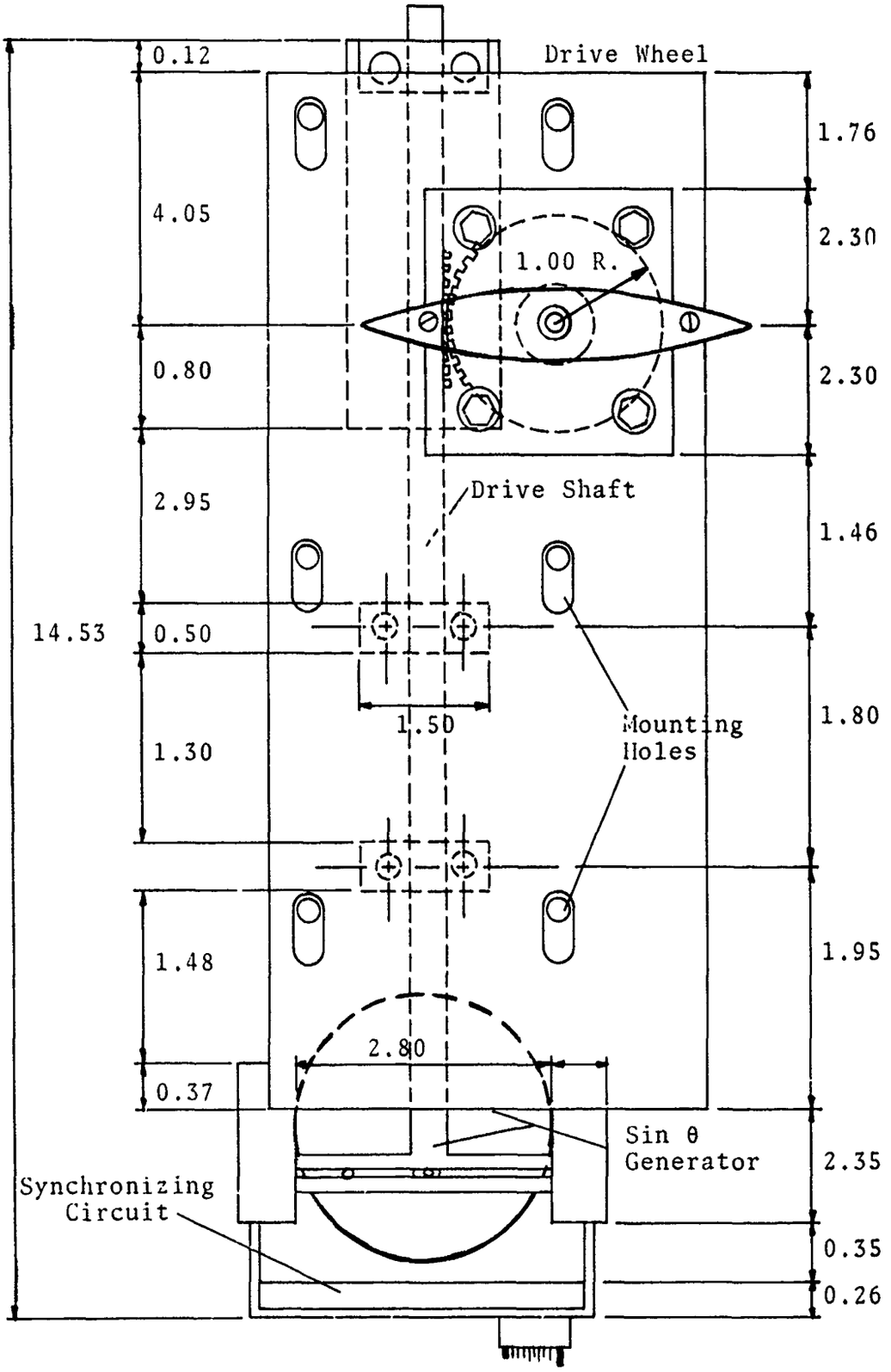

Figure II-16. Dynamic Walker Stand (Top View)

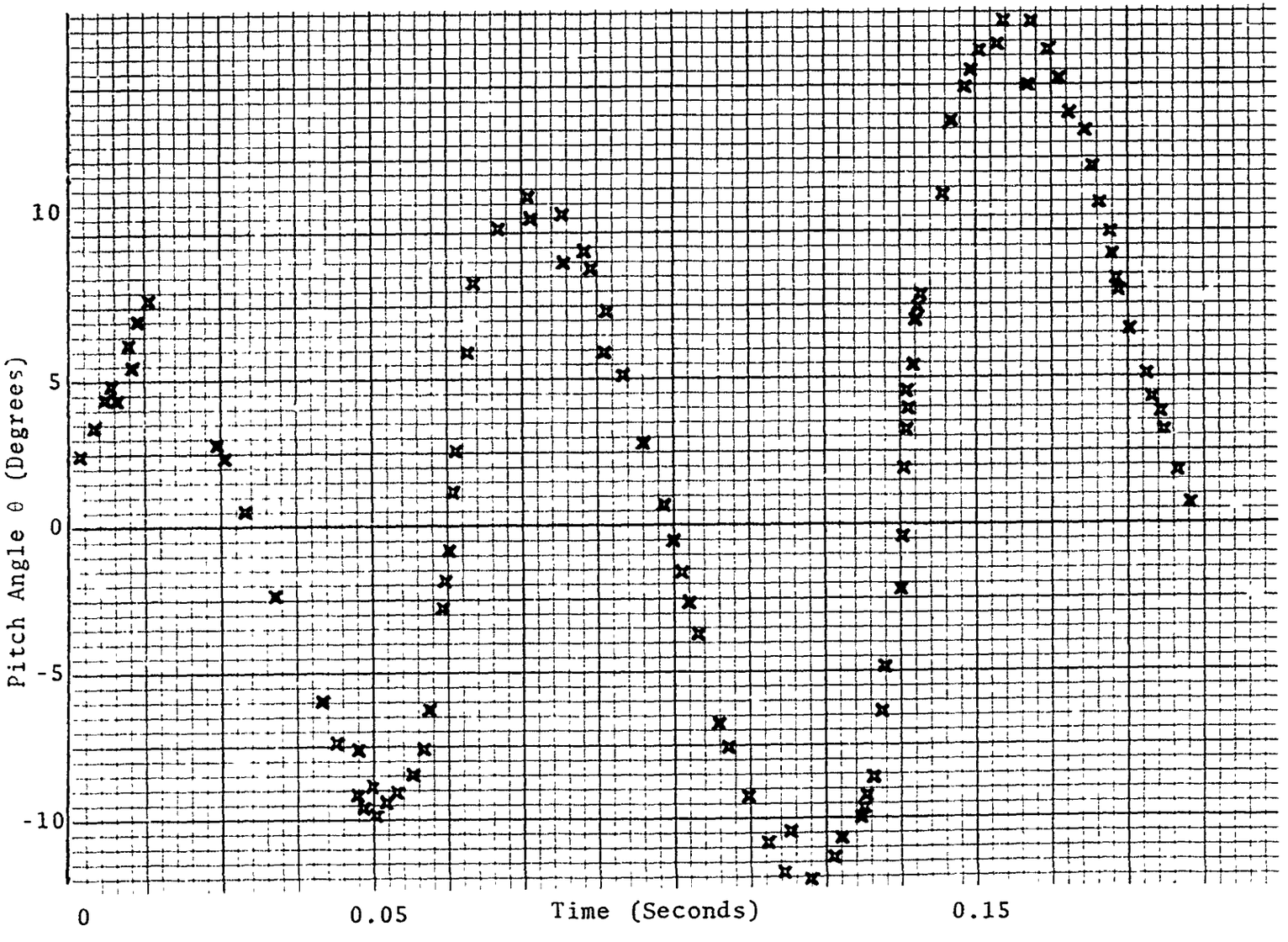

Figure II-17. Von Karman Data Sample, 0.75 Inch Cylinder With Small Volute

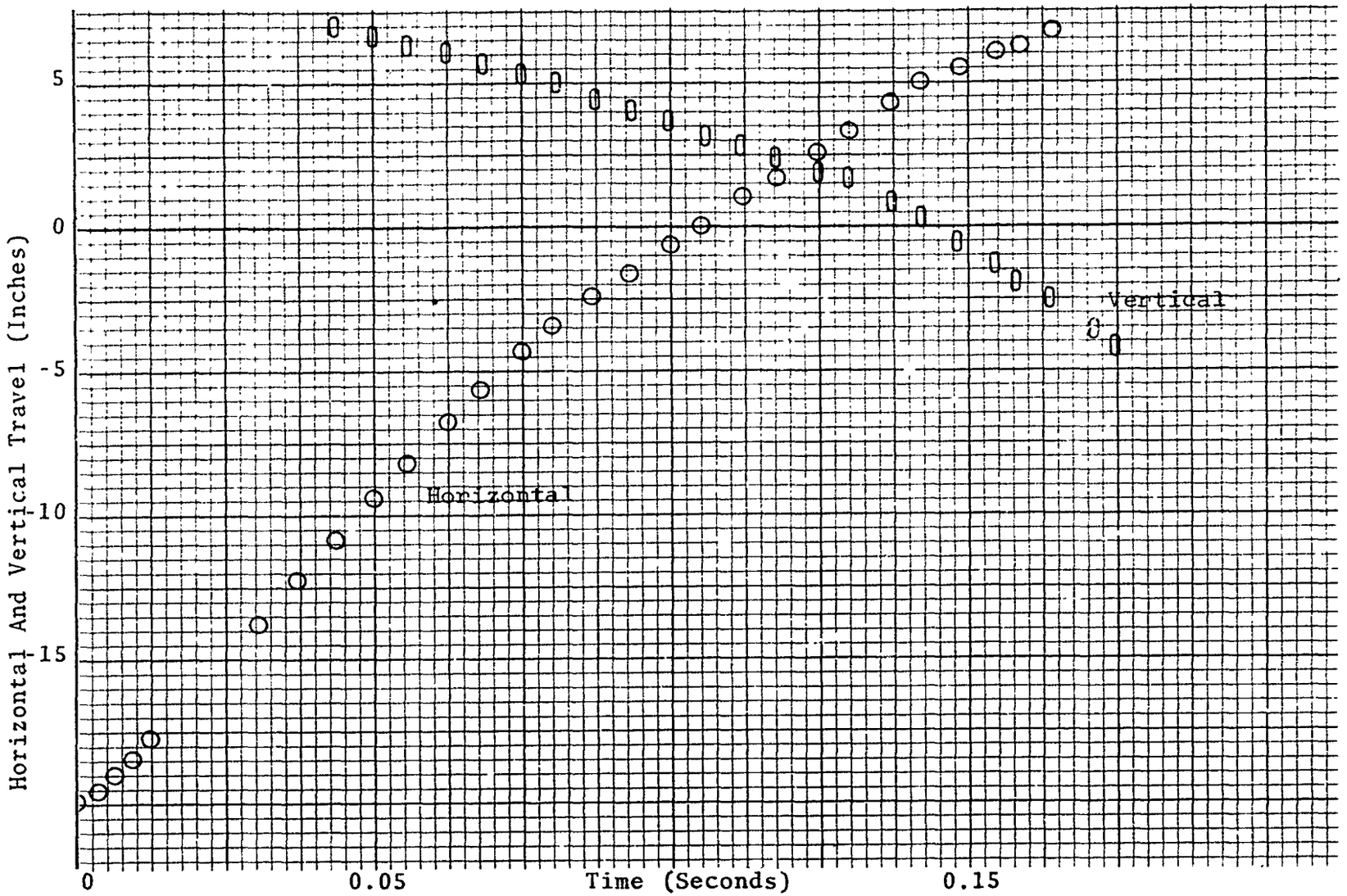

Figure II-18. Von Karman Data Sample, 0.75 Inch Cylinder With Small Volute

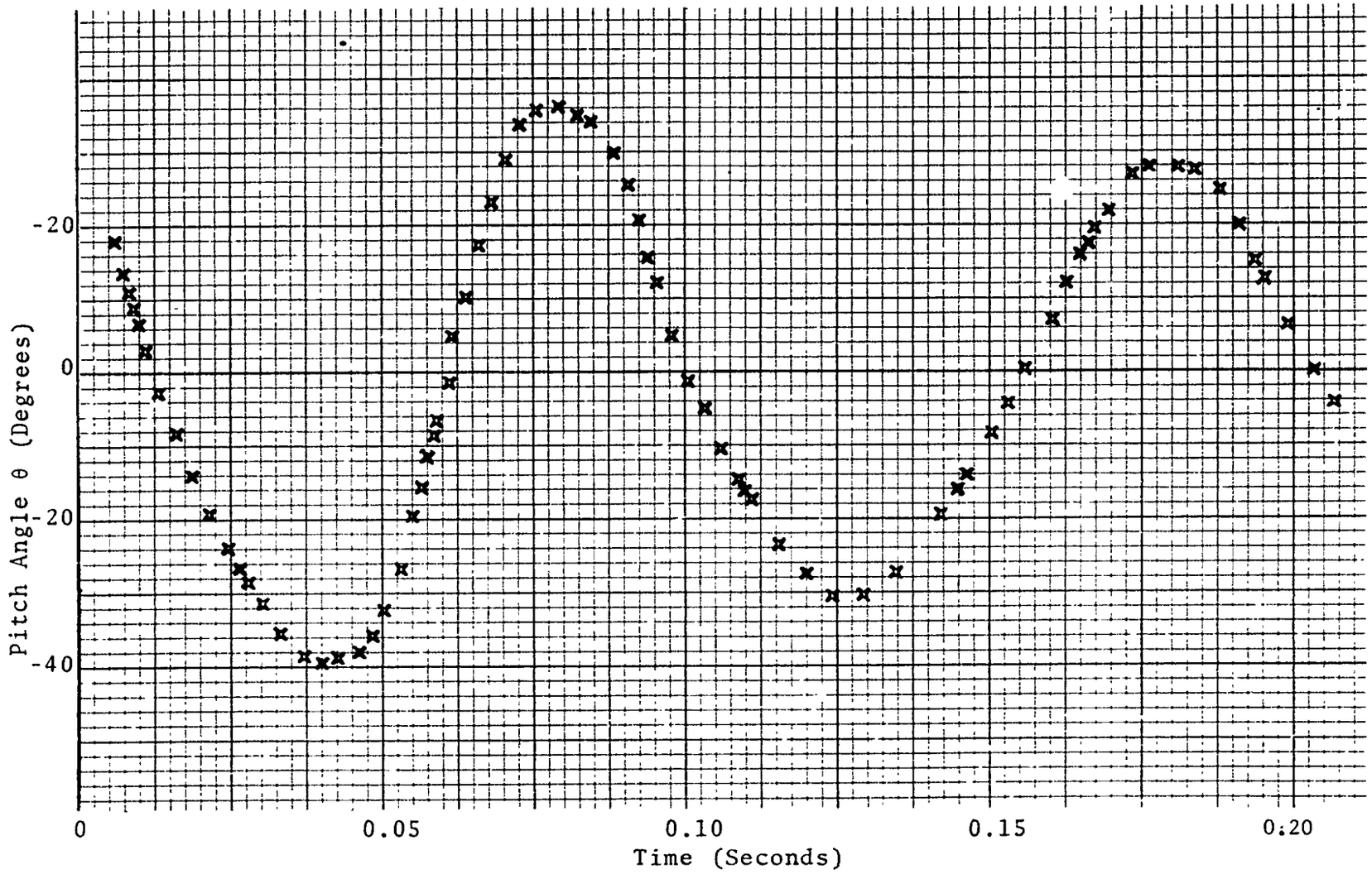

Figure II-19. Von Karman Data Sample, 1.25 Inch Cylinder With Small Volute

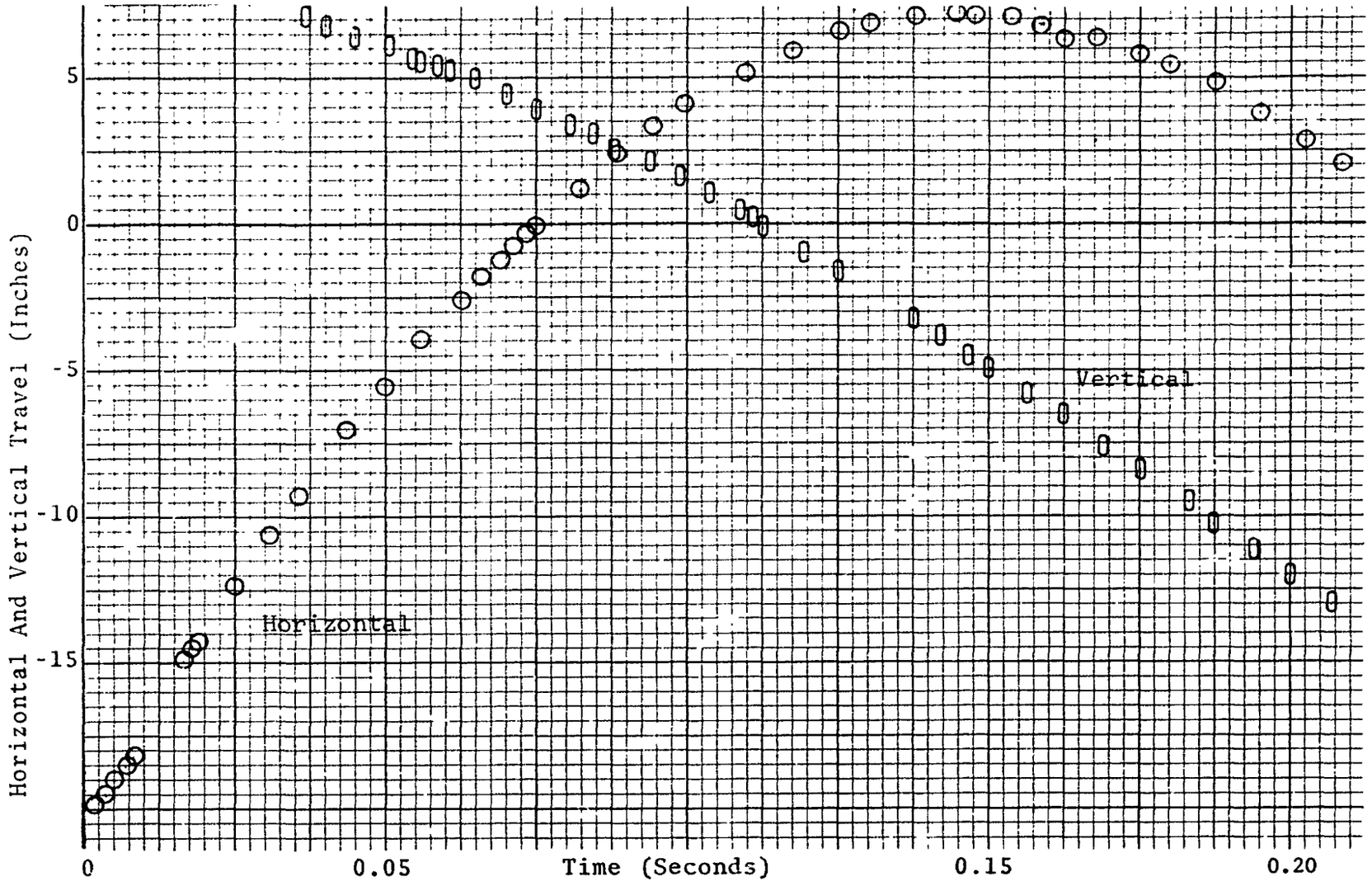

Figure II-20. Von Karman Data Sample, 1.25 Inch Cylinder With Small Volute

TABLE II-2. CYLINDER MODEL CHARACTERISTICS

Cylinder Length (Inches)	Weight (Pounds)	Moment of Inertia (Slugs-Ft^2)	X_{cg} (Inches)
0.75	0.059	2.2×10^{-6}	0.45
1.00	0.079	3.4×10^{-6}	0.55
1.25	0.088	4.3×10^{-6}	0.72
2.08	0.380	1.36×10^{-3}	1.25
2.78	0.500	2.05×10^{-3}	1.65
3.48	0.610	2.95×10^{-4}	1.96

Table II-2 lists only the cylinder forebody without the volute tail. Only two different type tails were used for the Von Karman tests. These two types are shown in Figure II-21. The smaller of the two was used on cylinder lengths 0.75, 1.00, and 1.25 inches. The larger volute was used on the remaining larger cylinders. Both volutes were constructed of epoxy or silicon rubber corresponding to rigid and flexible volutes. In both cases, the volute tail was hollow to give a more realistic value for I_V. This is especially important in order to have meaningful free flight data.

During the tests with the above mentioned volutes, it was decided to use a number of coiled spring tails since these were available in one size (Figure II-4,Flexible Volute 2). These small spring tail volutes stabilized the smaller cylinder forebodies as previously mentioned. Data listed in Table II-3 pertains to this particular tail for configurations 075-1, 100-1, and 125-1.

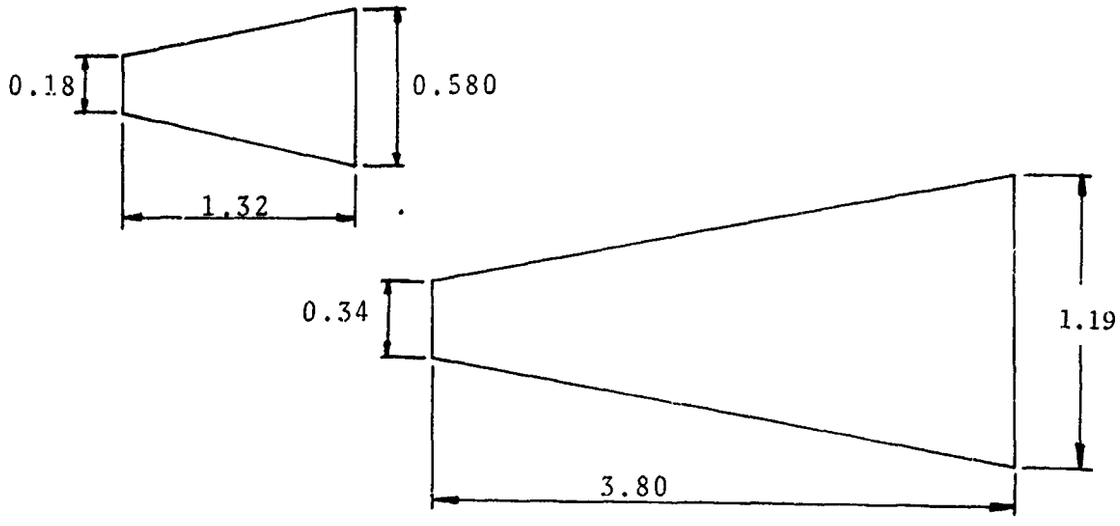

Figure II-21. Volute Tails Used In Von Karman Test Program

TABLE II-3. VOLUTE STABILIZATION DATA

Group	Configu-ration	M	Re_∞ Ft^{-1} x 10^{-6}	Launch Angle of Attack (Degrees)	C_D	$C_{m_q} + C_{m_{\dot{\alpha}}}$ Rad^{-1}	C_{m_θ} Rad^{-1}
2	075-0	0.19	1.04	0	1.2	---	-2.4
3	100-1	0.18	1.03	0	1.1	---	-3.9
4	125-0	0.19	1.04	0	1.0	---	-2.3
5	075-0	0.18	0.99	0	1.6	---	-0.9
6	100-0	0.18	1.06	0	1.3	---	-2.4
7	125-1	0.18	0.99	0	1.6	---	-1.4
8	075-0	0.19	1.06	45	1.7	---	-1.7
9	100-0	0.19	1.09	45	1.6	---	-1.2
10	125-0	0.19	1.07	45	2.0	---	-0.9
11	075-1	0.20	1.08	45	1.7	-3	-1.2
12	100-1	0.18	1.04	45	1.9	---	-1.3
13	125-1	0.18	1.04	45	2.5	-4	-0.6
14	075-0	0.38	1.08	45	1.9	12	-1.5
15	075-0	0.39	1.08	45	2.0	---	---
16	100-0	0.39	1.08	45	2.0	---	---
17	125-0	0.39	1.07	45	2.2	-18	-1.1
18	075-1	0.38	1.07	45	2.0	---	-0.8
19	100-1	0.40	1.09	45	1.7	---	-1.0
20	125-1	0.40	1.06	45	2.5	---	-0.6
21	278-0	0.39	1.07	45	2.7	-55	-2.2
22	075-0	0.39	1.08	0	1.7	22	-3.1
23	100-1	0.40	1.09	0	1.5	-14	-3.0
24	125-0	0.39	1.08	0	1.5	---	-2.0

TABLE II-3. VOLUTE STABILIZATION DATA (Continued)

Group	Configu-ration	M	$R_{e\infty}$ Ft.$^{-1}$ x 10^{-6}	Launch Angle of Attack (Degrees)	C_D	$C_{m_q} + C_{m_{\dot{\alpha}}}$ Rad^{-1}	$\cdot C_{m_\theta}$ Rad^{-1}
25	075-1	0.19	1.04	0	1.4	3	-1.4
26	100-1	0.19	1.05	0	1.2	---	-2.2
27	125	0.20	1.09	0	0.9	---	-3.0
28	100	0.19	1.06	45	1.8	-13	-1.2
29	125	0.20	1.09	45	1.6	-11	-0.7
30	100	0.19	1.07	45	1.7	---	-1.2
31	075	0.19	1.03	90	2.3	---	---
32	100	0.19	1.06	90	2.6	---	---
33	125	0.19	1.05	90	3.0	-18	-1.1
34	075	0.19	1.06	90	2.1	-5	-1.2
35	100	0.19	1.06	90	2.1	-5	-1.1
36	125	0.19	1.06	90	2.6	-22	-0.6
37	075	0.37	1.02	90	2.5	---	-1.2
38	125-0	0.40	1.08	90	3.0	---	-1
39	075-1	0.38	1.04	90	2.3	---	-0
40	125-1	0.37	1.03	90	2.5	---	---
41	125-1	0.39	1.09	90	2.4	---	-0
42	100-1	0.39	1.08	90	2.1	---	-0
43	100-1	0.39	1.06	90	2.2	---	-0
44	208-0	0.39	1.06	45	2.2	-47	-3
45	278-0	0.38	1.04	45	2.5	-51	-2
46	248-0	0.38	1.04	45	2.7	-65	-1
47	100-0	0.58	1.04	45	2.4	---	-2
48	075-0	0.59	1.05	45	2.6	-7	-1

TABLE II-3. VOLUTE STABILIZATION DATA (Concluded)

Group	Configu-ration	M	Re_{∞} Ft.$^{-1}$ x 10^{-6}	Launch Angle of Attack (Degrees)	C_D	$C_{m_q} + C_{m_{\dot{\alpha}}}$ Rad^{-1}	C_{m_θ} Rad^{-1}
49	100-1	0.60	1.08	45	4.4	---	---
50	100-1	0.59	1.06	45	5.6	---	---
51	075-0	0.59	1.00	0	2.3	6	-2
52	100-0	0.59	1.06	0	1.9	---	-5
53	100-1	0.59	1.06	0	3.4	---	---
53	100-1	0.59	1.06	0	5.0	---	---
54	100-1	0.58	1.01	0	2.2	---	-4.4
54	100-1	0.58	1.01	0	2.2	---	-3.6
55	100-1	0.39	1.08	180	---	---	---
56	100-1	0.37	1.04	180	2.6	---	-1.0
57	100-0	0.37	1.03	180	3.8	---	-1.0
58	100-0	0.37	1.04	180	3.5	-10	-1.0
59	278-0	0.37	1.03	45	2.8	-49	-2.55
60	100-1	0.37	1.80	90	2.9	---	-1.33
61	100-1	0.37	1.35	90	2.5	---	-1.22

[1]To find the model size in the above table, interpret the first three digits as the cylinder length, the digit following the dash indicates 1 flexible, 0 rigid. The small volute in Figure II-21 were used on cylinders 0.75, 1.00, and 1.25 in length. The larger cylinders used the larger volute.

REFERENCES

1 Etkin Bernard, Dynamics of Flight, New York Wiley, 1959.

2 Timoshenko S. and Young D.H., Advanced Dynamics, McGraw-Hill Book Company Inc., 1948.

3 Wehrend R. W., An Experimental Evaluation of Aerodynamic Damping Moment of Cones With Different Centers of Rotation, Nasa TN D-1202, January 1962.

4 Glasgow Mark O., Some Methods For Extracting Aerodynamic Derivatives From Forced Oscillation Wind Tunnel Tests With Application To Volute Stabilized Models, AFATL-TR-70-58, June 1970.

(The reverse of this page is blank)